Technical Report **R 226**

BLAST LOADING OF CONCRETE BEAMS REINFORCED WITH HIGH-STRENGTH DEFORMED BARS

22 April 1963

U. S. NAVAL CIVIL ENGINEERING LABORATORY
Port Hueneme, California

BLAST LOADING OF CONCRETE BEAMS REINFORCED WITH HIGH-STRENGTH DEFORMED BARS

Y-F008-10-102A

Type C

by

William A. Keenan

ABSTRACT

Economical blast-resistant concrete structures can be constructed by reinforcing concrete members with high-strength deformed bars if such members can meet the requirements of: (1) adequate strength and ductility under blast loading, and (2) limited deflections and formation of cracks under static service loads. A theoretical study and a series of beam tests were made to determine if concrete members reinforced with high-strength deformed bars can meet the above requirements.

In the theoretical study, the influence of (1) the amount, yield strength and ductility of the tensile steel and (2) the amount, location and yield strength of the compression steel on the strength and ductility of a concrete beam is discussed. Then, the influence of the amount and yield strength of tensile steel on the stiffness of a beam is presented. The minimum yield-load factor (ratio of the beam's static yield resistance to the static service load) required to limit deflections to any given amount is presented as an equation and is plotted for various span-to-depth ratios.

In the tests, sixteen simply supported concrete beams reinforced with high-strength deformed bars (91,600 psi yield stress) were subjected to static and dynamic uniform loads and their behavior observed. Eight beams were conventionally reinforced, and eight were partially prestressed. The prime purpose of the prestressing was to limit the cracks and deflections. Both types of beams were subjected to long- and short-duration loads. Several beams were loaded dynamically more than once to determine their resilience and to study the problem of multiple-shot damage. The static and dynamic tests are reported, evaluated, and compared with theory. Equations for the static collapse deflection and the maximum dynamic deflection of a uniformly loaded concrete beam are presented.

It is concluded that the two major factors which may restrict the use of high-strength steel in blast-resistant design are (1) the inability of such a steel to elongate a required minimum amount, and (2) excessive deflections and/or cracks of beams reinforced with high-strength steels under static service loads.

The tests demonstrate that more resistance can be gained with a lesser amount of high-strength steel than lower grades of steel and that chromium-alloy steel of the type used in this investigation has a sufficient amount of ductility for use in simply supported beams. Both the theoretical study and the experimental tests indicate that excessive deflections may be controlled by prestressing the tensile steel.

Copies available at OTS $2.50
The Laboratory invites comment on this report, particularly on the results obtained by those who have applied the information.

CONTENTS

INTRODUCTION

The increasing need for economical blast-resistant structures has created interest in the use of high-strength* steel as reinforcement in concrete. Designing for greater pressures and longer durations has increased the cost of protective construction, forcing the designer to seek new materials and methods of construction.

Engineers have long desired to take advantage of the greater working stress and yield stress possible with high-strength steels. However, the use of high-strength steels in blast-resistant structures is finding slow acceptance among design engineers. This reluctance is due primarily to a need for more information about the strength and ductility of beams under blast loading, the deflections and cracks of beams under static service loads, and the bond and shear strength of beams reinforced with high-strength steels. In addition, more information is required concerning the weldability, bending qualities, uniformity (e.g., stress-strain characteristics), and the identification of special new grades of high-strength alloy steels with a yield stress exceeding 75,000 psi. The need for more information has led to an investigation at the Naval Civil Engineering Laboratory to contribute to a better understanding in these areas.

The purposes of this report are (1) to develop some fundamental theories regarding the use of high-strength steels for reinforcement in concrete beams; (2) to study the feasibility of partially prestressing concrete beams with high-strength deformed bars; and (3) to present the results of a series of tests designed to study the behavior of concrete beams reinforced with high-strength deformed bars when subjected to static and blast loads.

The first part of the report presents a study of the influence of the yield strength of reinforcing steel on the strength, ductility, and stiffness of concrete beams. These characteristics determine the ability of a beam to resist both static and blast loadings. The second part of the report presents the results of static and dynamic tests on concrete beams reinforced with high-strength deformed bars. Sixteen beams of the type shown in Figure 1 were tested. Eight were partially prestressed and eight were conventionally reinforced. A comparison of experimental and theoretical behavior is next discussed. Finally, significant findings and conclusions are presented.

---

* In this report, the term "high-strength" is used to designate steels having a yield stress in excess of 60,000 psi.

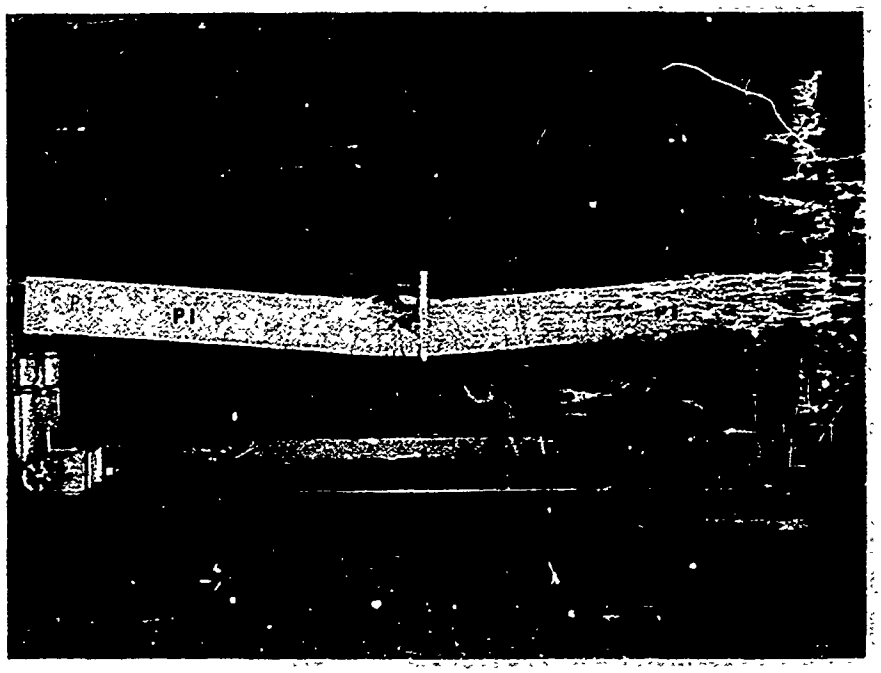

Figure 1. View of a typical concrete test beam.

In general, the symbols are defined where they first appear. A summary of all notation used is presented at the end of the report.

REQUIREMENTS OF BEAMS TO RESIST BLAST LOADS

General Considerations

For a reinforced concrete beam to resist blast loads it must have adequate strength and ductility. In addition, under static service loads,* the cracks and deflections of the beam must be limited. The feasibility of using high-strength steels in a concrete beam to resist blast loads depends upon how well such a beam can meet the above requirements. The influence of high-strength tensile reinforcement on each of these requirements is treated in the following sections.

* In this report, the static service load is defined as that proportion of dead plus live load which is used to compute the deflection of flexural members.

Theory Versus Design Practice

Theoretically, the amount of strength and ductility required in beams and the relative importance of each depends upon the duration of the blast load. For example, bombs in the megaton range normally produce long-duration loads with respect to the natural period of the member on which it acts ($T_e/T_n > 6$). The strength of the member is more important than its ductility for this type of load; i.e., increasing beam strength will increase the dynamic load-carrying capacity of the beam much more than if, instead, the beam ductility was increased by the same percentage. However, as the duration of the blast load decreases, the importance of ductility increases. For example, small weapons, especially high explosives, produce short-duration loads with respect to the natural period of the member on which it acts ($T_e/T_n < 3$). Therefore, it is more economical to design the member to deflect plastically without loss of strength for this type of load. This ductility will allow time for a short-duration load to decrease to a level which the member can support. However, the relative importance of strength and ductility under long- and short-duration loads is generally not considered in design practice.

In practice, the member is designed for a given load level and the load is generally assumed to be of infinite duration. This is a sound assumption since in all probability a large weapon will be used and should the load-duration be shorter, the design will be conservative. Next, a dynamic-deflection criterion is established (the amount of ductility that the member must possess). The dynamic-deflection criterion may either require that the beam be capable of deflecting to some ratio of the span length[1,2] or to some ratio of the yield deflection of the member.[3] The resistance or strength of the member is then adjusted until the maximum dynamic deflection under the blast load does not exceed the preselected deflection.

This beam-resistance can be obtained with considerably less high-strength steel. In addition, the relative reinforcement cost for a given load-carrying capacity for most high-strength steels is less than for lower-grade steels. Therefore, high-strength steel will generally be more economical provided such a steel has enough ductility to satisfy the preselected dynamic-deflection criterion and provided the deflection and cracks of the member under static service loads are within acceptable limits.

INFLUENCE OF HIGH-STRENGTH STEEL ON REQUIREMENTS OF BEAMS

Strength and Ductility

The strength and ductility of a concrete beam depend to a large degree upon the magnitude of the reinforcing index, ductility of the tensile steel, amount and location of compression steel, and the amount of tensile steel. Each of these

quantities, in turn, is influenced by the yield strength of the reinforcement. The allowable range of these quantities for various yield-strength steels and the influence of these quantities on the strength and ductility of a concrete beam are discussed in the following sections.

The succeeding discussion assumes that: (1) the reinforcement exhibits a "flat-top" stress-strain relationship with a well-defined yield stress, and (2) plane sections remain plane before and after bending. The first assumption is not valid for most high-strength steels. However, the error in this assumption is small for steels such as those used in the beam tests described later in this report.

Reinforcing Index. It is imperative that a concrete beam be under-reinforced to eliminate the possibility of a brittle failure and to gain the additional strength offered by high-strength steel. This requires that the reinforcing index, defined in the following paragraph, be less than the value corresponding to failure by initial yielding of the tensile steel followed by crushing of the concrete in compression. The allowable range of the reinforcing index for various grades of steel will be determined subsequently.

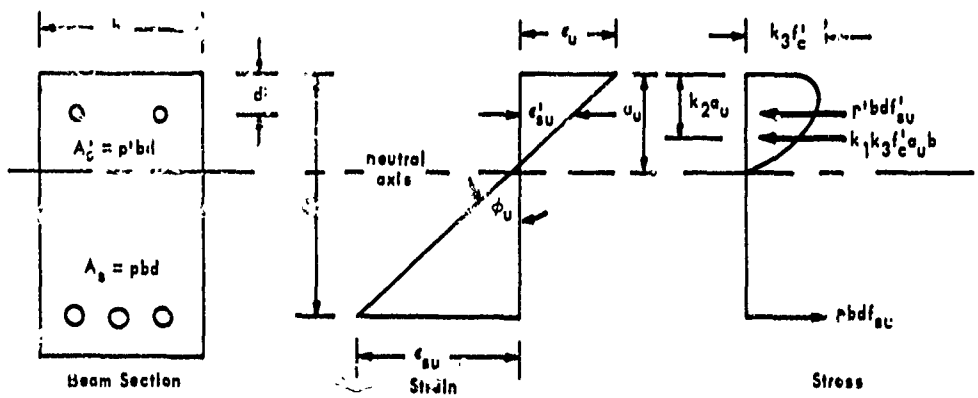

Figure 2. Stress and strain distribution at ultimate moment for R/C beam.

Figure 2 represents the assumed strain and stress distribution over a section of an R/C beam at ultimate-moment capacity. With reference to Figure 2, the position of the neutral axis is given by

$$\frac{a_u}{d} = \frac{\epsilon_u}{\epsilon_u + \epsilon_{su}} \qquad (1a)$$

For internal equilibrium of forces,

$$p'bdf'_{su} + k_1k_3f'_c a_u h = pbdf_{su} \tag{1b}$$

Combining Equations 1a and 1b, the reinforcing index is defined as

$$q = (pf_{su} - p'f'_{su})\frac{1}{f'_c} = k_1k_3\left(\frac{\epsilon_u}{\epsilon_u + \epsilon_{su}}\right) \tag{1}$$

For the special case of a "balanced" beam in which failure occurs by simultaneous yielding of tensile steel and crushing of the concrete, $\epsilon_{su} = \epsilon_y$ and $f_{su} = f_y$. Thus the "balanced" reinforcing index is defined as

$$q_b = (p_b^c f_y - p'f'_{su})\frac{1}{f'_c} = k_1k_3\left(\frac{\epsilon_u}{\epsilon_u + \epsilon_y}\right) \tag{2}$$

For beams with no compression reinforcement, $p' = 0$, $p_b^c = p_b$, and Equation 2 becomes

$$q_b = \frac{p_b f_y}{f'_c} = k_1k_3\left(\frac{\epsilon_u}{\epsilon_u + \epsilon_y}\right) \tag{2a}$$

Based on an extensive compilation of experimental data, empirical equations for k_1k_3 and ϵ_u have been established.[4]

$$k_1k_3 = \frac{3,900 + 0.35f'_c}{3,200 + f'_c} \tag{3}$$

$$\epsilon_u = 0.004 - \frac{f'_c}{6.5 \times 10^6} \tag{4}$$

From Equations 2, 3, and 4, the balanced reinforcing index, q_b, for various grades of concrete and reinforcement, is plotted in Figure 3. The member is over-reinforced if the reinforcing index, q, of a member is greater than the value given in Figure 3, and only a portion of the strength offered by the tensile steel will be utilized.

Curve	f_y (psi)	Steel
A	40,000	ASTM, A15-58T (intermediate grade)
B	60,000	ASTM, A432-59T (billet)
C	75,000	ASTM, A431-59T (high-strength billet)
D	90,000	ASTM Std in Progress

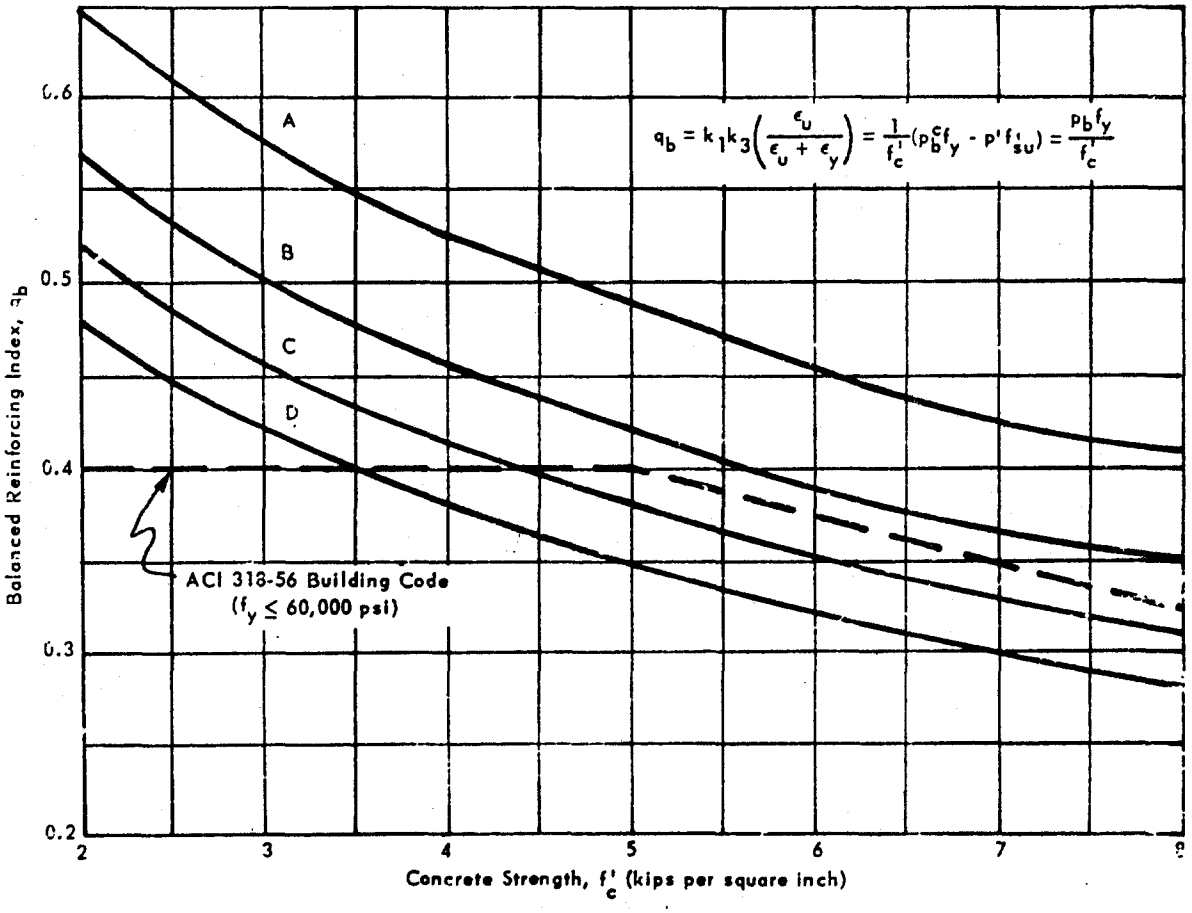

Figure 3. Balanced reinforcing index for various grades of steel.

A beam which is under-reinforced insures that the yield strength of the tensile steel will be utilized (tensile steel will yield) but does not insure that the beam has sufficient ductility to resist the imposed blast loading. For example, if $q = q_b$ the beam will provide the greatest resistance and least ductility, and it will fail by simultaneous yielding of the tension steel and crushing of the concrete. If q is much smaller than q_b, the beam will not provide maximum resistance but will be capable of undergoing large plastic deformations before collapse. Beams with intermediate values of q will have resistance and ductility characteristics between the two extremes described above. The value of q to be used in blast-resistant design will depend on the relative requirements of strength and ductility.

For reasons of safety, to account for the increased yield strength of steel under blast loads, and because the values of q_b are only theoretical, the maximum-allowable value of q to be used in design must be significantly less than q_b. The percent increase in the yield strength of steel under blast loading decreases with an increase in the static yield strength.[5,6] For steels with $f_y < 60,000$ psi, the increase is about 30 percent for the strain rates in most beams ($0.05 < \dot{\epsilon} < 0.20$). For $f_y > 60,000$ psi, the increase is less than 20 percent. Therefore, the limiting value of q to be used in blast-resistant design should be about $0.60q_b$ for intermediate-grade steel and about $0.70q_b$ for high-strength steels.

The limiting value of q recommended by the ACI Building Code (318-56)[7] is shown in Figure 3. The figure shows that within the practical range of concrete strengths, the value of q prescribed by the ACI Code is only safe for $f_y < 60,000$ psi (as stated in Section A603 of the Code). An empirical equation proposed by the author for the maximum-allowable value of q to be used in blast-resistant design, which covers the practical range of steel and concrete strengths, is

$$q_a = 0.510 - (1.9f_y + 22f'_c)10^{-6} \qquad (5)$$

This expression insures that q_a will never exceed 62 to 68 percent of q_b for the range of steel and concrete strengths shown in Figure 3.

It is desirable, under certain conditions, to partially prestress the tensile steel of a concrete beam; this has the effect of increasing the balanced reinforcing index.

Figure 4 shows the stress and strain distribution at ultimate moment at a section of a partially prestressed concrete beam. From equilibrium of forces and by relating the strains,

$$q = (p\frac{f_{su}}{f'_c} - p'\frac{f'_{su}}{f'_c}) = k_1 k_3 \left(\frac{\epsilon_u}{\epsilon_u - \epsilon_{se} - \epsilon_{ce} + \epsilon_{su}}\right) \qquad (6)$$

For the special case of a balanced beam,

$$q_b = (p_b\frac{f_y}{f'_c} - p'\frac{f'_{su}}{f'_c}) = k_1 k_3 \left(\frac{\epsilon_u}{\epsilon_u - \epsilon_{se} - \epsilon_{ce} + \epsilon_y}\right) \qquad (7)$$

This equation shows that the higher the prestress (i.e., the larger ϵ_{se}), the greater the balanced reinforcing index. Therefore, Equation 5 can also be used to obtain a conservative estimate of the maximum-allowable reinforcing index for beams which are partially prestressed.

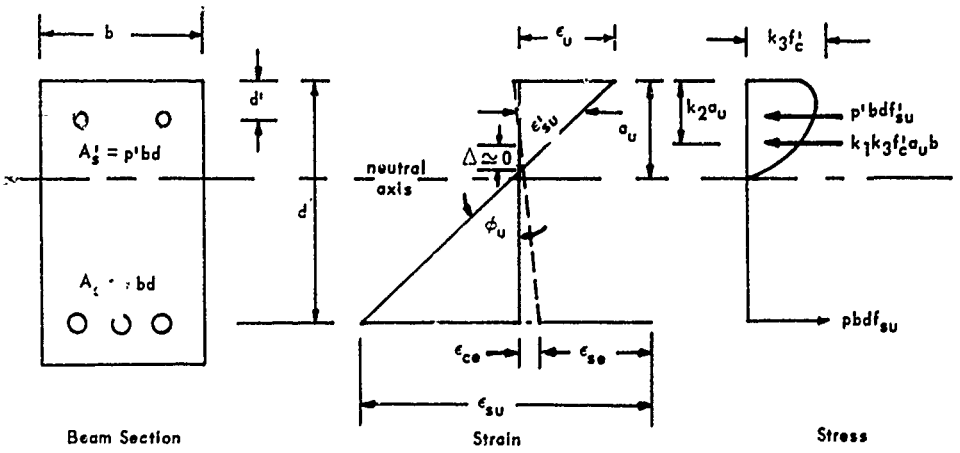

Figure 4. Stress and strain distribution at ultimate moment for P/C beam.

Steel Ductility. A beam must be capable of large inelastic deformations prior to collapse to meet the dynamic-deflection criterion established for a given design. This requires that the tensile reinforcement be capable of elongating a certain minimum amount, ϵ_{su}. By rearranging Equation 1,

$$\epsilon_{su} = \epsilon_u \left(\frac{k_1 k_3}{q} - 1 \right) \tag{8}$$

Equation 8 gives the maximum strain in the tensile steel at ultimate-moment capacity and is plotted in Figure 5. The required strain capacity of the tensile steel in simply supported beams can be estimated from Figure 5. This figure may also be used to estimate the required strain capacity of the tensile steel at the point of maximum positive moment in restrained beams. Also shown in Figure 5 is the approximate strain-hardening strain, ϵ_o, for intermediate-grade steel and a chromium-alloy steel with a well-defined yield stress of 91,600 psi.

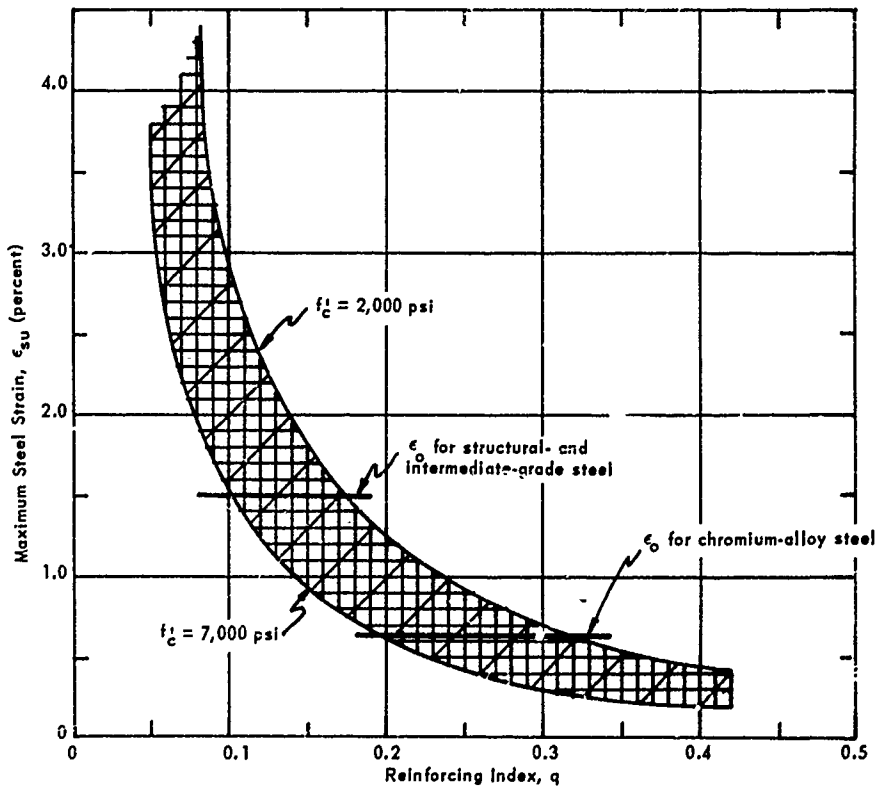

Figure 5. Maximum steel strain at ultimate moment in simply supported beams.

The reinforcing index must be quite small in order to gain the ductility required in blast-resistant design. Experience has shown that it is generally greater than 0.08 and rarely exceeds 0.2. Within this range of the reinforcing index the following conclusions can be drawn from Figure 5 about the tensile steel in simply supported beams:

1. The strain in the tensile steel at ultimate moment, ϵ_{su}, is greater than ϵ_o for all grades of steel except possibly structural- and intermediate-grade; i.e., all grades of steel except possibly structural- and intermediate-grade. will be strain-hardened.

2. The maximum ductility required of the tensile steel will occur in beams with a low q and f'_c. For this condition, the maximum strain in the tensile steel will be about 4 to 5 percent. Therefore, the minimum ductility of reinforcement used in blast-resistant design should be 5 percent. However, the ductility should be greater than 5 percent (a) for reasons of safety, (b) because Equation 8 is only theoretical and (c) to account for the possible variation in the elongating capacity of any one type of steel. Therefore, it is recommended that the tensile reinforcement be capable of elongating at least 10 percent.

Compression Steel. In concrete beams designed to resist blast loads, compression steel is required in order to obtain enough ductility in the beam and to protect against negative moments. Whether full advantage is taken of high-strength steel for compression reinforcement will depend upon its location in the beam and the magnitude of the reinforcing index. From the strain distribution in Figure 2, if $\epsilon'_{su} < \epsilon'_{sy}$

$$\frac{a_u}{a_u - d'} = \frac{\epsilon_u}{\epsilon'_{su}} = \frac{\epsilon_u E_s}{f'_{su}} \tag{9a}$$

Rearranging Equation 1b,

$$a_u = \left(\frac{pf_{su} - p'f'_{su}}{f'_c}\right) \frac{d}{k_1 k_3} \tag{9b}$$

Combining Equation 1, 9a, and 9b, if $f'_{su} = f'_y$

$$\frac{d'}{d} = \frac{q}{k_1 k_3}\left(1 - \frac{f'_y}{E_s \epsilon_u}\right) \qquad (9)$$

Any d'/d less than that given by Equation 9 will insure that the compression steel yields before the beam section reaches its ultimate-moment capacity. Equation 9 is plotted in Figure 6 for a 3,000-, 5,000-, and 7,000-psi concrete strength. Values for $k_1 k_3$ and ϵ_u were determined from Equations 3 and 4, respectively.

As stated, the reinforcing index seldom exceeds 0.2 for beams properly designed to resist blast loads, and, except for very deep beams, the practical lower limit for d'/d is about 0.15. Figure 6 shows that within these limits for q and d'/d the maximum stress that can be developed in the compression steel is about 45,000 psi. This suggests that, except in very deep beams, the additional strength offered by high-strength steel cannot be utilized before the concrete crushes in compression. Therefore, in special cases, it may be more economical to use two different grades of steel, i.e., high-strength steel for tensile reinforcement and intermediate grade for compression reinforcement. However, in general, it may be cheaper to make all steel of the same type, since this will reduce construction problems.

The dashed line in Figure 6 gives the ratio d'/d which at ultimate moment would cause the neutral axis to be located at the level of the compression steel. For ratios of d'/d greater than those corresponding to this curve, the "compression steel" will lie below the neutral axis and actually be in tension.

Equation 9 was compared with reported beam tests.[8] In the reported series-C beams, d'/d was 0.17 and f'_c was 5,100 psi. For $f'_{su} = 0$, the value of q calculated from Equation 1 was 0.09. In several tests the strain gages on the top and bottom face of the compression steel showed that the neutral axis was located in the compression steel prior to beam collapse. Figure 6 supports this behavior.

From the standpoint of beam strength, Equation 18 shows that the contribution from compression steel is relatively small. Therefore, the error in computing the ultimate-moment capacity resulting from an error in the calculated stress in the compression steel is relatively small.

From the standpoint of beam ductility, the contribution from compression steel is large. This follows because the ultimate deflection (Equation 19) increases considerably with an increase in the ultimate rotational capacity (Equation 19b) of a beam section. The ultimate rotational capacity, in turn, is inversely proportional to the reinforcing index (Equation 18d) which, in turn, decreases with an increase in the amount of compression steel. This latter point, of course, assumes that the ratio d'/d is small enough to permit the compression steel to carry its share of the load. For example, if d'/d is such that the neutral axis is in the compression steel at ultimate-moment capacity, beam ductility will not be increased by increasing the amount of compression steel.

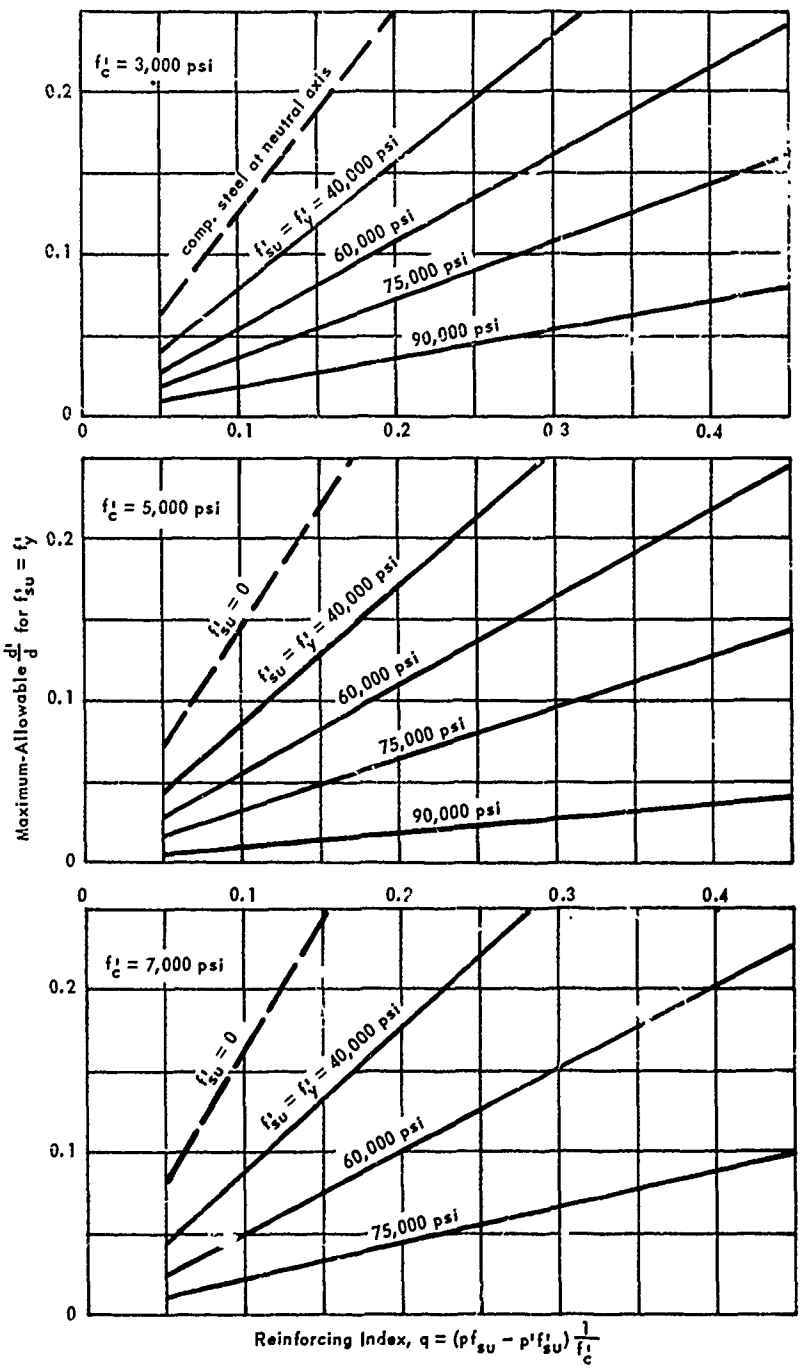

Figure 6. Maximum-allowable d'/d for various grades of steel.

Therefore, an error in the calculated stress in the compression steel can result in a large error in computing beam ductility but a small error in computing beam strength.

Tensile Steel Ratio. In design, the steel and concrete strength are generally selected first and then the dimensions of the cross section and the amount of reinforcement are adjusted to give the necessary strength and ductility. Therefore, when the designer adjusts the reinforcing index he is actually limiting the amount of tensile steel that can be used. In other words, he is adjusting the tensile steel ratio to a value less than the steel ratio corresponding to the maximum-allowable reinforcing index, q_a.

The equation for the tensile steel ratio corresponding to q_u is determined for beams without compression steel ($p' = 0$) by rearranging Equation 2a and letting $q_b = q_a$.

$$p_a = q_a \left(\frac{f'_c}{f_y}\right) \qquad (10)$$

Equation 10 gives the maximum-allowable steel ratio p_a for beams with no compression steel and is plotted in Figure 7. The values for q_a were computed from Equation 5.

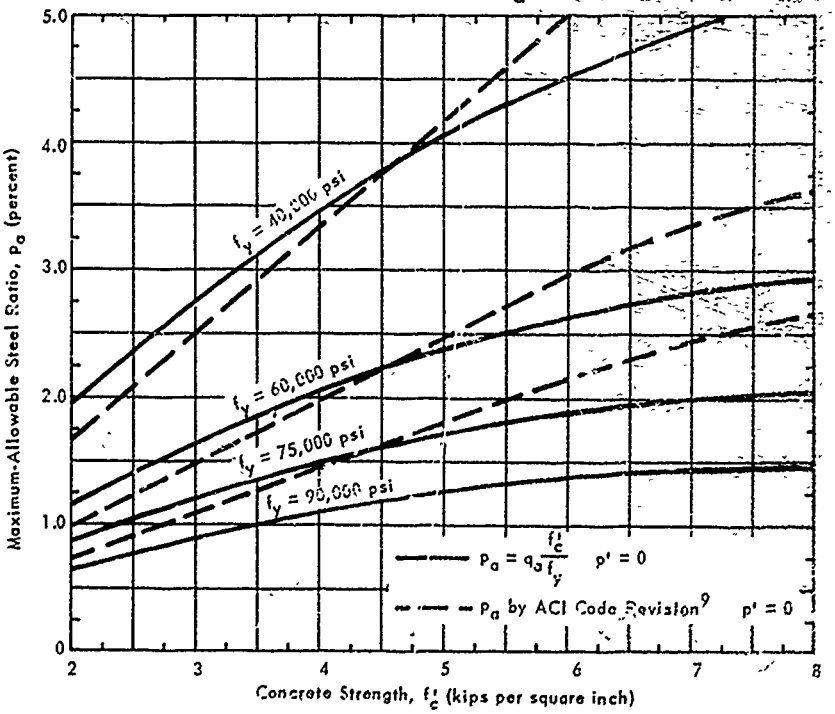

Figure 7. Maximum-allowable steel ratio for R/C beams with no compression steel.

In section 1601 of the "Proposed Revision of Building Code Requirements for Reinforced Concrete (ACI 318-56)"[9] the allowable ratio of tensile steel is given by

$$p_a = 0.75\left[\frac{0.85k_1 f^*_c}{f^*_y}\left(\frac{90,000}{90,000 + f^*_y}\right)\right]$$

where $f^*_y = 0.8f_y$, for $f_y \leq 75,000$ psi

$f^*_c = 2f'_c/3$

$k_1 = 0.85$, for $f^*_c \leq 4,000$ psi

$k_1 = 0.85 - 0.05[(f^*_c - 4,000)/1,000]$, for $f^*_c > 4,000$ psi

The latter equation for p_a is compared with Equation 10 in Figure 7. The proposed revision to the 1956 ACI Code does not permit designs to be based on f_y in excess of 75,000 psi.[9] Therefore, no comparison is shown for a steel with a yield strength of 90,000 psi.

The addition of compression steel in beams permits increasing the amount of tensile steel, thus increasing the strength of the beam.

For beams with compression steel, the allowable tensile steel ratio is p^c_a. If $q_b = q_a$ then $p^c_b = p^c_a$ and Equation 2 becomes

$$q_a = (p^c_a f_y - p'f'_{su})\frac{1}{f'_c} \tag{11a}$$

Solving for q_a in Equation 10 and setting it equal to Equation 11a,

$$\frac{p_a f_y}{f'_c} = (p^c_a f_y - p'f'_{su})\frac{1}{f'_c} \tag{11b}$$

Rearranging

$$p^c_a = p_a + p'\left(\frac{f'_{su}}{f_y}\right) \tag{11}$$

where $f'_{su}/f_y \leq f'_y/f_y$

Equation 11 gives the maximum-allowable tensile steel ratio, p_a^c, corresponding to the maximum-allowable reinforcing index, q_a, for beams with compression steel.

The steel-stress ratio f'_{su}/f_y, for the case when the compression steel does not yield, is determined by rearranging Equation 9 and letting $q = q_a$.

$$\frac{f'_{su}}{f_y} = E_s \epsilon_u \left[1 - \frac{d'}{d}\left(\frac{k_1 k_3}{q_a}\right)\right] \tag{12}$$

where $q_a = 0.510 - (1.9 f_y + 22 f'_c)\, 10^{-6}$ (5)

Equation 12 is plotted in Figure 8 for various steel and concrete strengths and ratios of d'/d.

The value of the steel-stress ratio to be used in Equation 11 will depend upon whether or not the compression steel has yielded. If the compression steel has not yielded, $f'_{su}/f_y < f'_y/f_y$, and the steel-stress ratio taken from Figure 8 should be used in Equation 11. If the compression steel has yielded, $f'_{su}/f_y = f'_y/f_y$, and the ratio f'_y/f_y should be used in Equation 11. Thus, from Equation 11 and Figures 7 and 8, the maximum-allowable tensile steel ratio can be determined for a beam with compression steel.

In the proposed revision to the ACI Code 318-56,[9] the stress ratio to be used in Equation 11 is either zero or unity. If the compression steel stress is less than the yield stress, f'_y, the stress ratio is assumed to be zero except when a general analysis is made.[9] Thus, for this case no increase is permitted in the allowable tensile steel ratio; i.e., $p_a^c = p_a$. If the compression steel does yield, the stress ratio is assumed to be unity. For this case, a stress ratio greater or less than unity is not permitted because the ACI Code does not specify for beams reinforced with two different grades of steel.

It is interesting to note from Figure 7 that, within the practical range of steel ratios used in design, there is little chance of over-reinforcing a beam with structural- or intermediate-grade steel. However, the designer should pay particular attention to the amount of tensile reinforcement when designing with high-strength steels.

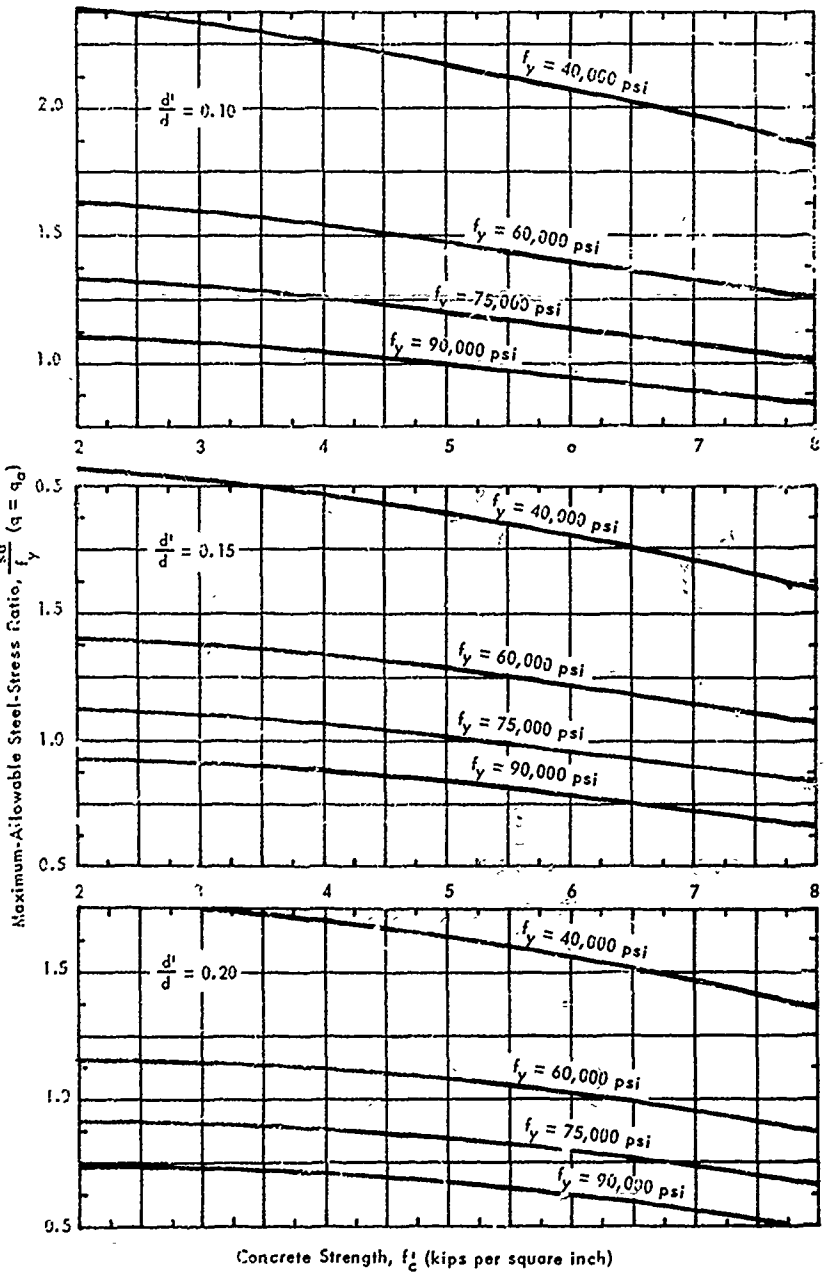

Figure 8. Maximum-allowable steel-stress ratio for R/C beams with compression steel.

Cracks and Deflections

The engineering requirements for a reinforced concrete structure may be roughly classified as:[10]

1. Adequate safety against failure
2. Limited crack formation
3. Limited deflection (sufficient rigidity)

Each of these requirements can impose an upper ceiling on allowable steel stresses and, therefore, the grade of steel to be used in a concrete structure. Item 1 has already been discussed. The influence of the grade of steel on items 2 and 3 is examined in the following paragraphs.

In general, the higher the yield strength of a steel, the less desirable it becomes to use such a steel in unprestressed concrete because of excessive deflection and cracking under static service loads. Although, as stated, a given yield resistance can be obtained more economically with high-strength steel, the beam will not be as stiff and will deflect more under static service loads. Therefore, another factor which will influence the feasibility of using high-strength steel in unprestressed concrete will be the acceptable limit for deflections. However, this factor will become less important as the magnitude of the blast load increases.

Yield-Load Factor. The greater the ratio between the static service load and the static yield resistance required to withstand the imposed blast loading, i.e., the greater the yield-load factor, the more feasible it becomes to use high-strength steel in unprestressed concrete. The physical properties necessary to resist large blast loads (e.g., depth of beam and steel percentage) will generally put deflections under static service loads within acceptable limits.

The acceptable limit for deflections depends upon the type and intended function of the structure. However, the maximum-allowable deflection is commonly limited to some fraction of the span. The minimum yield-load factor required to limit deflections to some fraction of the span is a function of the support conditions, span-to-depth ratio, yield strength of the reinforcement, the percentage of steel, and effective prestress level. The relationship between each of these variables is discussed below.

Shown below is the distribution of curvature along a uniformly loaded simple beam. The mid-span deflection at first yielding of the tensile steel can be expressed as

$$y_y = \left(\frac{5}{48}\right)\varphi_y L^2 \tag{13a}$$

From the resistance diagram shown below,

$$y_s = y_y\left(\frac{w_s}{r_y}\right) \tag{13b}$$

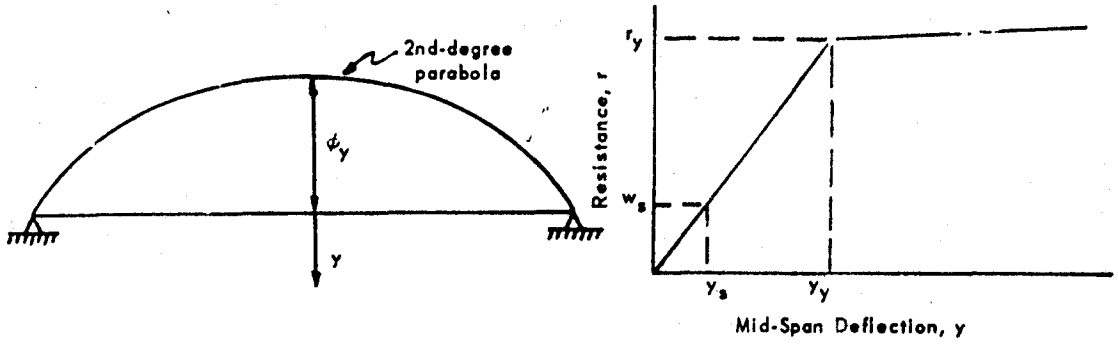

a) Curvature diagram at $y = y_y$

b) Resistance diagram

From the strain diagram shown in Figure 9, the unit rotation of the beam at mid-span when $y = y_y$ is

$$\varphi_y = \frac{\epsilon_y - \epsilon_{se}}{d(1-k)} = \frac{f_y - f_{se}}{E_s d(1-k)} \tag{13c}$$

Let the allowable deflection under static loads be

$$y_s = \frac{L}{N} \tag{13d}$$

Then, combining Equations 12a through 13d,

$$\text{minimum yield-load factor (M.L.F.)} = \left(\frac{5}{48}\right) N \left(\frac{L}{d}\right) \left[\frac{f_y - f_{se}}{E_s (i - k)}\right] \qquad (13)$$

For beams with no prestress, $f_{se} = 0$. Equation 13 gives the yield-load factor at which the mid-span deflection, y_s, of a simply supported beam under a static service load, w_s, will be L/N. This equation indicates that excessive deflections under static service loads may become a limiting criterion in blast-resistant design and should be checked by the designer in the case of:

1. Long spans
2. Shallow beams
3. High-strength steels
4. Low prestress levels
5. Low steel percentages

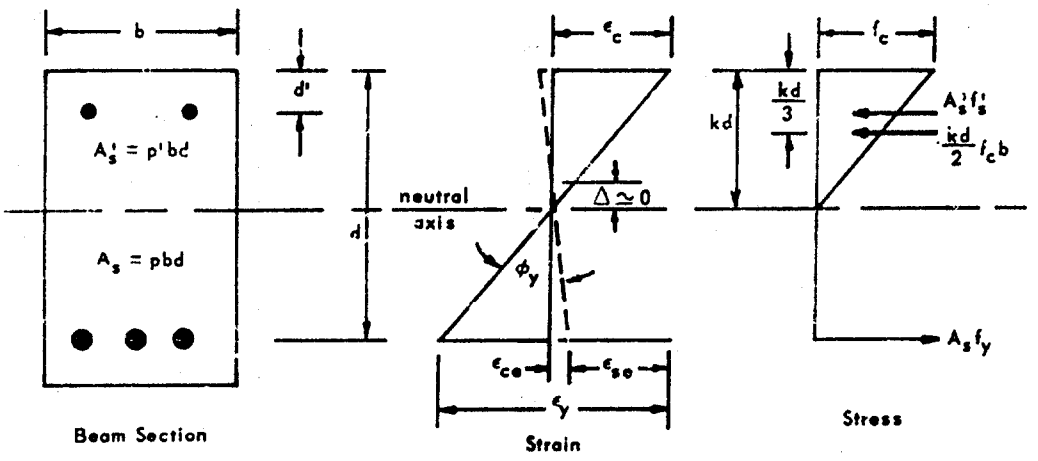

Figure 9. Stress and strain distribution at yield moment.

Equation 13 is plotted in Figure 10 for typical L/d ratios and steel percentages. The curves are based on a limiting deflection under static service loads of L/360. The minimum yield-load factor for any other deflection criterion, yield stress, or L/d ratio can be found by a direct proportion between the variables and those values used in Figure 10.

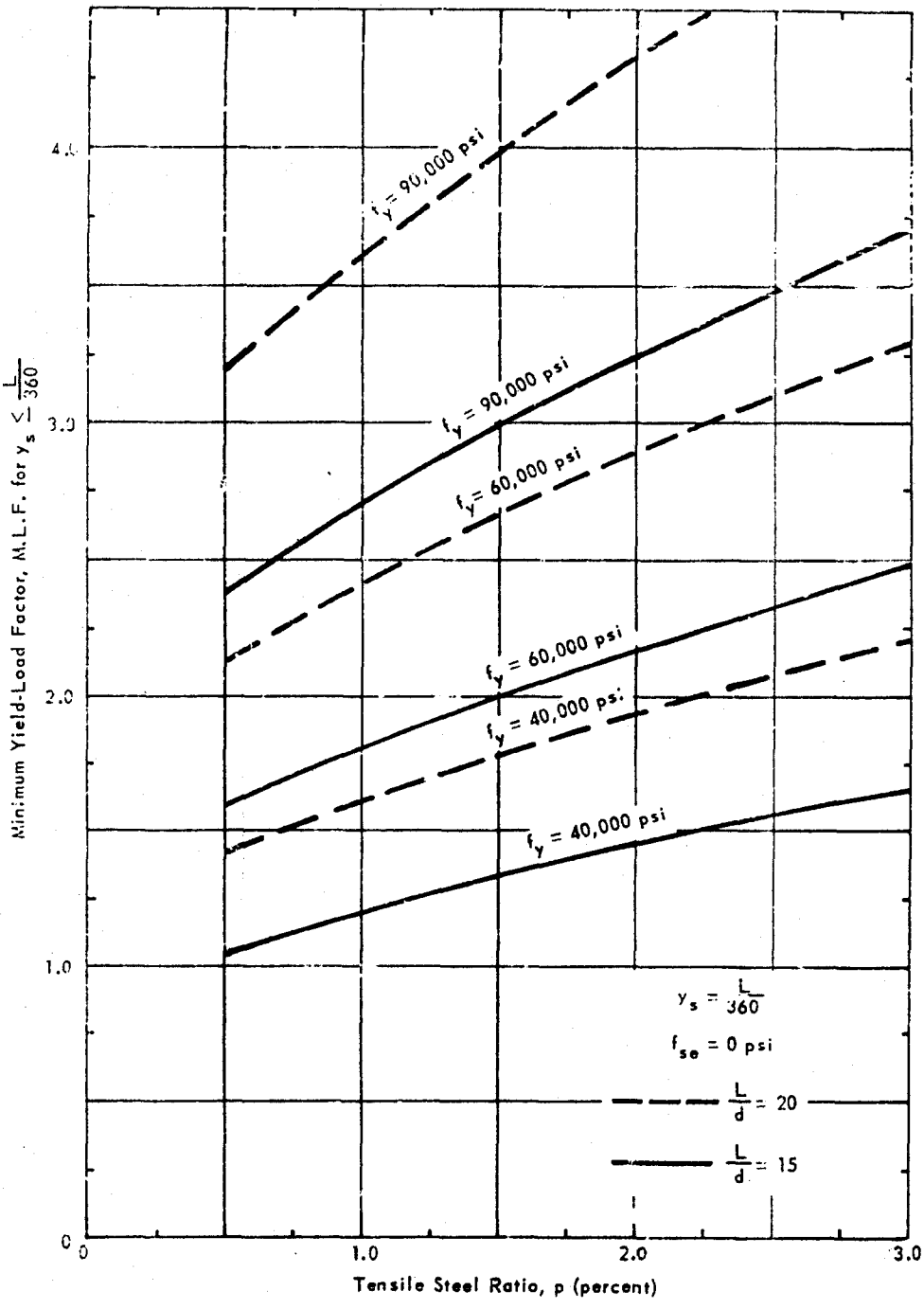

Figure 10. Minimum yield-load factor to limit deflections for varicus grades of steel.

For the deflection criterion and range of variables considered in Figure 10, the following conclusions can be drawn about simply supported unprestressed beams:

1. It is uneconomical to use steels with a yield strength much greater than 60,000 psi for unprestressed beams designed to resist only static loads. This assumes that the yield-load factor for static designs is generally less than 2.5.

2. Steels with a yield strength as high as 90,000 psi can be used in unprestressed beams if the yield-load factor is greater than about 4.5. A yield-load factor as large as 4.5 would seldom, if ever, be used for static designs. However, for blast-resistant design it is highly probable that the yield-load factor will be this large.

3. The smaller the L/d ratio, the more economical it becomes to use high-strength steels if deflection is the limiting criterion for design.

The minimum yield-load factor computed by Equation 10 such that $y_s \leq L/N$ agrees well with experimental data. A comparison is shown in the section of this report entitled "Theory Versus Experimental Results."

Control of Deflections. Prestressing the tensile reinforcement will reduce deflections and cracks, increase allowable working loads and provide more efficient utilization of the higher-strength steels and concrete. Therefore, it would seem reasonable that, in using high-strength ductile steels, a beam design should be selected which provides the necessary ultimate strength and ductility to resist the blast loading. Second, the ratio of the static yield resistance to the static service load, r_y/w_s, should be computed. If r_y/w_s is greater than the minimum yield-load factor required to limit deflections to L/N, the design is sufficient. If r_y/w_s is less than the minimum yield-load factor, deflections will be greater than L/N, and the design must be revised. Three alternatives may be used to revise the design:

1. Increase the depth of section and/or the steel ratio.

2. Redesign the section using a lower-yield-strength steel.

3. Partially prestress the tensile steel. The level of prestress should be adjusted to insure that the cracks and deflections at static service loads are within acceptable limits for the intended function of the structure.

EXPERIMENTAL WORK

Test Specimens

Description. Sixteen simply supported concrete beams were included in the test program. All beams were 12 inches deep, 7-3/4 inches wide, and 15 feet long. The longitudinal reinforcement consisted of high-strength deformed No. 6 bars (f_y = 91,600 psi, p = 1.135 percent) for tensile reinforcement and intermediate-grade No. 3 bars (f_y = 49,900 psi, p' = 0.426 percent) for compression reinforcement. The web reinforcement consisted of No. 3 intermediate-grade ties (f_y = 49,900 psi) hooked to the compression steel. Extra ties were placed in the center portion of the beam to contain the concrete and prevent buckling of the compression steel at large deflections. The arrangement of the reinforcement and the physical details of both the partially prestressed and conventionally reinforced concrete beams are illustrated in Figure 11. Eight beams were conventionally reinforced (zero prestress) and eight partially prestressed. The tensile steel in the partially prestressed beams was prestressed to 45,000 psi (seven beams) or 90,000 psi (one beam).

The reinforced concrete beams were designated R1 through R8 and the P/C beams P1 through P8. Most of the beams were loaded dynamically more than once, in which case an additional number is added to the beam designation to indicate the cycle of loading. For example, R3-4 means R/C beam No. 3, fourth dynamic loading.

Material Properties. The average physical and chemical properties of the reinforcing bars are summarized in Table I. A typical stress-strain curve for each size bar is shown in Figure 12. All bars of each size were from the same lot and met the deformation requirements of Specification A305-56T of the American Society for Testing Materials (ASTM).

The No. 3 bars were intermediate grade and met the requirements of ASTM A15-58T. The No. 6 bars were from a basic open-hearth chromium-alloy steel. These bars were made to meet the deformation requirements of ASTM A-431 Modified (90,000-psi minimum yield stress). The steel falls in the chemical requirement range of Specification A-5155H and A-5160H of the American Institute of Steel and Iron (AISI). These bars exhibited a linear stress-strain relationship up to a well-defined yield stress of 91,600 psi.

Some alloy-steel bars have less ductility than cold-worked bars and are relatively more difficult to bend. To determine the bending qualities of the chromium-alloy bars for stirrups, anchorage, etc., six random specimens were bent at room temperature through 90 degrees around a 3-inch-diameter pin. None of the specimens showed any signs of cracking on the outside of the bent portion of the bar. It is interesting to note that although ASTM A431-59T is most nearly applicable to these bars, they met the relatively severe bend-test requirements for structural-grade bars (ASTM A15-58T).

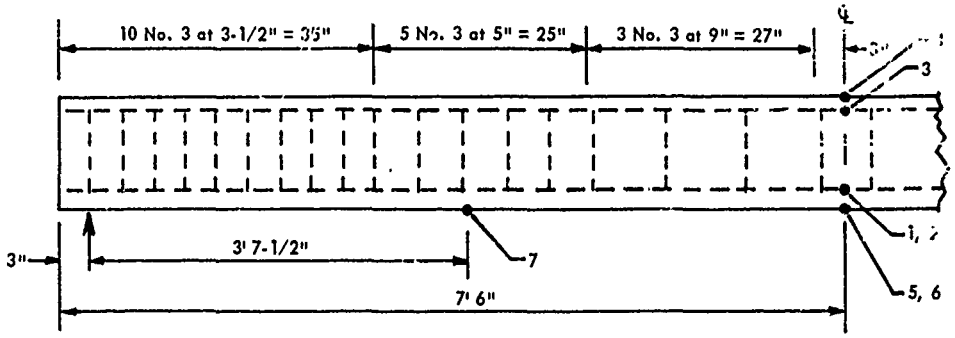

Typical Front View

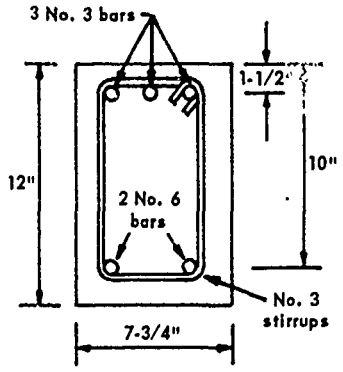

Typical Section

Instrumentation

Location	Mark	Measuring Device
1	S1	2, A12-2 electric strain gages
2	S2	2, A12-2 electric strain gages
3	S3	2, A12-2 electric strain gages
4	C1	1, A9-2 electric strain gage
5	a	Statham accelerometer
6	BP2	Bourns potentiometer and rotating drum
7	BP1	

Figure 11. Beam details and instrumentation.

Table I. Physical Properties of Reinforcing Bars

Tensile Properties[1/]

Bar Size	Yield Strength (psi)	Ultimate Strength (psi)	Modulus of Elasticity (10^6 psi)	Elongation in 8 Inches (percent)
No. 6	91,600	143,000	28.2	11.3
No. 3	49,900	71,500	27.3	24.2

Geometric Properties[1/]

Bar Size	Area ($in.^2$)	Deformations (inches)				
		Spacing (avg)	Height			Gap (avg)
			(min)	(avg)	(max)	
No. 6	0.43	0.340	0.038	0.039	0.042	0.155
No. 3	0.11	0.187	0.023	0.024	0.025	0.115

Chemical Properties

Bar Size	Chemical Composition (percent)					
	C	Mn	P	S	Si	Cr
No. 6	0.59	0.92	0.019	0.023	0.33	0.92

1/ Average for 5 bars of each size.

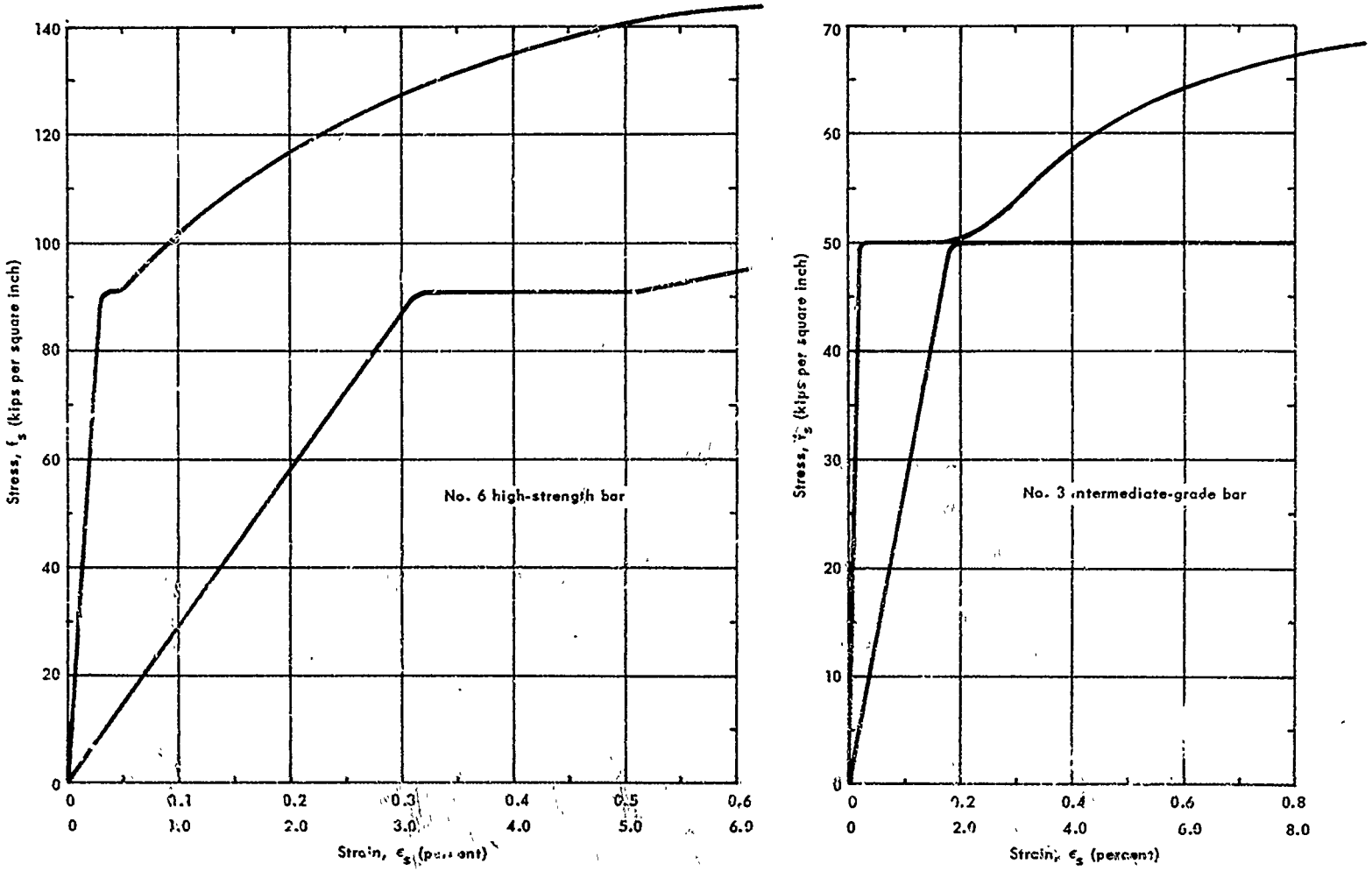

Figure 12. Typical stress-strain curve for reinforcing bars.

The average properties of the concrete are summarized in Table II. The concrete was made with type-III portland cement. The maximum size of the coarse aggregate was 3/4 inch. The concrete mix was 1:2.4:2.5 by weight, with a water-cement ratio ranging between 0.43 and 0.55. The slump of the concrete ranged from 1.5 to 3.5 inches.

Table II. Properties of Concrete[1/]

Beam No.	7-Day Compressive Strength f_c (psi)	Properties at Time of Beam Test			
		Age (days)	Compressive Strength f'_c (psi)	Secant Modulus[2/] E_c (10^6 psi)	Tensile Strength[3/] f_t (psi)
P1	5,780	48	7,300	3.49	600
P2	5,820	67	7,400	3.42	600
P3	4,750	61	6,320	3.15	670
P4	5,650	64	7,320	—	720
P5	5,300	56	6,620	—	690
P6	5,830	68	7,740	—	725
P7	4,840	62	6,130	—	685
P8	5,630	42	6,690	3.41	625
R1	6,160	61	7,630	3.58	665
R2	5,600	56	7,160	3.42	700
R3	5,800	58	7,200	3.33	785
R4	6,010	69	7,530	—	730
R5	5,840	62	7,630	—	725
R6	6,240	68	8,100	—	770
R7	5,140	62	6,750	—	655
R8	5,500	42	6,790	3.41	720

1/ Each value listed is the average for two control specimens.

2/ Secant modulus at $0.5f'_c$.

3/ From modulus-of-rupture specimen.

Methods of Prestressing. Many methods of prestressing steel entail intricate operations and the use of highly skilled labor. In addition, most methods are adaptable only to plain bars, wire strands, and cables.[11]

Three methods of prestressing high-strength No. 6 deformed bars were evaluated. In all three methods, the prestress force was applied to the bar by tightening a nut onto a 1-inch-diameter threaded stud. The first method involved welding a stud to each end of the deformed bar for gripping. A maximum bar stress of 30,000 psi could be developed before fracture at the weld. The second method involved threading each end of the bar. This method proved inefficient but a maximum bar stress of 70,000 psi could be developed. The third method of prestressing consisted of welding the threaded stud to a Howlett Grip Coupler (Figure 13a) which in turn gripped the reinforcing bar. The Howlett Grip Coupler consists of an outer casing and an inner sleeve, joined together by buttress threads. The sleeve is slotted to permit its diameter to be reduced. When tension is applied to the bar, the sleeve moves. This movement decreases the sleeve diameter forcing its teeth to compressively engage and grip the periphery of the bar. Before assembling the grips, the deformations on each end of the bar were scored with a file. This permitted the sleeve to be twisted onto the bar to provide an effective gripping surface. The reaction for the prestressing force was provided by anchor plates bearing against each end of the steel form used to cast the beams. The stud had a square cross section and passed through a square hole in the anchor plate. This prevented the bar from twisting when the nut was tightened onto the stud. Details of the method of prestressing are shown in Figure 13b. The latter method was chosen; it was simple to use and its application is broad.

Fabrication. The beams were cast right side up in steel forms which had a movable side plate to facilitate removal of the beams. After the reinforcing cage was assembled, a Howlett sleeve was twisted onto each end of the bars to be prestressed. Next, a cage was positioned in each of three steel forms by hydrostone spacers placed at the quarter-points of the cage, with a wooden spacer box at each end. The prestressing jig was then assembled on the bars of the cages to be prestressed, and the anchor plates were bolted onto each end of the three forms (Figure 13b).

The prestress was applied simultaneously to each bar by tightening snug-tight nuts (Figure 13b) in increments of 1/8 of a revolution. At each increment of nut revolution, the required torque and corresponding bar strains were measured with a torque wrench and strain indicator, respectively. The bar stress computed from the strain gage measurements on the bar was also compared with the bar stress as determined by a load-cell measurement. A typical curve of the measured torque, nut revolutions, and bar stress versus load-cell stress is shown in Figure 14.

Six days after casting the concrete, the prestress force was transferred to the beam. The force was released by slowly loosening the nuts at each end of the bars. The beams were then removed from the forms and stored to field-cure until they were tested.

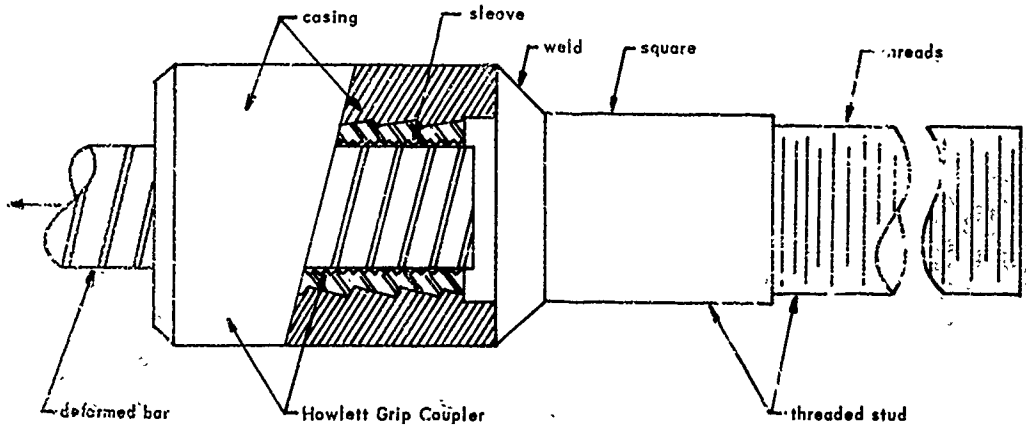

a) Gripping device

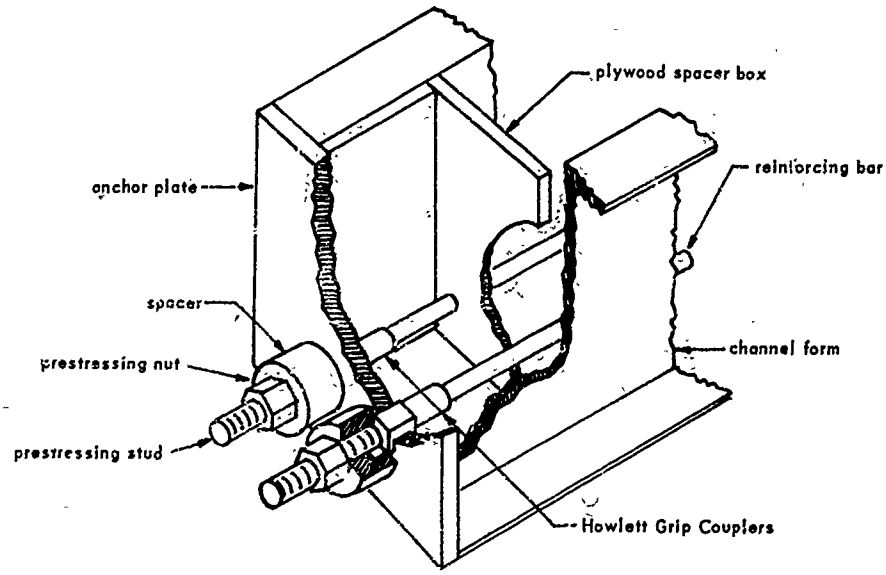

b) Anchorage assembly

Figure 13. Anchorage and gripping apparatus used to prestress bars.

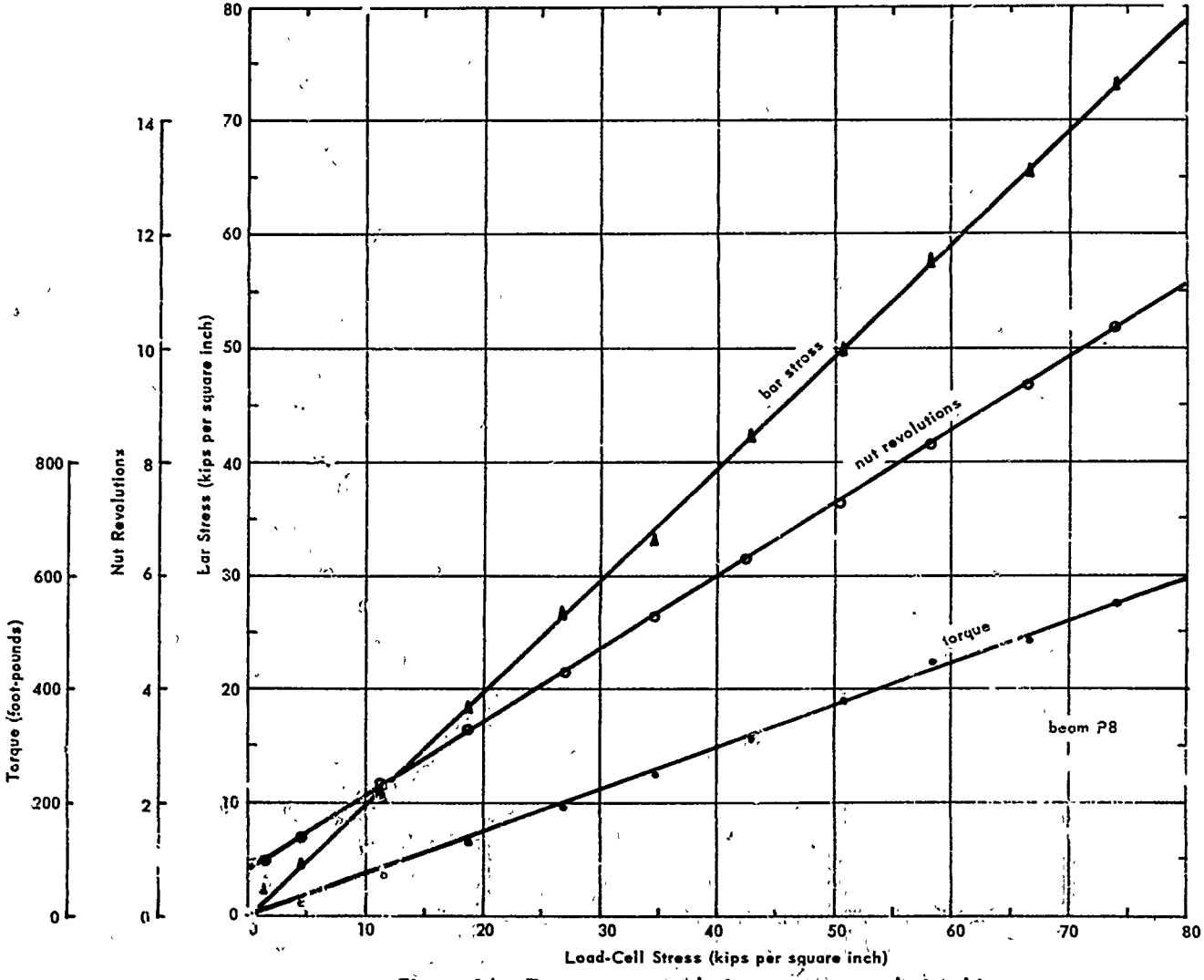

Figure 14. Torque–nut revolutions–prestress relationship.

The loss in prestress of each P/C beam was measured at periodic intervals between the time of casting and testing. The instantaneous losses at transfer were measured with strain gages mounted on the bar at mid-span. These losses agreed well with computed losses due to elastic shortening and bending. Estimates of the total loss in prestress were determined from strain-gage readings and measurements of the increase in mid-span deflection. A typical relationship between the prestress loss and time, for beams with an initial prestress of 90,000 psi and 45,000 psi, is shown in Figure 15.

Test Equipment

Loading Machine. The beams were tested in the NCEL blast simulator (Figure 16). A schematic of the beam in the simulator is shown in Figure 17. The simulator consists basically of a cylindrical pressure chamber to contain an air over-pressure and two parallel walls which extend vertically down from the bottom of the tank. These walls extend the full length of the cylinder and enclose the sides of the beam to contain the air over-pressure on the top surface of the member.

A uniformly distributed static or blast pressure may be applied over the top surface of a beam. A static pressure is achieved by introducing compressed air into the chamber. A blast pressure is generated by detonating explosives inside the chamber, and the peak pressure is controlled by the amount of explosive. The rate of decay and duration of the pressure is controlled by a series of valves which vent the chamber to the atmosphere.

Instrumentation. Pressure, acceleration, deflection, and strain at the locations shown in Figure 11 were recorded as a function of time. The applied pressure was measured by pressure transducers at three locations, two at the center and one at the end of the blast simulator, 1 inch above the top of the beam. The acceleration was measured with a 100-g accelerometer. The deflections at the quarter-points of the beam were measured by a linear potentiometer and a direct-recording rotating-drum deflection gage. The strain in the two tensile bars and the center compression bar was measured at mid-span by two A12, SR-4 strain gages placed diametrically opposite each other. This arrangement of gages permitted an accurate measurement of the force in the bars at large beam deflections. Strain in the top fiber of the concrete at mid-span was measured by an A9-2, SR-4 gage. The signal output from each transducer, except the rotating-drum deflection gages, was sent through a carrier amplifier and recorded by an oscillograph.

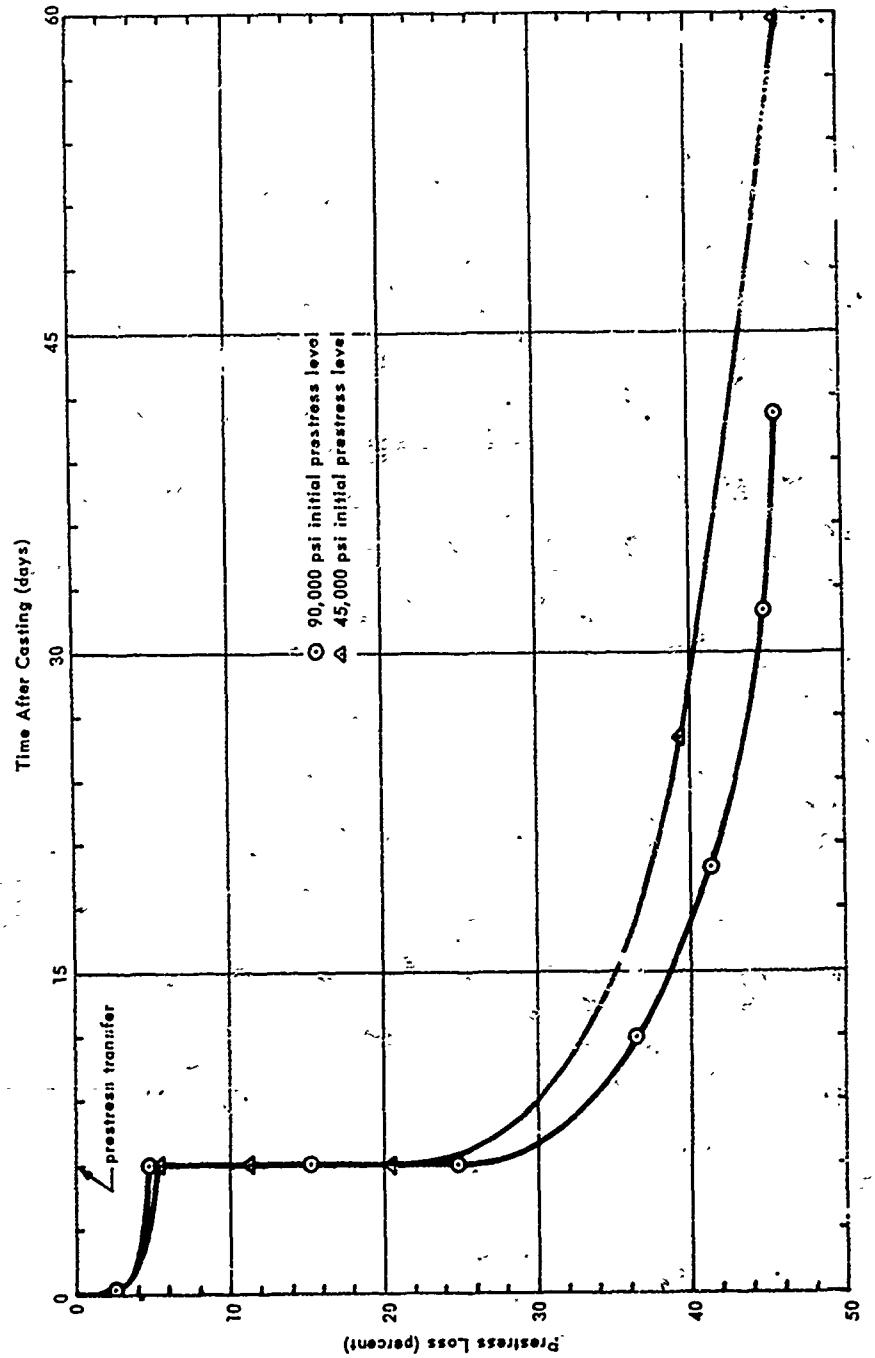

Figure 15. Curves of typical prestress loss versus time.

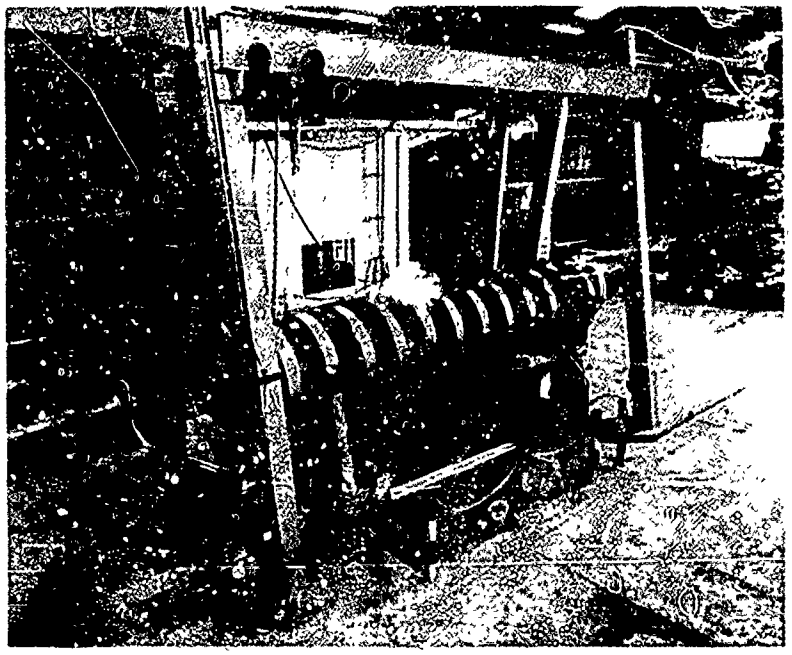

Figure 16. Blast simulator.

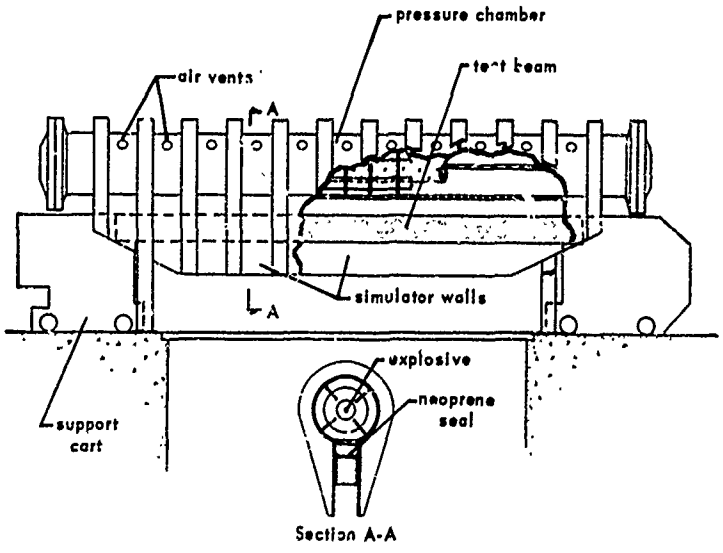

Figure 17. Schematic of beam in blast simulator.

Test Procedure

Preparation of a beam for a test was the same whether the test was static or dynamic. First, the beam was positioned on movable carts which served as end supports. A sheet of Teflon was then draped over the top and down the sides of the middle quarter of the beam. The Teflon was very effective in reducing frictional forces if the beam rubbed against the simulator walls. It also contained the crushed concrete at collapse of the beam. The whole unit was then rolled between the walls of the blast simulator, and the carts were anchored to the concrete foundation. Finally, all measuring instruments were fastened to the beam, all electrical connections were made, and a strip of neoprene was placed over the top of the beam to seal the chamber. A beam ready for testing is shown schematically in Figure 17.

Before testing, the natural period of vibration of several beams was measured by displacing the center of the beam upward with a wedged block and suddenly removing it. The induced free vibrations were measured by the strain gages and the deflection transducers and were recorded by the oscillograph. The natural period was measured with and without the Teflon seal in place and with the beam cracked and uncracked.

Static Tests. In the static tests the beams were uniformly loaded by introducing compressed air into the pressure chamber of the blast simulator. The pressure level was monitored from a master-control panel. The R/C beams were loaded up to the cracking load, unloaded, and then reloaded to failure. The P/C beams received only one cycle of loading. During loading, the pressure, deflections, and strains were recorded at regular intervals of pressure by the oscillograph up to the yield deflection. Thereafter, the oscillograph was operated continuously until the maximum resistance of the beam was overcome. The pressure on the beam was then released, and measurements of residual strains and deflections were taken.

Dynamic Tests. In the dynamic tests the beams were loaded by detonating an explosive charge in the pressure chamber. First, one channel of the electro-mechanical programmer was set to control the firing sequence and delay-time of the air vents. The amount of explosive charge required to obtain the desired peak pressure was then loaded into the pressure chamber. The blasting caps were inserted and wired to the master-control circuit. Next, a zero and calibration trace for each transducer were recorded by the oscillograph. Finally, a switch was closed which started the programmer which in turn started the recording equipment, automatically ignited the explosive charge, and controlled the air vents.

After the shot, the permanent strains and deflections were recorded, and the beam-cart assembly was rolled out of the simulator. The beam was inspected, crack patterns were recorded, and photographs taken. If the beam was not seriously damaged, it was rolled back into the simulator and the above procedure repeated.

Table III. Summary of Static-Test Results[1/]

Beam No.	Cracking		Yield		Ultimate			
	Load r_c (kips/ft)	Defl. y_c (in.)	Load r_y (kips/ft)	Defl. y_y (in.)	Load r_u (kips/ft)	Deflection (in.)		
						Mid-Span y_u	Quarter-Points	
							y_u	y_u
R1	—	—	2.35	1.60	2.72	3.92	2.55	2.55
R2	—	—	2.39	1.61	2.92	4.00	2.55	2.57
P1	1.16	0.25	2.36	1.11	2.80	—	—	—
P2	1.02	0.25	2.20	1.20	2.70	3.99	2.47	2.48
P8	1.30	0.30	2.28	0.80	2.86	3.93	2.46	2.47

1/ Values listed correspond to the straight-line approximation of the experimental load-deflection curves shown in Figures A1-A10 of Appendix A.

Test Results

Static Tests. Five beams were tested statically to failure to provide a comparison with similar beams tested dynamically. Beam R1 received two cycles of loading. It was loaded until sufficient cracking developed (approximately 0.5 kips per ft), unloaded, and then reloaded to failure. Beams R2, P2, and P8 received continuous loading to failure. Beam P1 received five cycles of loading. This test gave some measure of the resilience and load-deflection characteristics of the P/C beams under repeated loads.

The results of the static tests are plotted in Figures A1-A10 of Appendix A. These figures include load versus mid-span deflection and load versus steel and concrete strains. An idealization of the load-deflection curves as two straight lines is also shown.

The results of the static tests are summarized in Table III. The values given in Table III correspond to the idealization of the experimental load-deflection curve.

Photographs of the beams tested statically are shown in Figures C1 and C5.

Dynamic Tests. The results of the dynamic tests are presented in the form of tables, figures, and photographs. The load and response characteristics, maximum and permanent strains, damping characteristics, and dynamic yield resistance are summarized in Tables IVa, IVb, IVc, and V, respectively. Figures B1 and B2 (Appendix B) contain plots of effective peak load versus initial maximum deflection for the R/C and P/C beams, respectively. The deflected shape versus time for a beam which rebounded is shown in Figure B3. A damage curve for each type of beam is presented in Figures B4 and B5. Photographs showing the extent and distribution of cracking of each beam are included in Figures C2 through C5 (Appendix C). Typical oscillograms showing the time variation in the measured quantities are presented in Figures D1 through D3 (Appendix D).

Most of the tables and figures are self-explanatory. The logarithmic decrement and damping factor shown in Table IVc are based on the assumption of viscous damping. The values were obtained from the oscillograph traces by measuring successive peak amplitudes of free vibration A_n and A_{n+1} after the beam had reached its initial maximum displacement. Then the logarithmic decrement was computed from the following relationship:

$$\delta = \ln \frac{A_n}{A_{n+1}} \tag{14}$$

It was not possible to calculate the logarithmic decrement by considering the reduction in displacement amplitude over more than one cycle of oscillation because the free vibrations damped out so quickly.

The amplitudes of free vibration were very small for the beams which experienced large plastic deflections. Therefore, the logarithmic decrement was not measured for these beams because of the accuracy of the amplitude measurements.

Finally, the viscous damping factor was calculated from

$$\beta = \frac{\delta}{2\pi} \tag{15}$$

Table IVa. Results of Dynamic Tests — Load and Response Characteristics

Beam No.	Loading			Mid-Span Deflection					Strain [illegible] 2/	
	Peak B (kips/ft)	Duration		Max y_m (in.)	Accum. Perm. y_{ap} (in.)	Accum. Max y_{am} (in.)	Time to Max t_m (msec)	Damped 1/ Period T_{nd} (msec)	Tens. Steel ϵ_s (in./in./sec)	Comp. Steel ϵ'_s (in./in./sec)
		Effec. T_e (msec)	Actual T (msec)							
R3-1	0.64	230	850	0.40	0.03	0.40	25	52	—	—
R3-2	1.36	450	900	1.33	0.16	1.36	32	66	—	—
R3-3	1.89	330	1,030	2.04	0.66	2.20	37	64	0.20	0.03
R3-4	2.29	245	1,020	2.92	1.67	3.58	42	63	0.27	0.04
R3-5	2.24	260	1,100	2.81	2.42	4.48	39	70	—	0.04
R4-1	2.20	350	1,100	3.57	1.66	3.57	49	66	0.21	0.05
R5-1	1.22	250	1,140	1.15	0.23	1.15	33	60	—	—
R5-2	2.19	225	1,120	2.64	1.16	2.87	41	68	0.22	0.04
R5-3	2.16	270	1,100	2.90	2.07	4.06	40	72	—	0.04
R5-4	2.04	270	1,150	2.75	2.73	4.82	38	67	—	0.05
R6-1	2.44	290	1,120	3.74	1.85	3.74	48	61	0.24	0.04
R6-2	2.15	385	1,170	2.74	2.54	4.59	39	63	—	0.05
R7-1	1.21	100	140	0.92	0.16	0.92	30	63	—	—
R7-2	1.75	95	145	1.46	0.26	1.62	32	67	0.15	0.02
R7-3	2.42	90	145	2.45	0.96	2.71	36	73	0.18	0.07
R7-4	2.55	545	1,190	5.51	4.20	6.47	63	59	—	0.07
R8-1	1.84	85	140	1.66	0.23	1.66	35	70	0.15	0.03
R8-2	2.54	375	1,180	4.41	2.54	4.64	55	62	0.31	0.06
P3-1	0.52	830	1,010	0.22	0.00	0.22	19	40	—	—
P3-2	1.13	280	900	0.84	0.06	0.84	27	51	—	—
P3-3	1.76	250	920	1.57	0.32	1.63	33	63	0.17	0.06
P3-4	1.89	335	840	2.02	0.80	2.34	36	63	0.24	0.05
P3-5	2.85	545	940	7.46	5.85	8.26	83	—	—	0.07
P4-1	0.58	400	1,000	0.23	0.00	0.23	18	39	—	—
P4-2	0.51	225	900	0.18	0.00	0.18	17	40	—	—
P4-3	2.40	420	1,060	3.36	1.35	3.36	53	60	0.17	0.07
P4-4	2.46	270	1,040	3.91	3.34	5.46	52	66	—	0.07
P5-1	1.72	200	900	1.11	0.09	1.11	30	55	—	—
P5-2	2.18	285	930	2.32	0.81	2.41	40	64	0.18	0.06
P5-3	2.33	250	920	2.95	1.83	3.76	44	70	0.29	0.06
P5-4	2.28	270	940	3.11	2.88	4.94	45	58	—	0.06
P6-1	2.64	315	910	3.74	1.85	3.74	52	54	0.17	0.09
P6-2	2.30	210	920	2.74	2.54	4.59	38	69	—	0.05
P7-1	0.86	90	125	0.32	0.00	0.32	20	45	—	—
P7-2	1.92	85	140	1.14	0.03	1.14	30	58	—	—
P7-3	2.11	95	150	1.78	0.34	1.81	33	66	0.21	0.06
P7-4	2.37	825	1,000	4.00	2.34	4.34	56	—	—	0.07

1/ Value corresponds to the period of the beam oscillations at mid-span after initial maximum response.

2/ Values given only for tests where tension steel yielded and gages not damaged.

Table IVb. Results of Dynamic Tests — Maximum and Permanent Strains and Deflection

Beam No.	Deflection		Strain							
			Tension Steel				Comp. Steel		Concrete	
			Max		Perm.		Max	Perm.	Max	Perm.
	Max y_m (in.)	Perm. y_p (in.)	S1 (μin./in.)	S2 (μin./in.)	S1 (μin./in.)	32 (μin./in.)	S3 (μin./in.)	S3 (μin./in.)	C1 (μin./in.)	C1 (μin./in.)
R3-1	0.40	0.02	1,030	1,070	90	20	220	5	540	30
R3-2	1.33	0.13	2,840	2,920	200	140	550	10	1,440	35
R3-3	2.04	0.50	8,140	7,970	4,240	3,450	640	355	2,430	520
R3-4	2.92	1.01	7,970	8,140	3,610	2,100	660	500	2,900	500
R3-5	2.81	0.75	—	—	—	—	635	185	2,860	290
R4-1	3.57	1.66	12,800	12,300	8,120	7,850	865	125	3,280	940
R5-1	1.15	0.23	2,630	2,620	460	500	565	0	1,320	120
R5-2	2.64	0.93	10,800	10,200	6,440	5,880	815	465	3,070	845
R5-3	2.90	0.91	—	—	—	—	870	295	3,170	650
R5-4	2.75	0.66	—	—	—	—	970	—	3,160	—
R6-1	3.74	1.85	14,100	14,600	9,340	9,720	805	605	3,750	1,320
R6-2	2.74	0.69	—	—	—	—	1,020	350	2,750	—
R7-1	0.92	0.16	2,110	2,100	360	380	560	5	1,240	75
R7-2	1.46	0.10	6,440	6,210	2,540	2,350	905	55	2,120	45
R7-3	2.45	0.70	7,410	8,810	4,540	4,070	980	360	3,220	635
R7-4	5.51	3.24	—	—	—	—	—	—	3,580	—
R8-1	1.66	0.23	3,900	5,520	710	1,700	715	120	2,480	105
R8-2	4.41	1.71	17,200	16,900	12,400	11,900	975	290	3,840	—
P3-1	0.22	0.00	340	315	25	20	335	20	460	25
P3-2	0.84	0.06	2,000	1,990	145	140	825	30	1,330	70
P3-3	1.57	0.26	7,530	7,460	3,540	3,450	1,070	65	2,380	430
P3-4	2.02	0.48	6,190	6,380	1,950	2,100	990	160	2,550	320
P3-5	7.46	5.05	—	—	—	—	1,110	—	3,610	—
P4-1	0.23	0.00	410	400	50	50	390	15	415	70
P4-2	0.18	0.00	320	320	0	15	320	5	330	0
P4-3	3.36	1.55	13,400	12,800	8,730	8,390	1,120	270	2,090	1,030
P4-4	3.91	1.79	—	—	—	—	1,220	—	2,620	—
P5-1	1.11	0.09	2,380	2,360	170	185	925	50	1,520	70
P5-2	2.32	0.72	8,390	7,400	4,220	3,330	1,060	85	2,600	670
P5-3	2.95	1.02	8,560	8,220	3,770	3,470	1,040	260	2,750	465
P5-4	3.11	1.05	—	—	—	—	1,240	—	2,960	—
P6-1	3.74	1.85	13,700	15,100	8,810	10,300	1,020	510	3,930	1,360
P6-2	2.74	0.69	—	—	—	—	1,040	155	3,310	545
P7-1	0.32	0.00	880	860	70	75	500	30	745	20
P7-2	1.14	0.03	3,190	2,910	400	115	990	85	1,750	270
P7-3	1.78	0.31	8,380	8,470	—	3,680	1,140	25	2,950	335
P7-4	4.00	2.00	—	—	—	—	1,070	—	3,790	—

Table IVc. Results of Dynamic Tests — Damping Characteristics

Beam No.	Max Defl. y_m (in.)	Logarithmic Decrement, δ		Damping Factor, β		Damping Ratio[1] β_p/β_E	Remarks
		S1	BP2	S1 (%)	BP2 (%)		
R3-1	0.40		1.34		21		$y_m < y_y$ medium duration load
R3-2	1.13		1.13		18		
R5-1	1.15		1.22		20		
R7-1[2]	0.92		1.24		20		
R7-2[2,3]	1.46		0.95		15		$y_m \leq y_y$ short duration load
R8-1[2,3]	1.66		0.85		14		
P7-1[2,3]	0.32		0.88		14		
P7-2[2,3]	1.14		0.83		13		
P3-1	0.22	0.723	0.722	11	11		$y_m \leq y_c$ medium duration load
P4-1	0.23	0.595	0.615	10	10		
P4-2	0.18	0.612	0.674	10	11		
R3-3	2.04		1.56		25	1.25	
R3-4	2.92		1.57		25	1.25	
R3-5	2.81		1.67		27	1.35	
R4-1	3.57		1.70		27	1.35	
R5-2	2.64		1.65		26	1.30	$y_y \leq y_m \leq y_u$ medium duration load
R5-3	2.90		1.55		25	1.25	
P3-3	1.57		1.52		24	2.18	
P3-4	2.02		1.79		28	2.54	
P5-1	1.11		1.54		24	2.18	
P7-3[2,3]	1.78	—		—		—	
R3	0 psi[4]	0.146	0.191	3	3[5]		vibration test
R3	5 psi[4]	0.982	0.764	16	12[6]		
R3	0 psi[4]	0.352	0.392	6	6[6]		
R8-1[2]	0 psi[4]	0.385	0.356	6	6[6]		
P3	0 psi[4]	0.182	0.248	3	4[5]		

1/ Based on β_E = 20 percent for R/C beams and β_E = 11 percent for P/C beams.

2/ No seal, short duration load.

3/ Beam rebounded.

4/ Static pressure on beam during vibration test.

5/ Uncracked.

6/ Cracked.

Table V. Measured Increase in Yield Resistance

Beam No.	Strain Rate $\dot{\epsilon}$ (in./in./sec)	Strain		Deflection		Reference 6 Increase in Yield Stress $(f_{yd} - f_y)/f_y$ (%)
		Dynamic[1] Yield Strain ϵ_{yd} (μin./in.)	Increase[2] in Yield Strain $(\epsilon_{yd} - \epsilon_y)/\epsilon_y$ (%)	Dynamic[3] Yield Defl. y_{yd} (in.)	Increase[4] in Yield Defl. $(y_{yd} - y_y)/y_y$ (%)	
P3-3	0.17	3,880	21	1.29	12	11
P4-3	0.17	3,730	16	1.31	14	11
P5-2	0.18	4,050	26	1.38	20	11
P6-1	0.17	3,960	24	1.36	18	11
R4-1	0.22	4,100	28	1.99	25	12
R5-2	0.22	3,900	22	1.65	3	12
R6-1	0.24	3,760	18	1.89	18	13
R7-2	0.15	3,750	17	1.53	0	10

1/ ϵ_{yd} = elastic strain in tension steel prior to test plus measured strain to yield.

2/ Based on a static yield strain of 3,200 μin./in. (see Figure 12).

3/ y_{yd} = mid-span deflection at first yielding of tension steel.

4/ Based on a static yield deflection of 1.60 in. for R/C beams, 1.15 in. for P/C beams.

THEORY VERSUS EXPERIMENTAL RESULTS

Static Tests

The accuracy of a dynamic analysis depends to a large degree on how well the shape of the static resistance diagram (load-deflection curve) of a beam can be predicted. Therefore, a theoretical analysis was made of those beams which were tested statically. The material properties listed in Table II and VI were used in the theoretical calculations. Computations were made of the load and deflection corresponding to initial yielding of the tensile steel and ultimate collapse of the beams. The load corresponding to first cracking of the concrete was also computed. The results of the theoretical analysis and a comparison with the experimental values (Table III) are summarized in Table VI.

Table VI. Comparison Between Experimental and Calculated Static Results[1/]

Beam No.	f_{se} (ksi)	f_y (ksi)	Cracking		Yield				Ultimate						
			r_c (kips/ft)	Exp./Calc.	r_y (kips/ft)	Exp./Calc.	y_y (in.)	Exp./Calc.	r_u (kips/ft)	Exp./Calc.	y_u (in.)	Exp./Calc.	y_u (1/4-pt.) (in.)	Exp./Calc.	q
R1	0	91.3	—	—	2.17	1.08	1.47	1.08	2.60	1.04	4.02	0.98	2.61	0.98	0.139
R2	0	92.1	—	—	2.18	1.09	1.50	1.07	2.59	1.12	4.04	0.99	2.62	0.98	0.146
P1	28.5	93.0	0.82	1.41	2.20	1.07	1.06	1.04	2.61	1.07	3.81	—	2.37	—	0.145
P2	23.4	89.5	0.73	1.40	2.12	1.03	1.09	1.08	2.63	1.03	4.26	0.94	2.74	0.91	0.144
P8	41.4	92.4	1.05	1.24	2.19	1.04	0.83	0.97	2.62	1.09	3.84	1.02	2.41	1.02	0.156

1/ The experimental values are listed in Table III. Calculated values are based on f_t, E_c, and f'_c listed in Table II.

The procedure used to calculate the various loads and deflections is outlined in the following sections.

Cracking Load. The cracking load for the P/C beams is given by

$$r_{cr} = \frac{8}{L^2}\left[f_{se}A_s\left(d - k'd\right) + \frac{f_{se}A_s I}{bd\,(h - k'd)} + \frac{f_t I}{h - k'd}\right] \tag{16}$$

where $I = (1/12)bh^3 + (n-1)A_s(d - kd)^2 + (n-1)A_s'(kd - d')^2$ (16a)

$$k'd = [h^2(b/2) + A_s'(n-1)d' + A_s d(n-1)]/[(n-1)(A_s + A_s') + hb] \tag{16b}$$

Yield Load and Deflection. With reference to Figure 9, the yield load is given by

$$r_y = \frac{8}{L^2}\left[A_s d f_y\left(1 - \frac{k}{3}\right) + A_s' f_s' d\left(\frac{k}{3} - \frac{d'}{d}\right)\right] \tag{17}$$

where $k = \sqrt{2n[p + p'(d'/d)] + n^2(p + p')^2} - n(p + p')$ (17a)

$$f_s' = \{[k - (d'/d)]/(1 - k)\}(f_y - f_{se}) \tag{17b}$$

The yield deflection is given by Equations 13a and 13c and is repeated here for completeness.

$$y_y = \left(\frac{5}{48}\right)\omega_y L^2 \tag{13a}$$

$$\omega_y = \frac{f_y - f_{se}}{E_s d\,(1 - k)} \qquad f_{se} = 0 \text{ for R/C beams} \tag{13c}$$

Ultimate Load and Deflection. The ultimate load capacity of all beams was computed from the following equation:

$$r_u = \frac{8}{L^2}\left\{A_s f_{su} d\left[1 - \left(\frac{k_2}{k_1 k_3}\right)q\right] + A_s' f_{su}' d\left[\left(\frac{k_2}{k_1 k_3}\right)q - \frac{d'}{d}\right]\right\} \tag{18}$$

Equation 3 was used to compute k_1k_3. The value of k_2 was taken from Reference 4 as

$$k_2 = 0.50 - \frac{f'_c}{80,000} \tag{18a}$$

By a process of iteration, f_{su}, f'_{su}, and q were determined from the following equations and Figure 12.

$$\epsilon_{su} = F\epsilon_u\left(\frac{k_1k_3}{q} - 1\right) + \epsilon_{se} \tag{18b}$$

$$f'_{su} = E_s\epsilon_u\left[1 - \left(\frac{d'}{d}\right)\frac{k_1k_3}{q}\right] \tag{18c}$$

$$q = \frac{pf_{su} - p'f'_{su}}{f'_c} \tag{18d}$$

The value of ϵ_u was taken from Figures A1-A10. The compatability factor, F, was assumed equal to unity (e.g., good bond). The iteration procedure involved the following steps: (1) A reasonable value of q was assumed (for the first assumption, q was computed from Equation 18d by assuming that $f_{su} = f_y$ and $f'_{su} = f'_y$); (2) This value was substituted in Equation 18b and 18c to determine ϵ_{su} and f'_{su}; (3) Knowing ϵ_{su}, f_{su} was determined from Figure 12; (4) Finally, q was calculated from Equation 18d and compared with the assumed value. If the assumed and computed value of q were not the same, the procedure was repeated using the computed value for the next trial. The procedure was found to converge in two to three trials.

The ultimate or collapse deflection can be computed if the relation between moment and rotation and the distribution of moment along the length of the beam are known.[12] A typical relation between moment and rotation for a section of a concrete beam is shown in Figure 18a. The values of ϕ_y, M_y, and M_u were computed with the use of Equations 13c, 17, and 18, respectively.

The relationship for ϕ_u was determined from the strain distribution over the beam cross section at ultimate-moment capacity. With reference to Figure 2 or Figure 4,

$$\varphi_u = \frac{\epsilon_u}{a_u} \tag{19a}$$

Combining Equation 19a with Equations 9b and 18d,

$$\varphi_u = \frac{\epsilon_u k_1 k_3}{qd} \tag{19b}$$

The distribution of moment at ultimate-load capacity along the length of a simply supported beam under a uniform load is shown in Figure 18b. The length of the yield hinge, αL, is given by[13]

$$\alpha L = \sqrt{1 - \frac{r_y}{r_u}} \tag{19c}$$

The distribution of curvature along a simply supported beam under a uniformly distributed ultimate load (Figure 19) is found by combining the diagrams shown in Figure 18. For the distribution of curvature shown in Figure 19, the mid-span deflection at ultimate-load capacity is

$$y_u = \frac{L^2}{120}\left[\varphi_y(10 - 14\alpha + 5\alpha^2) + \varphi_u(24\alpha - 10\alpha^2)\right] \tag{19}$$

and the deflection at the quarter-span is

$$y_u = \frac{L^2}{80}\left\{5\varphi_y\left[1 - \frac{1}{12(1-\alpha)}\right] + \alpha\left(8\varphi_u - 3\varphi_y\right)\right\} \tag{20}$$

Two simplifying assumptions were made in Figure 19: (1) The shape of the curvature diagram in the outer portions of the beam where $M < M_y$ has little influence on the mid-span deflection.[12] Therefore, the actual parabolic distribution of curvature can be replaced by a straight line; (2) The shape of the curvature diagram in the plastic yield range, αL, can be adequately described by a 4th-degree parabola. This shape was found to give the best agreement between the experimental and calculated ultimate deflection at both the mid-point and quarter-point of the span. Other shapes predicted the ultimate deflection at mid-span but not at the quarter-point of the span.

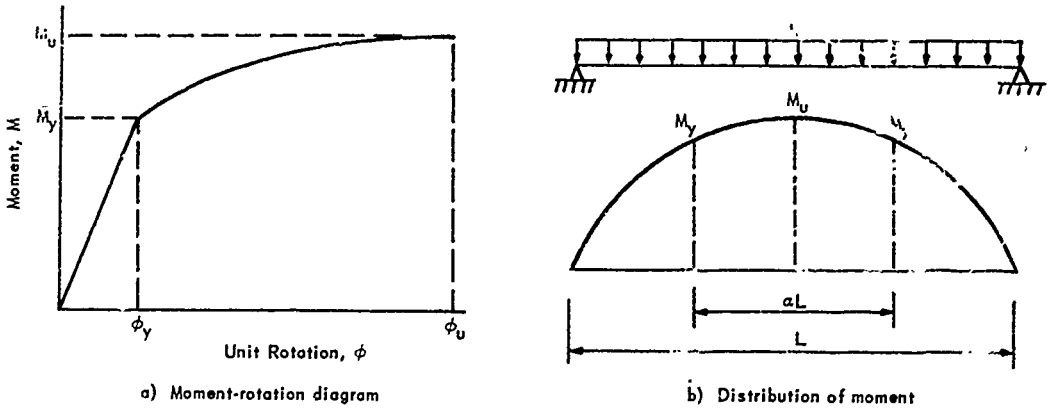

Figure 18 Moment-rotation diagram and distribution of moment.

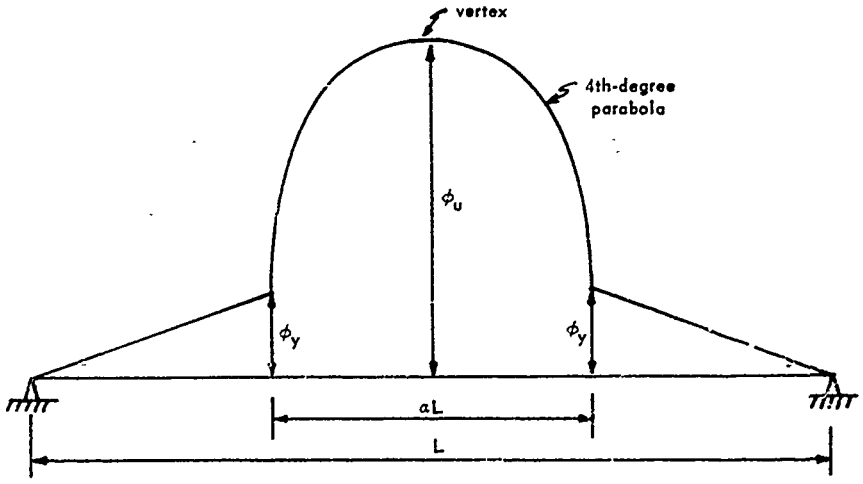

Figure 19. Distribution of curvature for a simple beam at ultimate load.

The effective prestrain in the concrete, ϵ_{ce}, was neglected in the theoretical analysis of the P/C beams. This simplifies the analysis and does not introduce significant inaccuracies since ϵ_{ce} is very small compared to the crushing strain of the concrete.

Dynamic Tests

The effect of viscous damping on beam response can be derived from a linear single-degree-of-freedom system with a viscous damper in parallel with a spring. The motion of the mass in the elastic range [$y(t) \leq y_y$] when subjected to a peak-triangular load pulse is

$$\frac{y(t)}{y_s} = 1 - \frac{t}{T_e} + \frac{2\beta}{\omega T_e} + e^{-\beta\omega t}\left[\frac{1}{\omega\sqrt{1-\beta^2}}\left(\frac{1}{T_e} - \beta\omega - \frac{2\beta^2}{T_e}\right)\sin\left(\omega\sqrt{1-\beta^2}\,t\right)\right.$$

$$\left. - \left(1 + \frac{2\beta}{\omega T_e}\right)\cos\left(\omega\sqrt{1-\beta^2}\,t\right)\right] \qquad (21a)$$

A close approximation for the time, t_m, when the mass will reach its initial maximum deflection is

$$t_m = \frac{T_{nd}}{2} \qquad (21b)$$

By combining the above equations and assuming that $T_n = T_{nd}$ (i.e., $\sqrt{1-\beta^2} \cong 1$), the dynamic load factor, D.L.F., can be expressed as follows if $y_m < y_y$ and $t_m < T_e$:

$$\text{D.L.F.} = 1 - \frac{T_{nd}}{2T_e} + \frac{\beta T_{nd}}{\pi T_e} + e^{-\beta\pi}\left(1 + \frac{\beta T_{nd}}{\pi T_e}\right) \qquad (21c)$$

Then the maximum dynamic deflection is

$$y_m = \text{D.L.F.}\left(\frac{B}{K}\right) \qquad (21)$$

The maximum dynamic deflection of the beams was computed from Equations 21c and 21. The results are compared with the experimental values in Table VII.

Table VII. Comparison Between Experimental and Calculated Maximum Dynamic Deflection

Beam No.	Experimental Parameters				Cal. Max Dyn. Defl.[3]			Exp.[1] Max Defl. y_m (in.)
	Effect.[1] Peak Load B (kips/ft)	Damp.[1] Factor β (%)	Beam[2] Stiffness K (kips/ft/in.)	T_e/T_{nd}[1]	Equiv. Static Defl. $y_s = B/K$ (in.)	Load Factor y_m/y_s	Max Defl. y_m (in.)	
R3-1	0.64	21	1.48	4.43	0.43	1.43	0.61	0.40
R3-2	1.36	18	1.48	6.81	0.92	1.51	1.39	1.33
R5-1	1.22	20	1.48	4.17	0.83	1.44	1.19	1.15
R7-1	1.21	20	1.48	1.62	0.82	1.28	1.05	0.92
R7-2	1.75	15	1.48	1.50	1.18	1.34	1.58	1.46
R8-1	1.84	14	1.48	1.21	1.24	1.29	1.61	1.66
P3-1	0.52	11	4.40	20.70	0.12	1.69	0.20	0.22
P4-1	0.58	10	4.40	10.30	0.13	1.69	0.22	0.23
P4-2	0.51	11	4.40	5.62	0.12	1.63	0.19	0.18
P7-1	0.86	14	4.40	2.02	0.20	1.43	0.28	0.32
P7-2	1.92	13	2.62[4]	1.46	0.73	1.37	1.00	1.14

1/ Values taken from Table IVa.

2/ Average stiffness computed from static tests (see Figure 20).

3/ From Equation 21 and 21c.

4/ The effective "elastic" stiffness found by balancing areas under resistance diagram up to y_m.

Beam No.	Variable								
	f_y (ksi)	f_{se}(ksi)	p (%)	p' (%)	q	d (in.)	b (in.)	d' (in.)	L (in.)
①	92	41	1.14	0.43	0.156	10.0	7.75	1.50	174
②	92	0	1.14	0.43	0.142	10.0	7.75	1.50	174
③	92	25	1.14	0.43	0.144	10.0	7.75	1.50	174
④	49	0	1.55	0.47	0.129	10.6	8.00	1.00	174

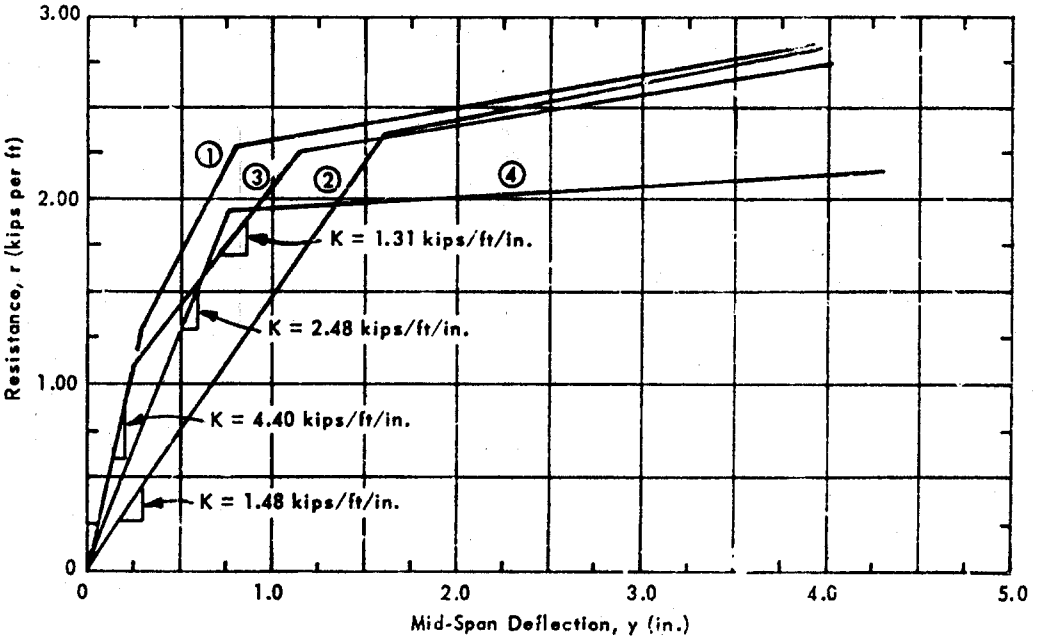

Figure 20. Idealized resistance diagram for four types of beams.

DISCUSSION

Static Tests

The individual and relative static behavior of the R/C and P/C beams was observed in terms of the shape of the resistance diagram, service load deflection, ultimate-load capacity, ultimate deflection, bond strength, and crack patte. Much of this information is summarized in Figure 20 which shows the idealized resistance diagram for the two types of P/C beams and the R/C beams. The curves were plotted from the average values listed in Table III. Also included in Figure 20 is the idealized resistance diagram obtained from tests of uniformly loaded R/C beams reinforced with intermediate-grade steel.[2] This curve provides an interesting comparison between the behavior of R/C beams reinforced with different grades of steel.

Shape of Resistance Diagram. In the stage below cracking, both beams exhibited a linear relationship between load and deflection. First cracking of the concrete in the P/C beams occurred at a considerably higher load and smaller deflection because of the action of the prestress. Thus, the high-strength bars in the P/C beams were more efficiently utilized. It is interesting to note that almost doubling the effective prestress only increased the cracking load about 18 percent (Figure 20).

After first cracking, the stiffness of both beams was gradually reduced until the fully cracked section was developed. Beyond this stage of loading, the post-cracking stiffness of both beams was approximately the same until the yield stress of the tension steel was exceeded.

The yield resistance of each type of beam was approximately the same, but the yield deflection of the P/C beams was considerably less, depending upon the effective prestress level. By developing an effective prestress of 41,000 psi, the yield deflection was reduced by 50 percent (see Figure 20). Thus the useful energy-absorbing capacity was higher in the inelastic range for the P/C beams than for the R/C beams.

Beyond the point of first yielding, the load increased only slightly, as deflection increased, until the point of ultimate load was reached. The ultimate-load and collapse deflection of both types of beams were approximately the same. In other words, the effect of prestress on the ultimate-load and deflection capacity was negligible. All beams failed in flexure, and failure was gradual and gentle.

Design-Load Deflections. It was previously shown in the discussion on cracks and deflections that the feasibility of using high-strength reinforcing bars in blast-resistant design may depend upon the deflection criterion established for static service

loads. Whether a given beam would meet this deflection criterion was found to depend upon the ratio between the yield resistance required to resist the impulsed blast loading and the static service load. These parameters were found to be related by Equation 13 and were plotted in Figure 10. In the following, Figure 10 is compared with experimental data. From Figure 20 for beam No. 2

$$p = 1.14\%,\ f_y = 92 \text{ ksi},\ r_y = 2.37 \text{ kips/ft},\ \frac{L}{d} = \frac{14.5 \times 12}{10} = 17.4$$

From Figure 10, to limit the static deflections to L/360 requires that

$$\text{M.L.F.} = 2.8, \text{ for } \frac{L}{d} = 15 \text{ and } f_y = 90 \text{ ksi}$$

Therefore, for beam No. 2 in Figure 20

$$\text{M.L.F.} = 2.8\left(\frac{17.4}{15}\right)\frac{92}{90} = 3.32$$

Thus, to limit the mid-span deflection to less than L/360, the static service load must not exceed

$$w_s = \frac{r_y}{\text{M.L.F.}} = \frac{2.37}{3.32} = 0.71 \text{ kips/ft}$$

From Figure 20, at $w_s = 0.71$ kips/ft

$$y_s = \frac{w_s}{K} = \frac{0.71}{1.48} = 0.48 \text{ inches}$$

which agrees well with the deflection criterion of

$$\frac{L}{360} = \frac{174}{360} = 0.48 \text{ inches}$$

Thus, assuming that the resistance diagram shown in Figure 20 (beam No. 2) has the proper strength and ductility to resist the imposed blast load, the design is sufficient if the anticipated static service loads will be less than w_s. If not, the tension steel must be prestressed or more steel and/or a deeper beam section used.

Repeating the same procedure for the beam reinforced with intermediate-grade steel (beam No. 4, Figure 20),

$$p = 1.55\%,\ f_y = 49 \text{ ksi},\ r_y = 1.96 \text{ kips/ft},\ \frac{L}{d} = \frac{14.5 \times 12}{10.5} = 16.6$$

From Figure 10,

$$\text{M.L.F.} = 1.34, \text{ for } \frac{L}{d} = 15 \text{ and } f_y = 40 \text{ ksi}$$

Therefore for beam No. 4,

$$\text{M.L.F.} = 1.34\left(\frac{16.4}{15}\right)\frac{49}{40} = 1.82$$

Thus,

$$w_s = \frac{r_y}{1.82} = \frac{1.96}{1.82} = 1.08 \text{ kips/ft} \left(\text{maximum allowable for } y_s < \frac{L}{360}\right)$$

From Figure 20, at $w_s = 1.08$ kips/ft,

$$y_s = \frac{w_s}{K} = \frac{1.08}{2.48} = 0.44 \text{ inches}$$

which agrees with the deflection criterion of

$$\frac{L}{360} = \frac{174}{360} = 0.48 \text{ inches}$$

It was assumed in the previous calculations that the deflection criterion was L/360. However, as shown by Equation 13, the designer may compute the minimum yield-load factor or maximum-allowable static service load for any other deflection criterion by direct proportion.

Ultimate-Load Capacity. All beams failed by initial yielding of the tension steel followed by eventual crushing of the concrete in compression. The concrete crushed at an average limiting strain of 0.004 in./in. In some of the tests, greatest destruction of the concrete occurred either to the left or right of mid-span where the spacing of the ties was greatest. This behavior supports the requirement that the compression steel be well tied with closely spaced ties in regions of high moment. This will reduce the effective buckling length of the compression steel and contain the concrete at collapse of the beam.

The maximum stress developed in the tension steel (108,000 psi) was approximately the same for the P/C and R/C beams. This is to be expected since the strains were in the inelastic region of the stress-strain curve (Figure 12). In this region there is little change in stress for large variations in strain. The measured maximum steel strains at collapse (1.35 to 1.50 percent) shown in Appendix A agree reasonably well with the values predicted by Figure 8 if the computed reinforcing index (0.14 to 0.16) given in Table VI is used. The maximum stress in the compression steel was generally reached at first yielding of the tension steel and remained fairly constant until the concrete crushed in compression. The maximum stress in the compression steel (Figures A1-A10) compares well with the values predicted from Figure 6.

The ultimate-load capacity of each type of beam was predicted with reasonable accuracy by the ultimate-strength theory (see Table VI for values). Evidently, the classical assumptions used in the ultimate-strength theory for the analysis of flexural failures can be satisfactorily applied to beams reinforced with high-strength steels.

Figure 20 shows an interesting comparison between the ultimate strength of R/C beams reinforced with different grades of steel. Approximately 32.5 percent more resistance was gained with 36.0 percent less high-strength steel.

It is commonly assumed that the effectiveness of reinforcement in strengthening a concrete member is almost proportional to the product of bar area and yield stress, $A_s f_y$. The accuracy of this assumption can be demonstrated by comparing beams No. 2 and 4 shown in Figure 20. The ratio of high-strength to intermediate-grade steel necessary to produce the relative ultimate resistance of these two R/C beams was

$$\frac{A_s^H}{A_s^I} = \frac{\text{area of high-strength steel}}{\text{area of intermediate-grade steel}} = \frac{0.88}{1.32} = 0.67, \text{ for } \frac{r_u^H}{r_u^I} = \frac{2.82}{2.18} = 1.29$$

Theoretically, to develop the same relative resistance, the ratio should be

$$\frac{A_s^H}{A_s^l} = \frac{r_u^H}{r_u^l}\left(\frac{f_y^l}{f_y^H}\right) = \frac{2.82}{2.18}\left(\frac{49,000}{92,000}\right) = 0.69$$

Therefore, the accuracy of this assumption, as demonstrated above, permits economies of high-strength steels to be compared in terms of costs per ton per psi yield stress. This comparison was made and it was found that the relative reinforcement cost per kip of load-carrying capacity for a 90,000-psi-yield-point steel is 58 percent of that for intermediate-grade steel.[14]

Ultimate Deflection. The ultimate deflection of the R/C and P/C beams was approximately the same, regardless of the level of prestress (Figure 20). The measured ultimate deflection at the mid-span and quarter-span of the beam compared well with the values predicted by Equations 19 and 20, as shown in Table VI.

Equations 19 and 19b lead to some interesting conclusions concerning the ultimate deflection of uniformly loaded R/C and P/C beams. The ultimate deflection increases with a decrease in the reinforcing index, q. Therefore, lowering the reinforcing index will not only assure "under-reinforced" beam behavior but will increase the deflecting capacity of beams. This point is demonstrated in Figure 20; beam No. 4 with the smallest q had the largest ductility and beam No. 1 with the largest q had the smallest ductility. The reinforcing index may be lowered and proper amounts of ductility "built into" beams by adding sufficient quantities of compression steel, as shown by Equation 1.

A major contributor to ultimate deflections of beams is the rotation of the beam within the length of the yield hinge (see Figure 19). Greater hinge lengths will produce greater ultimate deflections. The length of the yield hinge, αL, increases with an increase in the ratio of the ultimate to yield resistance, r_u/r_y, of beams. This ratio, in turn, will depend primarily on the stress-strain characteristics of the tensile reinforcement. The ratio will be small for reinforcement having "flat-top" stress-strain characteristics, as demonstrated by the resistance diagram of beam No. 4 (Figure 19). It follows, therefore, that the length of the yield hinge will be relatively short for this case. The ratio r_u/r_y will be larger if tension reinforcement has limited "flat-top" stress-strain characteristics, similar to that used in this investigation (see Figure 20, beams No. 1, 2, and 3). For this case, the unit rotational capacity of the beam may be less than for a "flat-top" steel, but the yield

hinge will be considerably longer. Thus a steel with limited "flat-top" stress-strain characteristics could develop ultimate deflections comparable with those obtained with mild-steel reinforcement. The relative importance of each of these variables deserves further study.

Bond and Cracks. The bond strength of the bars was sufficient to develop tensile steel stresses as high as 108,000 psi at mid-span. Even at these high stresses, the cracks along the span were uniform and closely spaced (see Figures C1-C5), indicating that the bond between the steel and concrete was not severely affected.

Care must be exercised in comparing the crack distribution of the beams shown in Appendix C since some of the beams experienced maximum dynamic deflections far in excess of the static collapse deflection (see y_{am} in Table IVa). However, in general, cracking in the P/C beams was less severe than in the R/C beams, as would be expected.

The height of the flexural cracks indicates that the yield hinge extended over a considerable portion of the span. Based on Equation 19c, the average length of the yield hinge for both the P/C and R/C beams was 69 inches or 40 percent of the span. This is approximately the hinge length indicated by the crack distribution shown in Appendix C, particularly for the beams which experienced cumulative maximum deflections not too much greater than the collapse deflection.

Dynamic Tests

The individual and relative dynamic performance of the two types of beams was observed in terms of maximum response, rebound and damping characteristics, resilience, and multiple-shot damage. Each of these phenomena are discussed in the following paragraphs.

Maximum Response. For a given load, the R/C and P/C beams experienced larger deflections when loaded dynamically (see Figures B1 and B2). The maximum dynamic deflections were greatest for the R/C beams. However, the ratio of the dynamic to static deflections (D. L. F.) was greater for the P/C beams for a given medium-duration load level. This phenomena is attributed to the smaller natural period and, therefore, greater ratio (T/T_e) of effective load duration to natural period for the P/C beams.

The maximum dynamic load-carrying capacity of both types of beams was approximately the same. This is to be expected since most of the experimental points in Figure B2 near the collapse deflection correspond to P/C beams which had lost their effective prestress from large deflections in previous tests. Having lost their effective prestress, the P/C beams had approximately the same stiffness and energy-absorbing capacity as the R/C beams. Therefore, the dynamic response of such a P/C beam should be similar to the response of the R/C beams.

Under a short-duration load both beams experienced maximum dynamic deflections which were considerably less than the corresponding deflections produced by the same load level of medium duration (Figures B1 and B2).

Table VII shows that the elastic response of both types of beams can be predicted by assuming a spring-mass system if the proper amount of viscous damping is considered. The excellent agreement between the experimental and theoretical results shown in Table VII suggests that: (1) damping in stressed concrete can be adequately represented by viscous damping, (2) the beam experiences the same amount of damping before and after the time of initial maximum response, therefore, (3) the amount of damping can be measured by the rate of decay in the free beam oscillations after initial maximum response, and (4) the elastic stiffness of a concrete beam does not increase under dynamic loads.

Rebound. None of the beams rebounded under a medium-duration load. The short-duration loads caused beams of both types to rebound (rise) off their simple supports. Figure B3 shows the extent of rebound for a P/C beam. The negative deflections were as large as 1/4 inch and 1/2 inch at the mid-span and supports, respectively.

The probability of a beam rebounding under dynamic loads appeared to be primarily a function of the amount of damping and the ratio of effective load duration to natural period, T_e/T_n. The beams rebounded under load durations as high as $T_e/T_n = 1.7$ when the viscous damping factor, β, was less than 15 percent. In comparison, beam R7-1 which had an effective load duration of $T_e/T_n = 1.4$ but a damping factor of 20 percent did not rebound. This comparison shows that the probability of rebound depends not only on the ratio of effective load duration to natural period but also the amount of damping. This conclusion supports the findings of other investigators.[15]

Damping. The damping capacity of materials is an important property in an engineering analysis or design involving the dynamic response of a structural system. Large amounts of damping can be important in controlling excessive vibrations from vibrating machinery or in controlling the response of a structural member subjected to a blast load or an earthquake. Small amounts of damping are important in that it increases the probability of a beam rebounding (deflecting in a negative direction) under short-duration blast loads.[15]

The effects of damping on the dynamic response of a structural system are generally accounted for by assuming viscous-type damping. The classical assumption is that the actual (non-linear) system can be approximated by a linear system with viscous-type damping where the damping force is proportional to velocity. However,

some investigators indicate that damping is often greatly affected by amplitude of stress.[15,16] In any case, knowledge of the mechanism of damping and the parameters which influence it, as applied to structural systems such as concrete beams, is meager and deserves further study.

Measurements of damping may vary widely depending upon the material, method of measurement, and the test procedure. Therefore, measurements should be taken under circumstances which closely resemble those for which the information is needed. In this respect, it could be expected that the values of damping listed in Table IVc are representative of the amount of damping experienced by beams under blast loading. However, caution must be exercised because large amounts of damping may be attributed to the support conditions, seal friction, and/or friction from the beam rubbing against the simulator walls.

The measured damping factor, β, was unusually high, particularly for the R/C beams, and the spread is large. The damping factor ranged between 10 and 28 percent (Table IVc). Under medium-duration loads the elastic damping factor for the R/C beams (20 percent) was almost twice as great as for the P/C beams (11 percent). Also, the damping factor increased as the load duration increased for the R/C beams. Whether this phenomenon is due to the higher average stress at which the beam vibrated when under the medium-duration load deserves further study. The largest damping factor for both types of beams (24 to 28 percent) was measured when the maximum dynamic deflection was in the plastic range of response; i.e., $y_m > y_y$.

The effects of concrete cracking, stress level, and the neoprene seal on the damping factor are further illustrated by the results of the vibration tests (Table IVc). Beams R3 (test 1) and P3, both uncracked and with the neoprene seal over each, had approximately the same damping factor of 3 percent. However, beams R3 (test 3) and R8-1, both cracked and with the seal only over beam R8-1, had the same damping factor of 6 percent. Comparison of these beams suggests that the seal had only a minor influence on damping, and that damping increases with the degree of cracking. The effect of stress level on damping is illustrated by the results of the vibration test on beam R3 (test 2). The damping factor almost quadrupled when the beam was vibrated under a static pressure of 5 psi. Apparently, concrete damping increases because stress level and degree of cracking cause increased dissipation of energy.

Resilience and Multiple-Shot Damage. Resilience and multiple-shot damage are interrelated. A beam which exhibits a very high capacity for recovery, even at deflections near incipient collapse, can absorb approximately the same amount of energy, regardless of how many times it is loaded.[14] The resilience and multiple-shot damage of the R/C and P/C beams are illustrated in Figures B4 and B5, respectively. Complete damage is arbitrarily defined by crushing of the concrete in compression and corresponds to a limiting cumulative maximum deflection, y_{am}, of 4.0 inches.

To illustrate the use of the damage curves, consider the curve for the P/C beams (Figure B5). The curves indicate that if the first "shot" on the P/C beam is a medium-duration load with a peak load of 2.00 kips/ft (indicated by an arrow in the figure), the post-shot deflection will be about 10 percent of the collapse deflection. Therefore, if complete damage (100 percent) of the P/C beam were desired on the second "shot," the maximum deflection would have to be 100 percent minus 10 percent — or 90 percent of the collapse deflection. Figure B5 shows that the medium-duration load corresponding to a maximum deflection of 90 percent of collapse is 2.48 kips/ft.

It is interesting to note from Figure B5 that regardless of the number of "shots" with a peak load less than about 1.4 kips/ft, the P/C beams will have no permanent damage. In comparison, Figure B4 indicates that for peak loads less than about 0.5 kips/ft, the R/C beams will have no permanent damage.

The resilience of a beam is related to its ductility. Each of these factors, in turn, is dependent upon the magnitude of the prestress, the reinforcing index, and the stress-strain characteristics of the reinforcing steel. Beam tests indicate that one of the main advantages of using P/C beams in blast-resistant structures is a high capacity for recovery, with 85- to 90-percent recoverability at incipient collapse.[15] Other beam tests indicate that P/C beams exhibit considerable capacity for recovery, whereas R/C beams have little capacity for recovery but a high capacity for absorbing energy by permanent deformation.[17] The author feels that P/C beams generally exhibit greater recoverability and less ductility than R/C beams not only because of the action of the prestress but also because the stress-strain characteristics of the reinforcement and the magnitude of the reinforcing index for the two types of concrete beams are generally different. The relative importance of each of these variables on the resilience and ductility of a concrete beam deserves further study.

FINDINGS AND CONCLUSIONS

Caution should be exercised in applying the following findings and conclusions to P/C beams in general because the level of prestress, size of the reinforcement, and the stress-strain characteristics of the steel used in this investigation are not generally found in practice.

Theory

Results of the theoretical study on the use of high-strength steels as reinforcement in concrete beams indicates that:

1. The reinforcing index should not exceed the value given by

$$q_a = 0.510 - (1.9f_y + 22f'_c)10^{-6} \quad (5)$$

for concrete beams reinforced with steels having a well-defined yield stress and adequate ductility.

2. The amount of tensile steel that can be used in a concrete beam depends upon the yield strength of the steel, the concrete strength, and the amount, location and yield strength of the compression steel.

a. For beams with no compression steel, the tensile steel ratio should never exceed

$$p_a = q_a\left(\frac{f'_c}{f_y}\right) \quad (10)$$

The value of p_a may be determined directly from Figure 7.

b. For beams with compression steel, the tensile steel ratio should never exceed

$$p_a^c = p_a + p'\left(\frac{f'_{su}}{f_y}\right) \quad (11)$$

where $f'_{su}/f_y \leq f'_y/f_y$

The value of p_a and f'_{su}/f_y may be determined directly from Figures 7 and 8, respectively.

3. The maximum strain in the compression steel is generally so low, except for very deep beams, that the additional strength offered by high-strength steels cannot be utilized before the concrete crushes in compression. Therefore, in special cases, it may be more economical to use two different grades of steel, i.e., high-strength steel for tensile reinforcement and intermediate or structural grade for compression reinforcement. However, in general, it may be more economical to make all steel of the same type, since this will reduce construction problems.

4. The amount of compression steel and its location in a beam has relatively little effect upon ultimate load but a large effect upon beam ductility. For beams designed to withstand large plastic deflections, the designer should make d'/d as small as practicable in order to gain the greatest advantage from compression steel. When computing collapse deflections the stress in the compression steel at ultimate moment can be estimated from Figure 6.

5. For the practical range of the reinforcing index generally required in blast-resistant design ($q \leq 0.2$), the tensile reinforcement should be capable of elongating at least 10 percent.

6. The feasibility of using high-strength steel in blast design may often depend upon the cracks and/or deflection criterion for static service loads. A beam will meet the deflection criterion, L/N, if the ratio between the static yield resistance required to withstand the imposed blast loading, r_y, and the static service load, w_s, is less than the minimum yield-load factor, M. L. F., given in Figure 10 and Equation 13. The M. L. F. increases with the yield strength of the tensile steel, tensile steel ratio, span-to-depth (L/d) ratio, and deflection criterion (L/N) and decreases with the effective prestress level f_{se}. However, in general, the greater the ratio r_y/w_s (i. e., the greater the blast pressure) the more feasible it becomes to use high-strength steels in unprestressed concrete.

Tests

Results of the static and dynamic testing of eight prestressed and eight conventionally reinforced concrete beams utilizing high-strength (f_y = 92,000 psi) chromium-alloy steel bars indicates that:

1. The static yield resistance of the R/C and P/C beams was approximately the same but the static yield deflection of the P/C beams was reduced considerably, depending upon the level of prestress. The yield resistance and deflection of both types of beams can be predicted by Equation 17 and 13a, respectively.

2. The ultimate resistance and collapse deflection of both types of beams was approximately the same and can be predicted by Equation 18 and 19, respectively, if the stress-strain characteristics of the tensile steel are known.

3. Increasing the effective prestress from 0 to 25,000 psi increased the cracking load 450 percent and decreased the yield deflection 39.1 percent.

4. The static service load corresponding to a limiting deflection of L/360 for the test beams compared well with the value predicted from Figure 10.

5. The cracks along the span of the R/C and P/C beams were uniformly distributed and closely spaced, indicating that the bond between steel and concrete was not severely affected.

6. A viscously damped spring-mass system may be used to predict the maximum dynamic response of the R/C and P/C beams in the elastic range if the correct amount of damping is employed.

7. The damping factor for the beams ranged between 10 percent and 28 percent. Under medium-duration loads the elastic damping factor for the R/C beams (20 percent) was almost twice that of the P/C beams (11 percent). Damping was about 43 percent greater under medium-duration loads than under short-duration loads.

8. The probability of rebound under dynamic loads increases with a decrease in the ratio of load-duration to natural period and/or a decrease in the damping factor. Both types of beams rebounded under load-durations of 0.14 seconds when the damping factor was less than 15 percent.

9. The resilience of the P/C beams was superior to the R/C beams when the maximum dynamic deflection was less than the cracking deflection. However, the resilience of both types of beams was approximately the same for large inelastic deflections.

ACKNOWLEDGMENTS

The author wishes to acknowledge his appreciation to the individuals who contributed to the completion of this investigation. Special appreciation is expressed to R. A. Breckenridge, Structural Research Engineer, for his assistance and guidance in the experimental phase of the program and for his critical review of this report; to Dr. K. Lensen of the University of Kansas for his help in designing the beams; to T. J. Landrum, Test Mechanic, for his able assistance in casting the test members and carrying out the test program; and to W. Q. Ginn, Engineering Technician, for his assistance in data reduction and preparation of the figures and tables for this report.

REFERENCES

1. Allgood, J. R., and G. R. Swihart. "Design of Flexural Members for Static and Blast Loading," to be published by American Concrete Institute, Redford Station, Detroit, Michigan.

2. U. S. Naval Civil Engineering Laboratory. Technical Report R-086, Blast Loading of 15 Ft R/C Beams, by J. R. Allgood, S. K. Takahashi and W. A. Shaw. Port Hueneme, California, January 1961.

3. Newmark, N. M. "An Engineering Approach to Blast Resistant Design," Proceedings of ASCE, Vol. 79 (October 1953).

4. Hognestad, E., et al. "Concrete Stress Distribution in Ultimate Strength Design." Journal of ACI, Vol. 27, No. 4 (December 1955), pp 455-480.

5. University of Illinois. Structural Research Series No. 197, The Yield Strength of Intermediate-Grade Reinforcing Bars Under Rapid Loading, by W. A. Keenan and A. Feldman. Urbana, Illinois, March 1960.

6. U. S. Naval Civil Engineering Laboratory. Technical Note N-427, Dynamic Tests on High Strength Steel, by W. L. Cowell and J. R. Keeton. Port Hueneme, California, February 1962.

7. ACI Committee 318. "Building Code Requirements for Reinforced Concrete (ACI 318-56)," Journal of ACI, Vol. 27, No. 8 (May 1956), pp 913-986.

8. U. S. Naval Civil Engineering Laboratory. Technical Memorandum M-130, Elasto-Plastic Response of Beams to Dynamic Loads, by J. R. Allgood and W. A. Shaw. Port Hueneme, California, March 1958.

9. ACI Committee 318. "Proposed Revision of Building Code Requirements for Reinforced Concrete (ACI 318-56)," Journal of ACI, Vol. 59, No. 2 (February 1962), pp 145-276.

10. Wastland, G. "Use of High-Strength Steel in Reinforced Concrete," Journal of ACI, Vol. 30, No. 12 (June 1959), pp 1237-1250.

11. Lin, T. Y. Design of Prestressed Concrete Structures. John Wiley and Sons, New York, 1955.

12. University of Illinois. Structural Research Series No. 40, An Investigation of the Load-Deformation Characteristics of Reinforced Concrete Beams Up to the Point of Failure, by J. R. Gaston, C. P. Siess and N. M. Newmark. Urbana, Illinois, December 1952.

13. Swihart, G. R., J. R. Allgood, and W. A. Shaw, "Static Resistance of Reinforced Concrete Beams," Proceedings of ASCE, Vol. 85, No. ST1, Part 1 (January 1959).

14. Hognestad, E. "High-Strength Bars as Concrete Reinforcement," Journal of PCA, Vol. 3, No. 3 (September 1961), pp 23-29.

15. U. S. Naval Civil Engineering Laboratory. Technical Report R-116, Blast Load Tests on Post-Tensioned Concrete Beams, by H. T. Miyamoto and J. R. Allgood. Port Hueneme, California, May 1961.

16. Crandall, S. H. Random Vibration. John Wiley and Sons, New York, 1958.

17. Bate, S. C. C. "Strength of Concrete Members Under Dynamic Loading," Symposium on the Strength of Concrete Structures, Session D, Paper No. 2. Building Research Station, England.

SYMBOLS

a = acceleration

a_u = depth of compression zone in concrete at ultimate moment

A_n = displacement amplitude of the n^{th} cycle of oscillation

A_{n+1} = displacement amplitude of the $n+1$ cycle of oscillation

A_s = area of tension steel

A'_s = area of compression steel

b = width of rectangular beam

B = effective peak dynamic load of the equivalent linearly decaying load pulse — found by passing a straight line through the point corresponding to t_m on the experimental pressure-time curve and adjusting the slope until the areas under each curve are equal up to time, t_m

d = distance from centroid of tension steel to compression face of beam

d' = distance from centroid of compression steel to compression face of beam

D.L.F. = dynamic load factor

E_c = secant modulus of elasticity of concrete corresponding to $0.5f'_c$

E_s = tangent modulus of elasticity

f_c = compressive stress in extreme fiber of concrete

f'_c = compressive strength of 6- x 12-inch concrete cylinders

f_s = stress in tension steel

f'_s = stress in compression steel

f_{se} = effective prestress in tensile steel

f_{su} = stress in tensile steel at ultimate-moment capacity

f'_{su} = stress in compression steel at ultimate-moment capacity

f_t = tensile strength of concrete

f_y = static yield stress of tensile steel corresponding to $\epsilon = 10^{-5}$ in./in./sec

f'_y = static yield stress of compression steel

f_{yd} = dynamic yield stress of tensile steel

F = apparent strain compatibility factor

h = depth of beam

I = moment of inertia of uncracked transformed section (elastic theory)

k = coefficient defining location of neutral axis of cracked transformed section (elastic theory)

k' = coefficient defining location of centroidal axis of uncracked transformed section (elastic theory)

k_1k_3 = coefficient defining average stress in compression zone of concrete at ultimate moment

k_2 = coefficient defining position of compression force in concrete at ultimate moment

K = stiffness of beam

L = clear span of beam

M = moment

M_u = ultimate moment

M_y = yield moment

M.L.F. = minimum yield-load factor

$n = E_s/E_c$ = modular ratio

N = a constant describing the ratio between the span length and the maximum-allowable service load deflection

$p = A_s/bd$ = tensile steel ratio

$p' = A'_s/bd$ = compression steel ratio

p_a = maximum-allowable tensile steel ratio for beam with no compression steel

p_a^c = maximum-allowable tensile steel ratio for beam with compression steel

p_b = balanced tensile steel ratio for beam with no compression steel

p_b^c = balanced tensile steel ratio for beam with compression steel

$q = (pf_{su} - p'f_{su})/f'_c$ = reinforcing index

q_a = maximum-allowable reinforcing index

q_b = balanced reinforcing index

r = static load or resistance

r_c = static cracking load or cracking resistance

r_u = static ultimate load or ultimate resistance

r_y = static yield load or yield resistance

t = time measured from beginning of load application

t_m = time required for beam to reach initial maximum deflection

T = load duration of applied load

T_e = effective load duration of the equivalent linearly decaying load — found by passing a straight line through the point corresponding to t_m on the experimental pressure-time curve and adjusting the slope until the areas under each curve between $t = 0$ and $t = t_m$ are equal

T_n = undamped natural period of vibration

$T_{nd} = T_n\sqrt{1 - \beta^2}$ = damped natural period of vibration

w_s = static service load — defined as that proportion of dead plus live load which shall be used to compute the deflection of flexural members

y = deflection

$y_{am} = y_m + y_{ap}$ = accumulative maximum deflection

$y_{ap} = \Sigma y_p$ = cumulative permanent deflection

y_c = cracking deflection

y_m = maximum deflection

y_p = permanent deflection

y_s = static service load deflection

y_u = ultimate or collapse deflection

y_y = yield deflection

y_{yd} = dynamic yield deflection

α = coefficient defining length of plastic yield hinge at ultimate-load capacity

β = viscous damping factor

β_E = viscous damping factor in elastic range

β_p = viscous damping factor in plastic range

$\delta = \ln(A_n/A_{n+1})$ = logarithmic decrement

ϵ = strain

$\dot{\epsilon}$ = strain rate

ϵ_c = strain in concrete

ϵ_{ce} = effective pre-strain in concrete

ϵ_o = strain-hardening strain

ϵ_s = strain in tension steel

ϵ'_s = strain in compression steel

ϵ_{se} = effective pre-strain in tension steel

ϵ_{su} = strain in tension steel at ultimate moment

ϵ'_{su} = strain in compression steel at ultimate moment

ϵ_u = ultimate compressive strain in concrete

ϵ_y = static yield strain in tension steel

ϵ_{yd} = dynamic yield strain in tension steel

φ_u = unit rotation of beam section at ultimate moment

φ_y = unit rotation of beam section at yield moment

ω = fundamental circular frequency

Appendix A

STATIC LOAD-DEFLECTION AND LOAD-STRAIN CURVES
(Figures A1-A10)

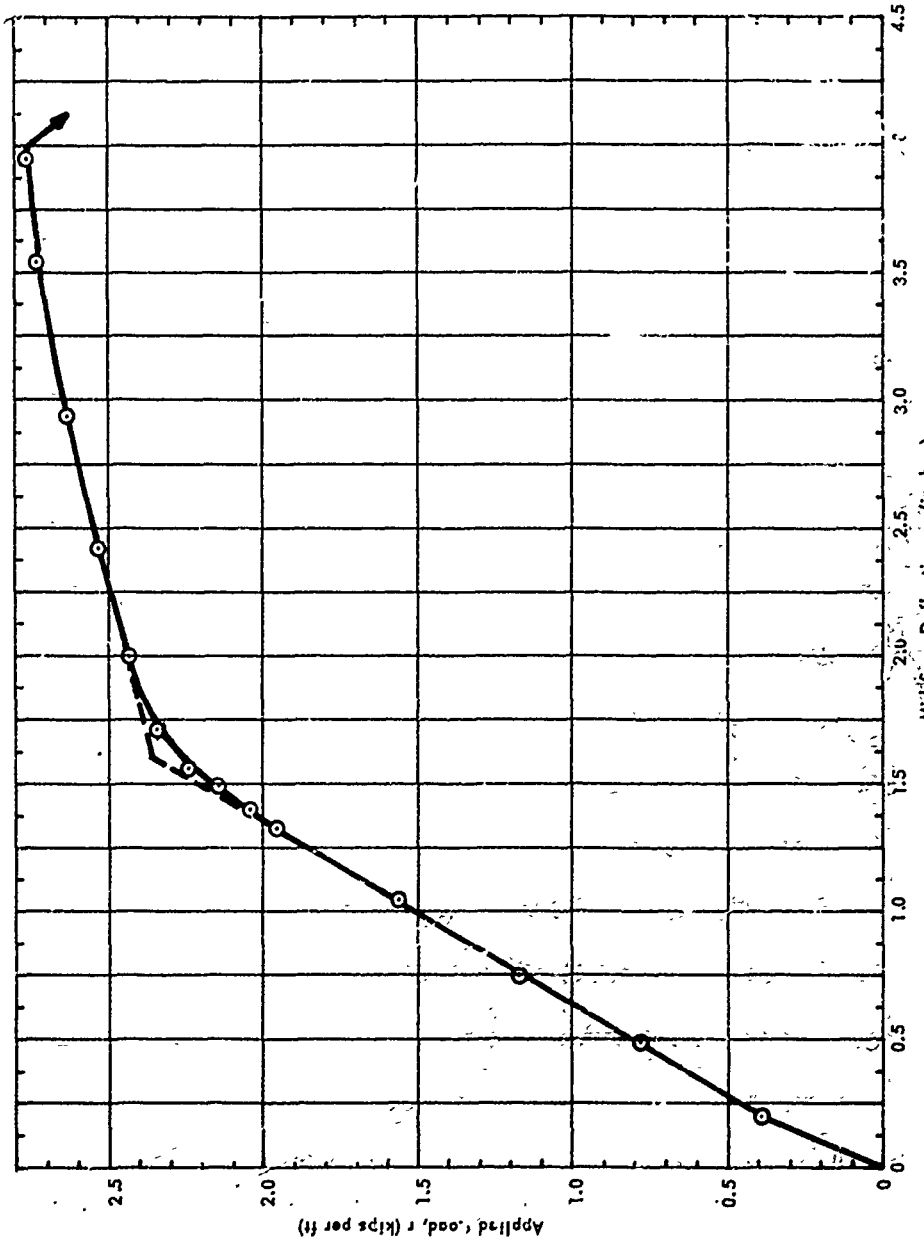

Figure A1. Static load-deflection curve, beam R1.

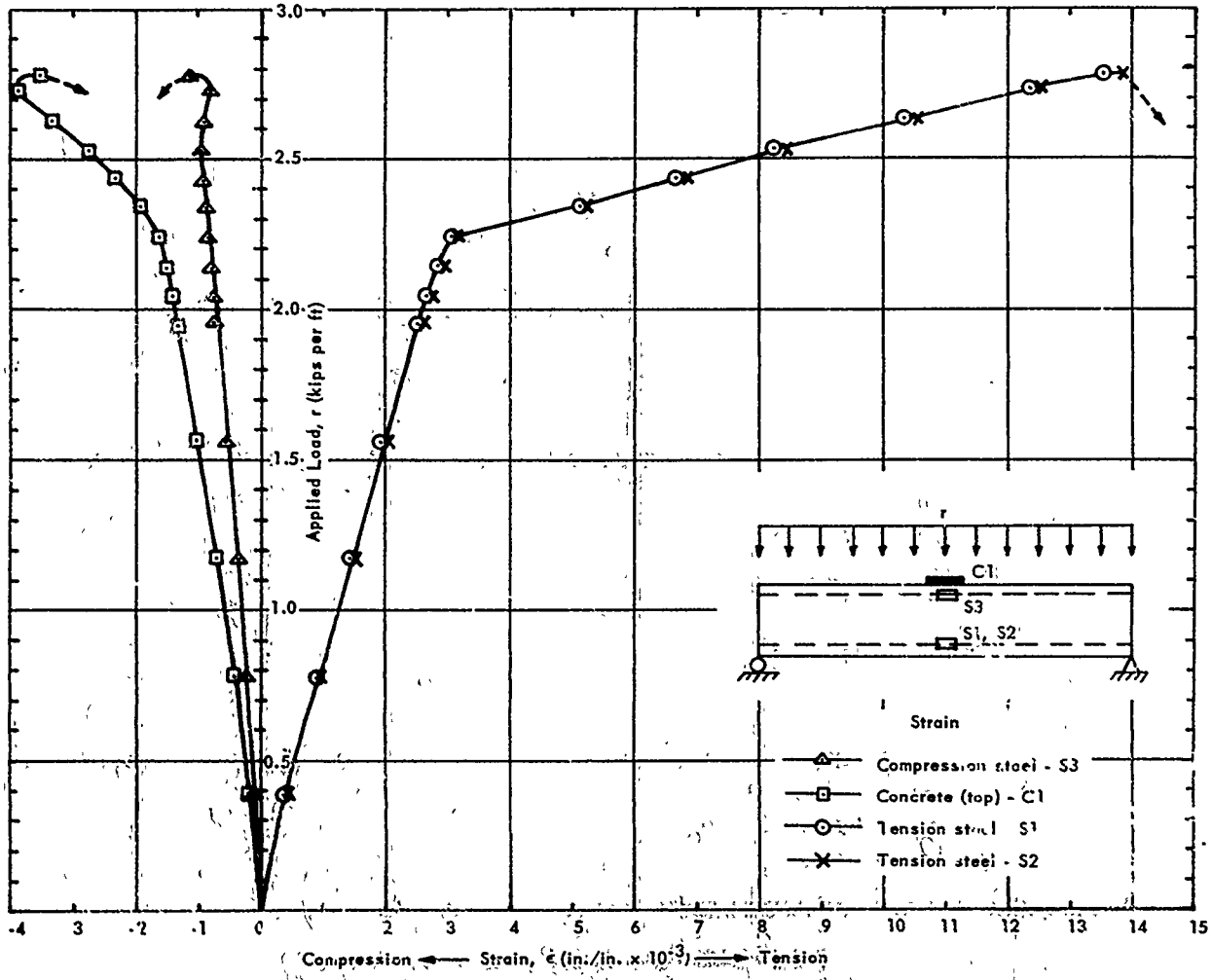

Figure A2. Static load-strain curves, beam R1.

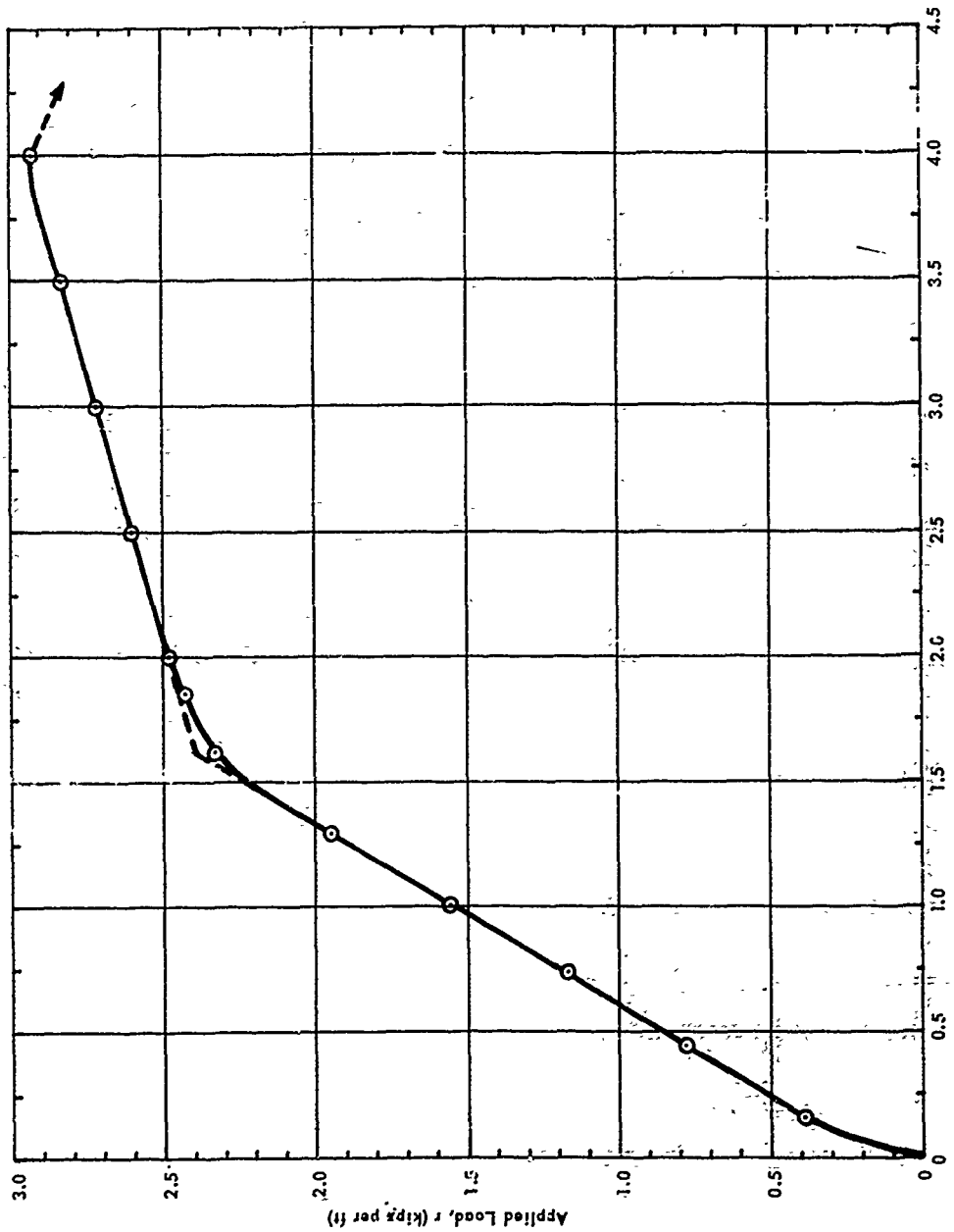

Figure A3. Static load-deflection curve, beam R2.

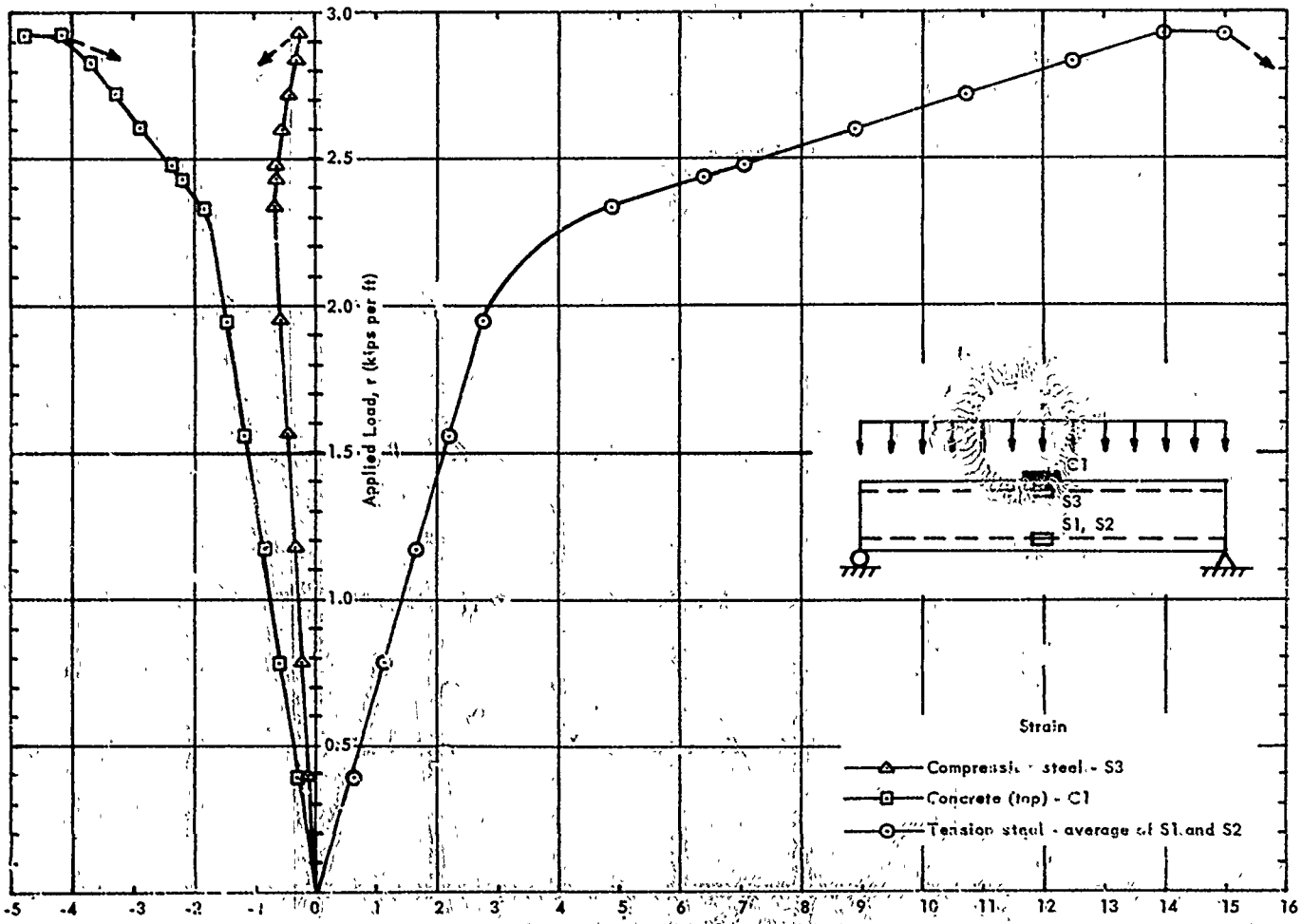

Figure A4. Static load-strain curves, beam R2.

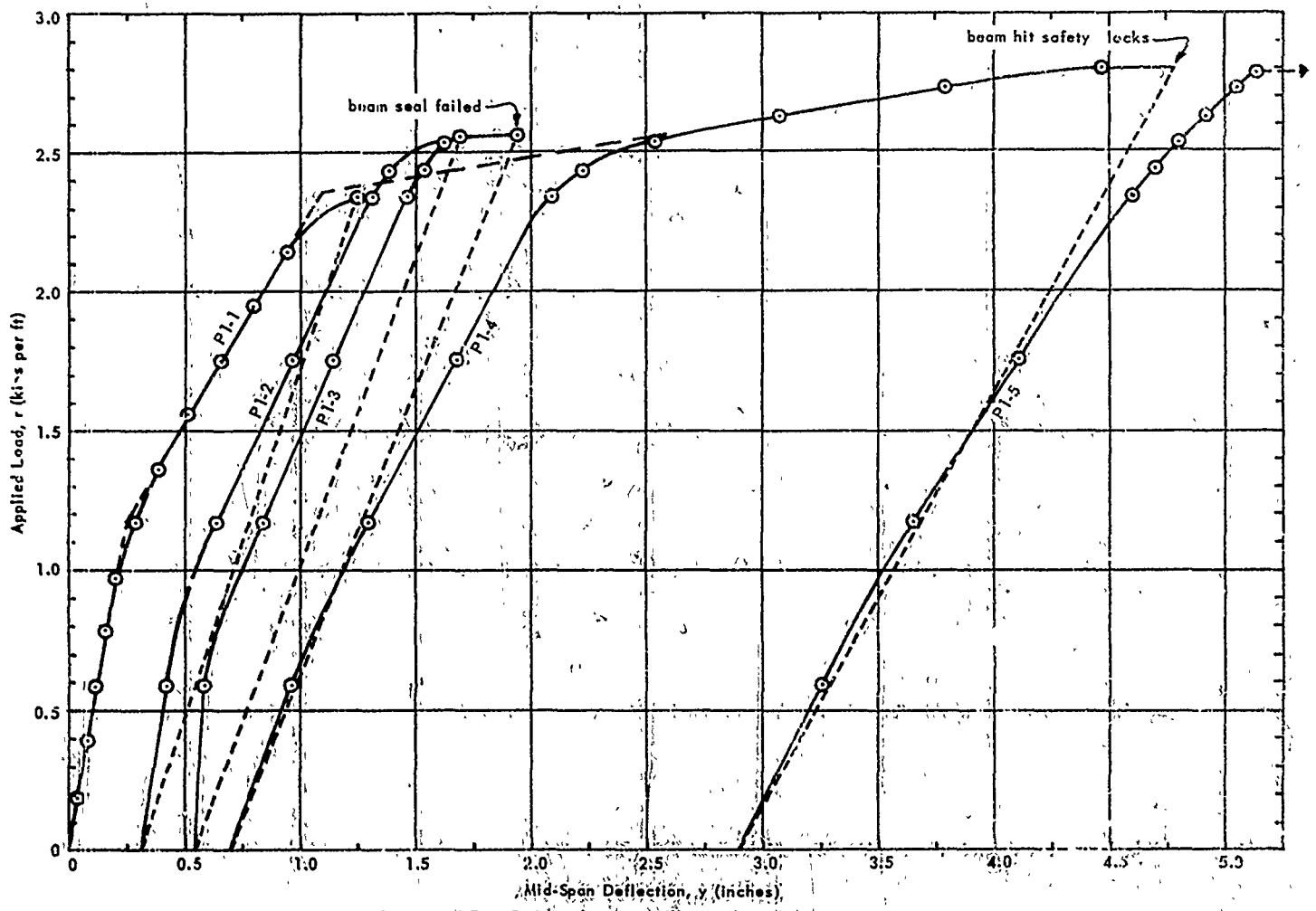

Figure A5. Static load-deflection curve, beam P1.

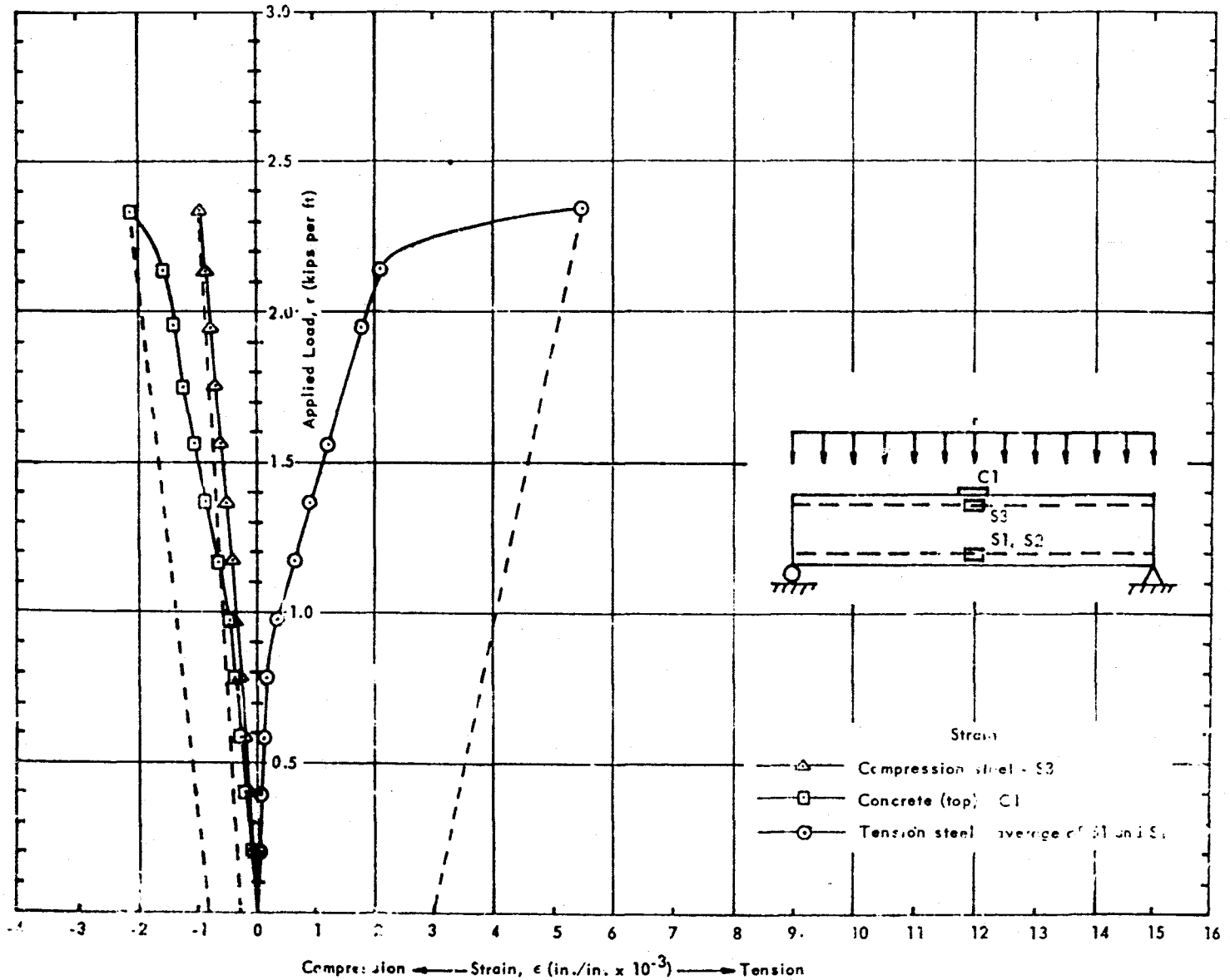

Figure A6. Static load-strain curves, beam P1.

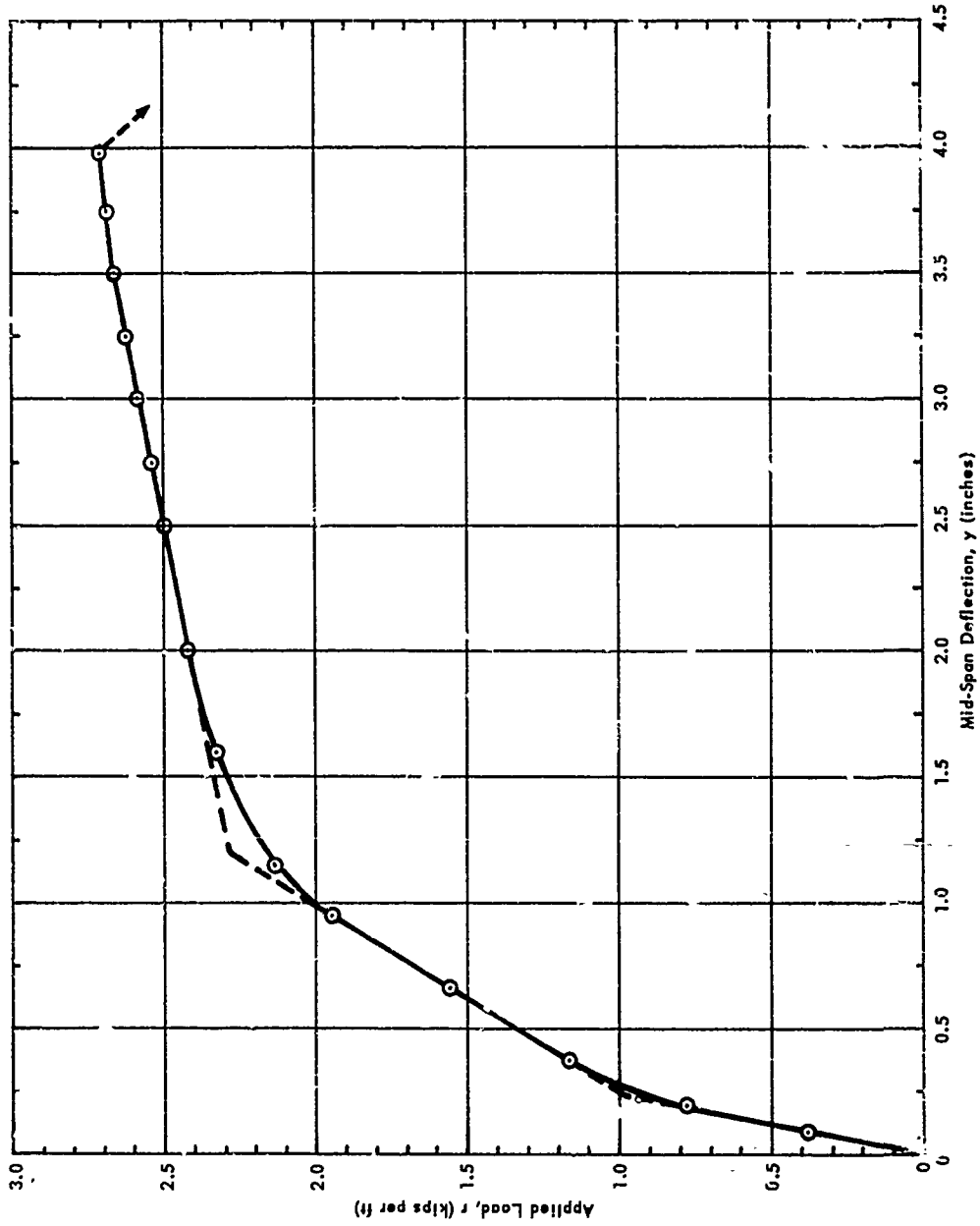

Figure A7. Static load-deflection curve, beam P2.

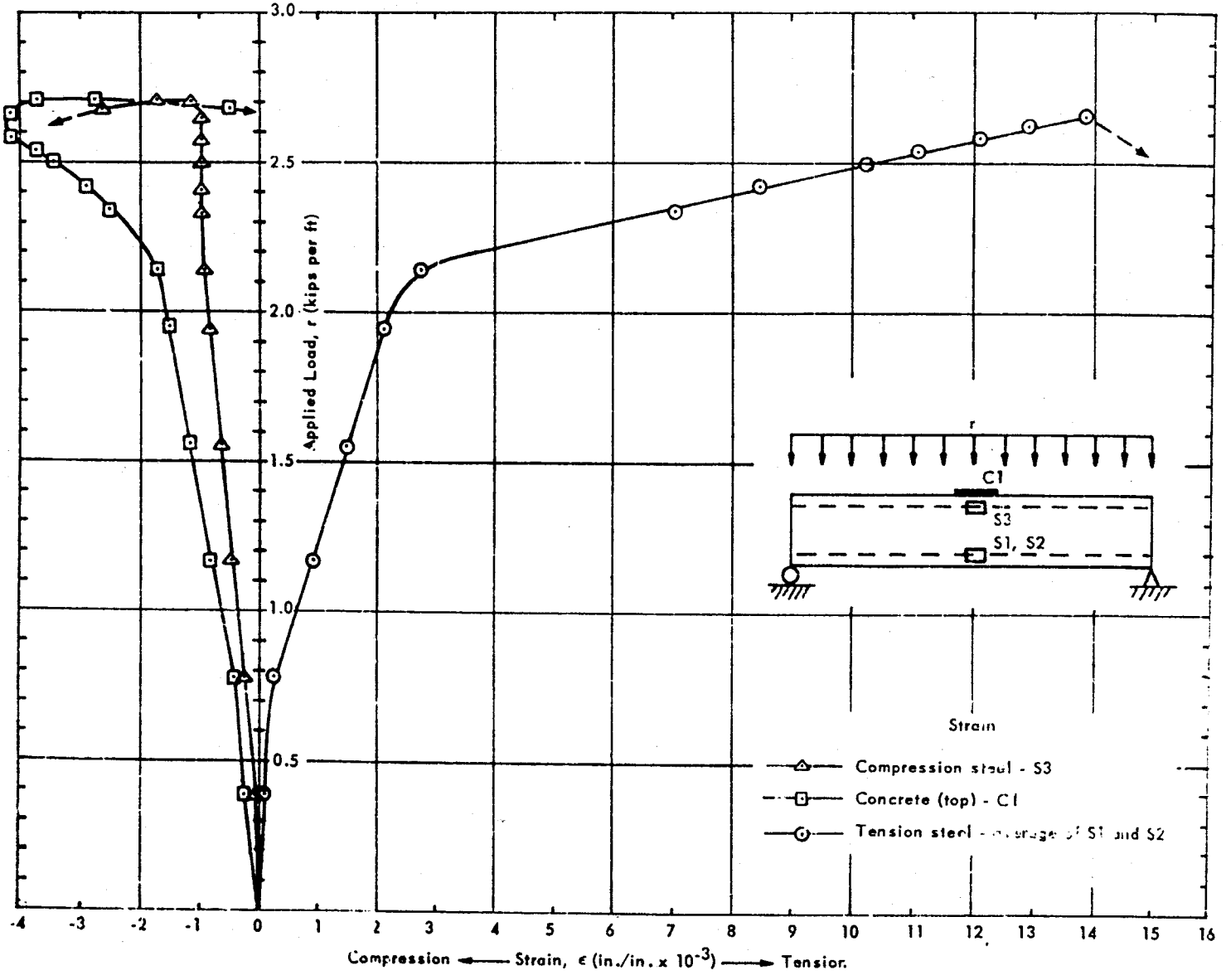

Figure A8. Static load-strain curves, beam P2.

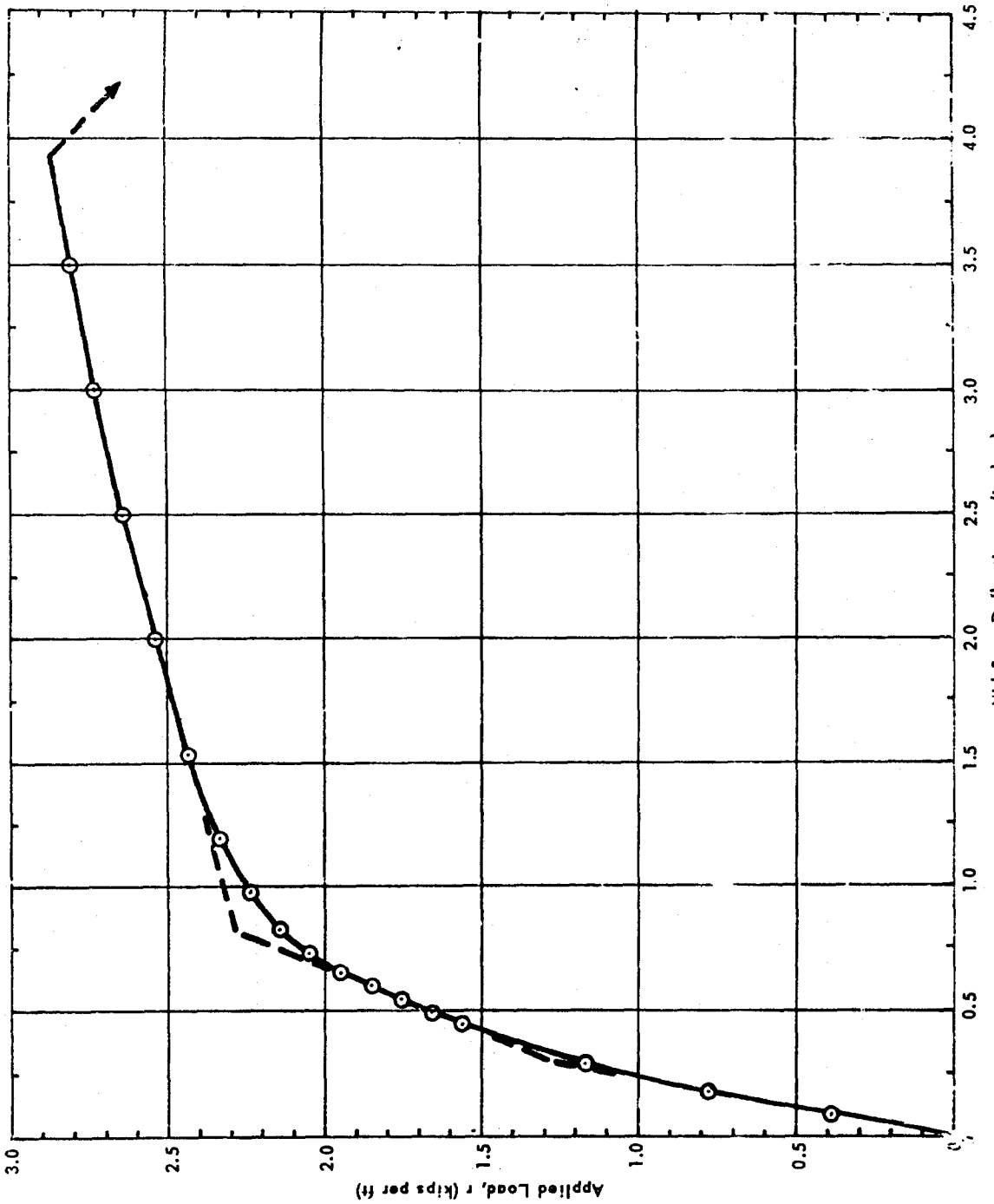

Figure A9. Static load–deflection curve, beam P8.

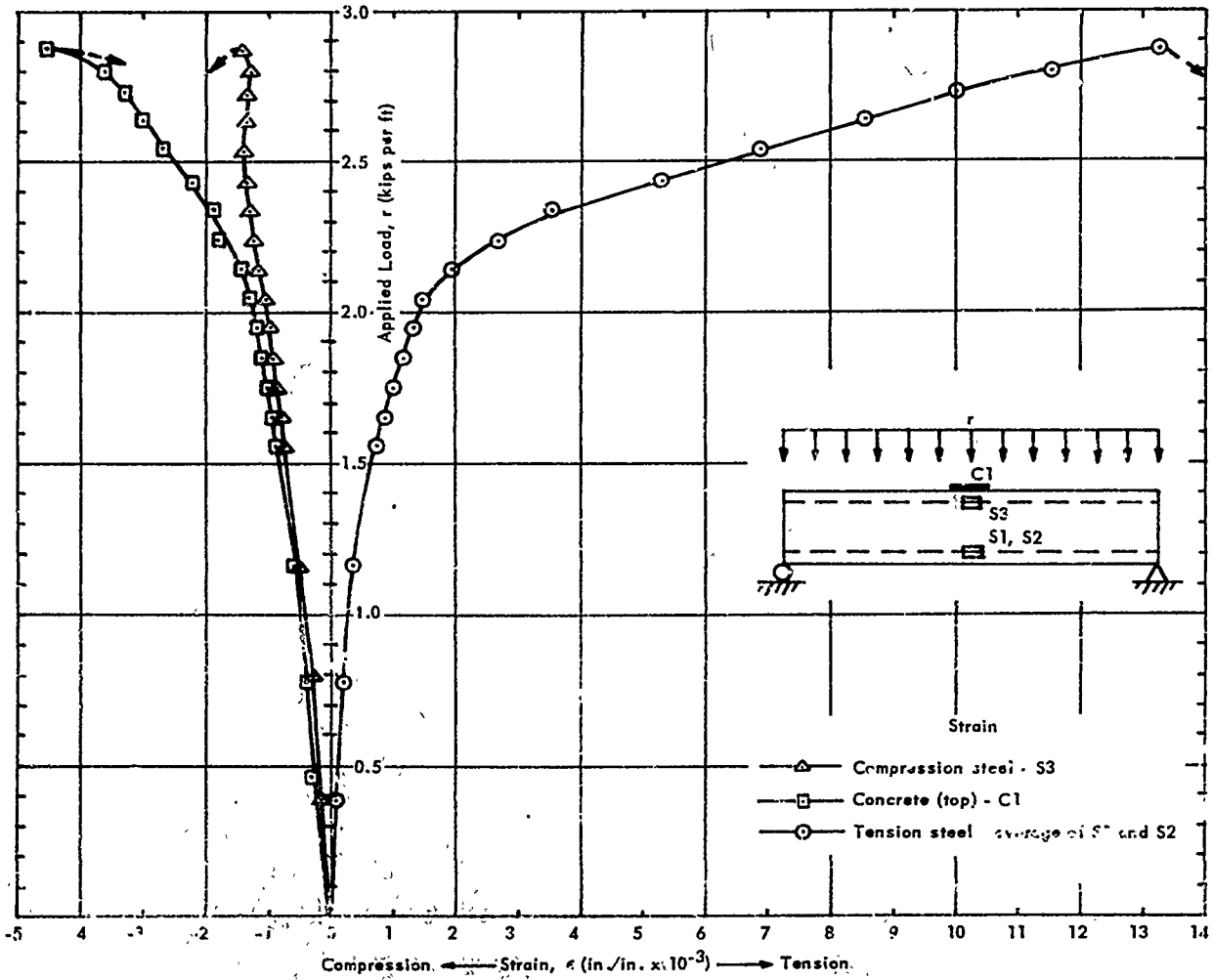

Figure A10. Static load–strain curves, beam P8.

Appendix B

DYNAMIC RESPONSE, REBOUND, AND DAMAGE CURVES
(Figures B1-B5)

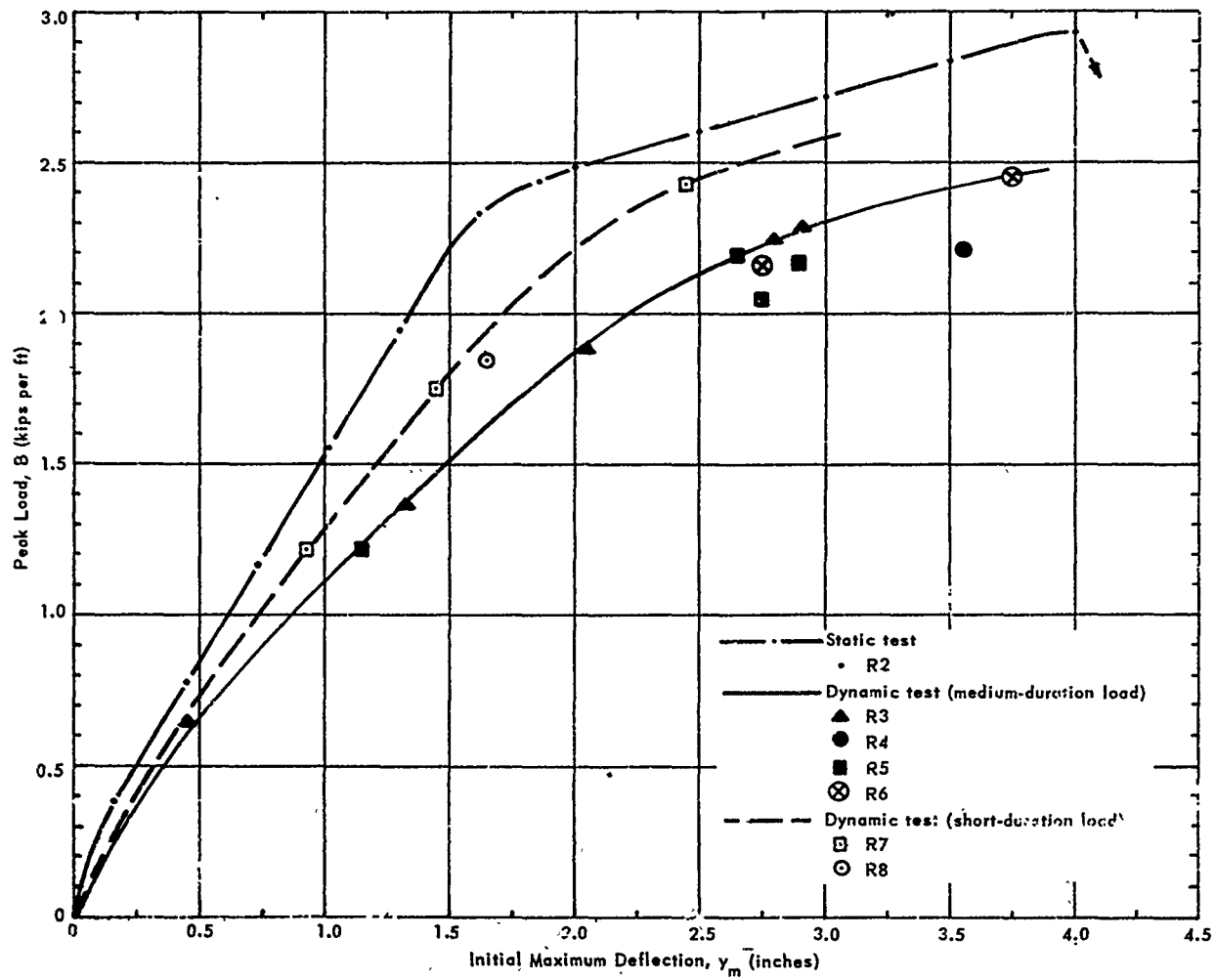

Figure B1. Comparison between static and dynamic load-deflection curves for R/C beams.

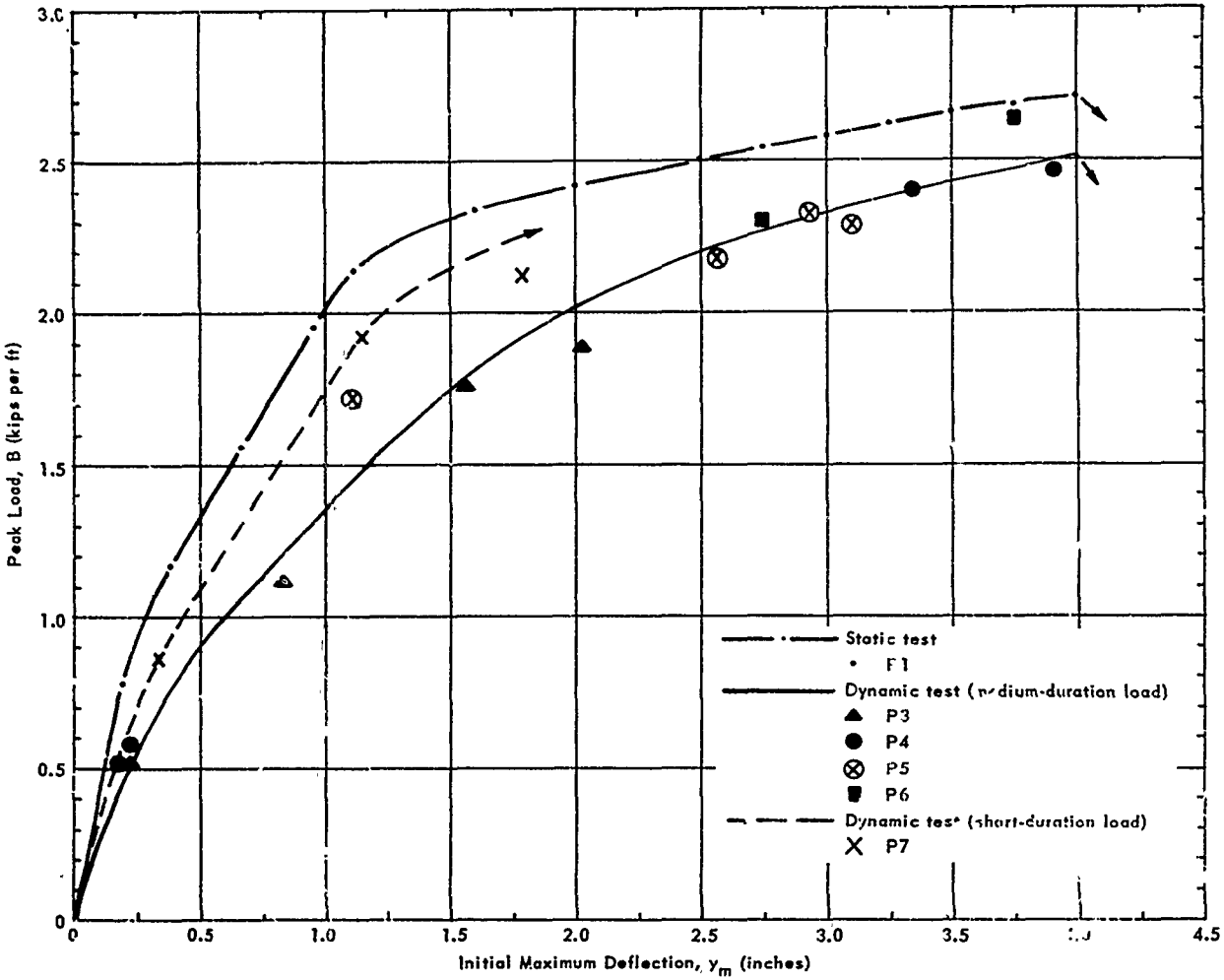

Figure B2. Comparison between static and dynamic load-deflection curves for P/C beams.

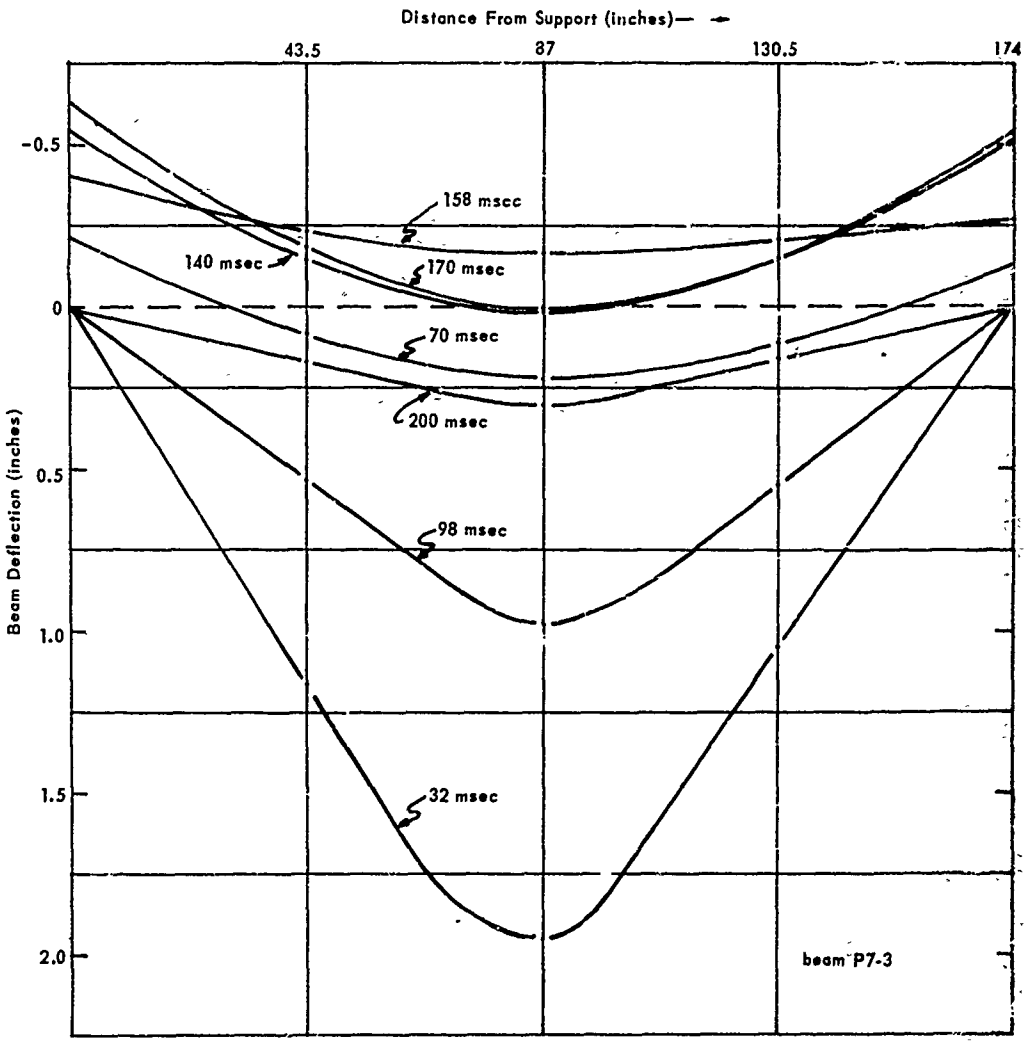

Figure B3. Deflected shape versus time (short-duration load).

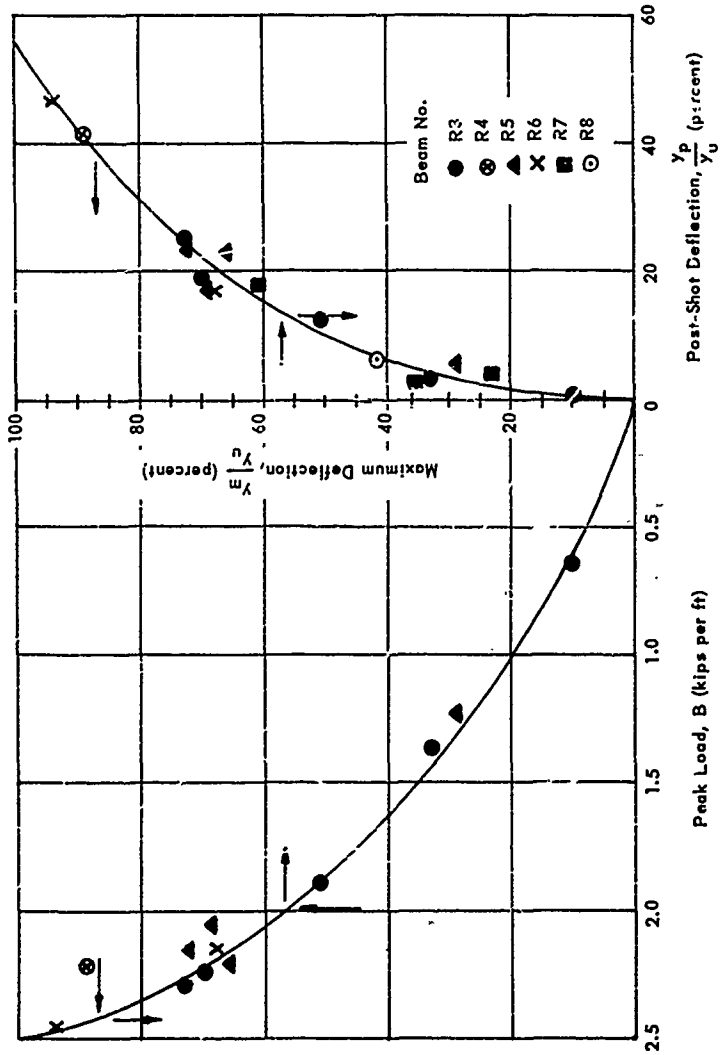

Figure B4. Damage curve for R/C beams.

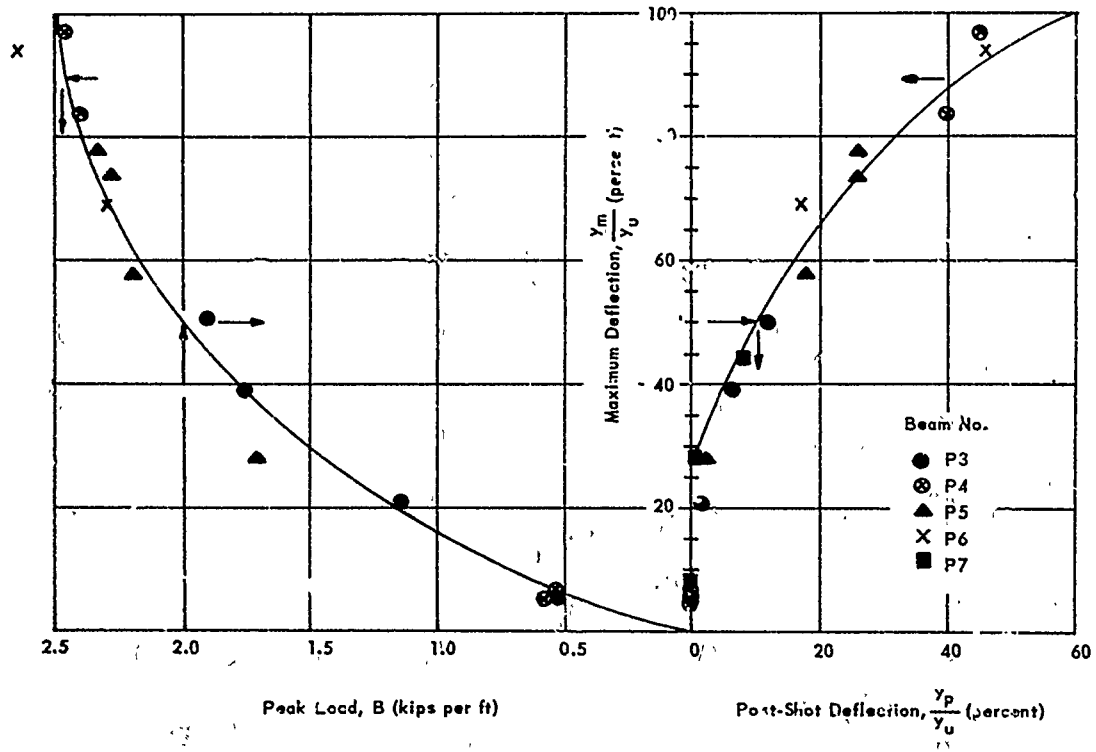

Figure B5. Damage curve for P/C beams.

Appendix C

STATIC AND DYNAMIC CRACK PATTERNS OF BEAMS
(Figures C1-C5)

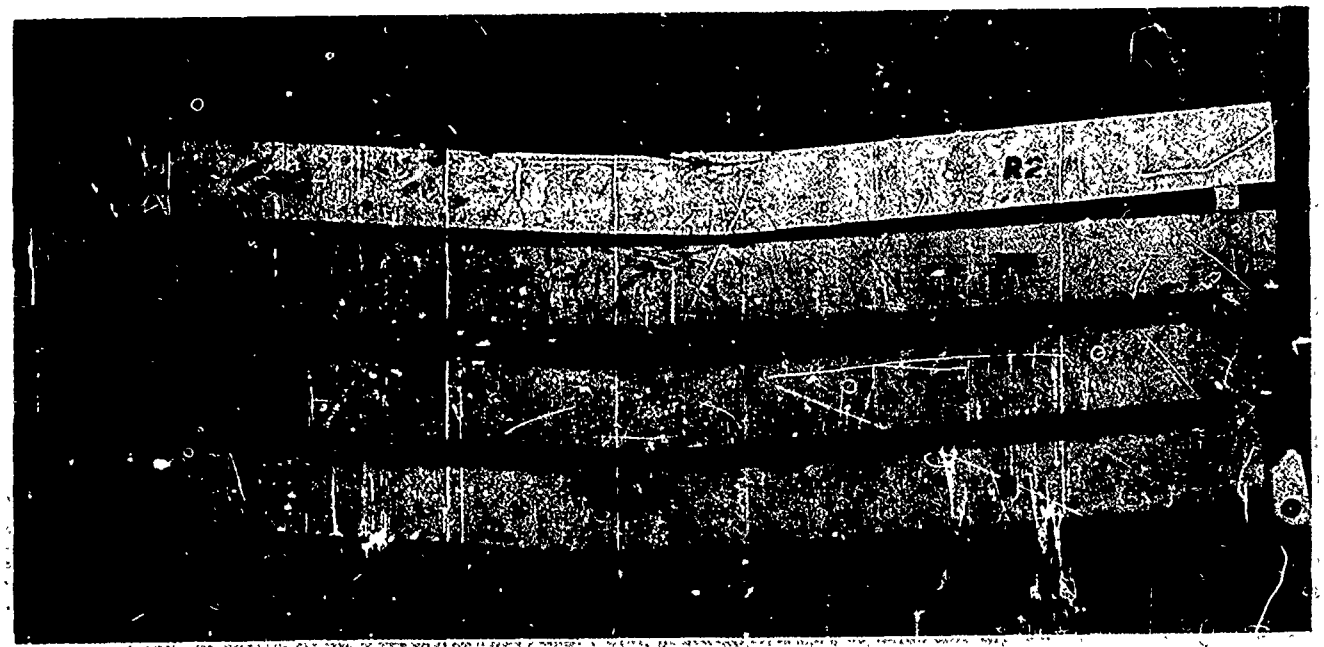

Figure C1. Post-shot view of crack pattern for beams P1, R1, P2, and R2.

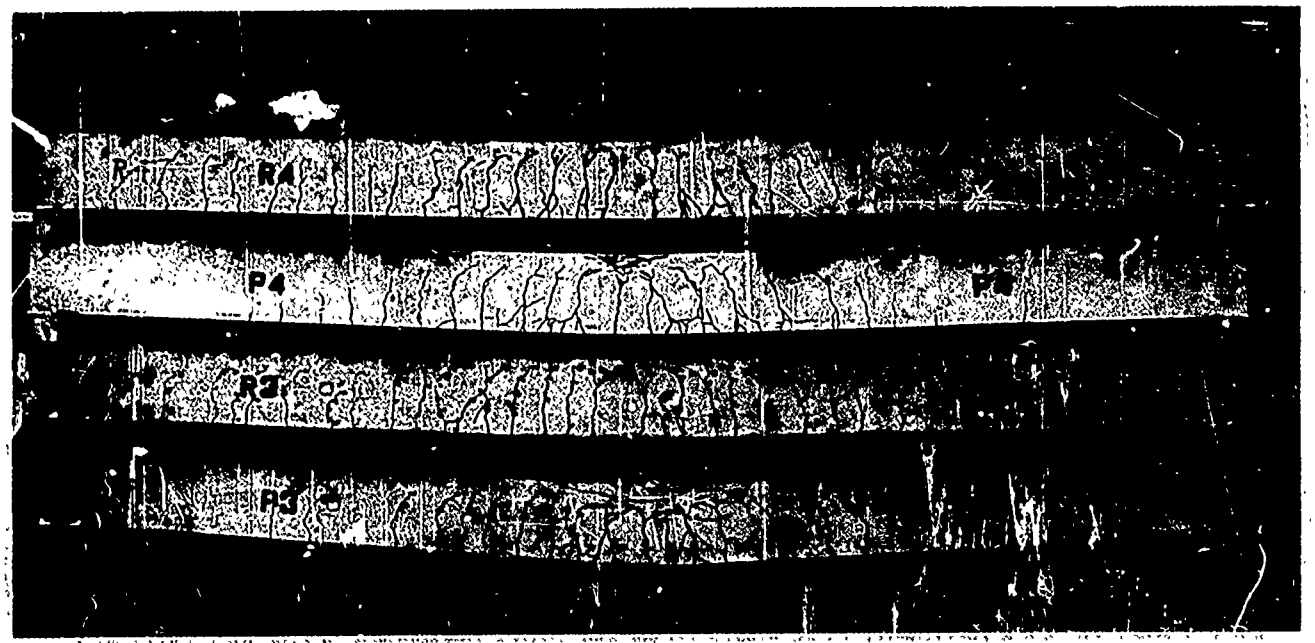

Figure C2. Post-shot view of crack pattern for beams P3-5, R3-5, P4-4, and R4-1.

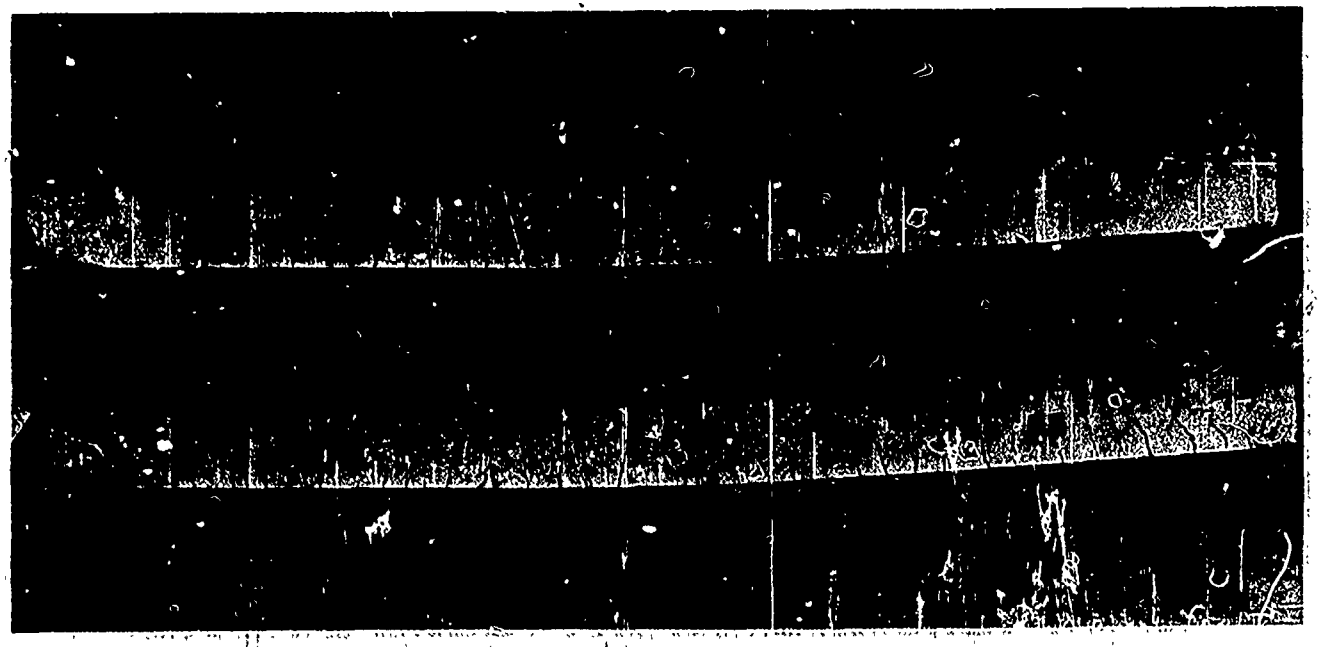

Figure C3. Post-shot view of crack pattern for beams P5-4 and R5-4.

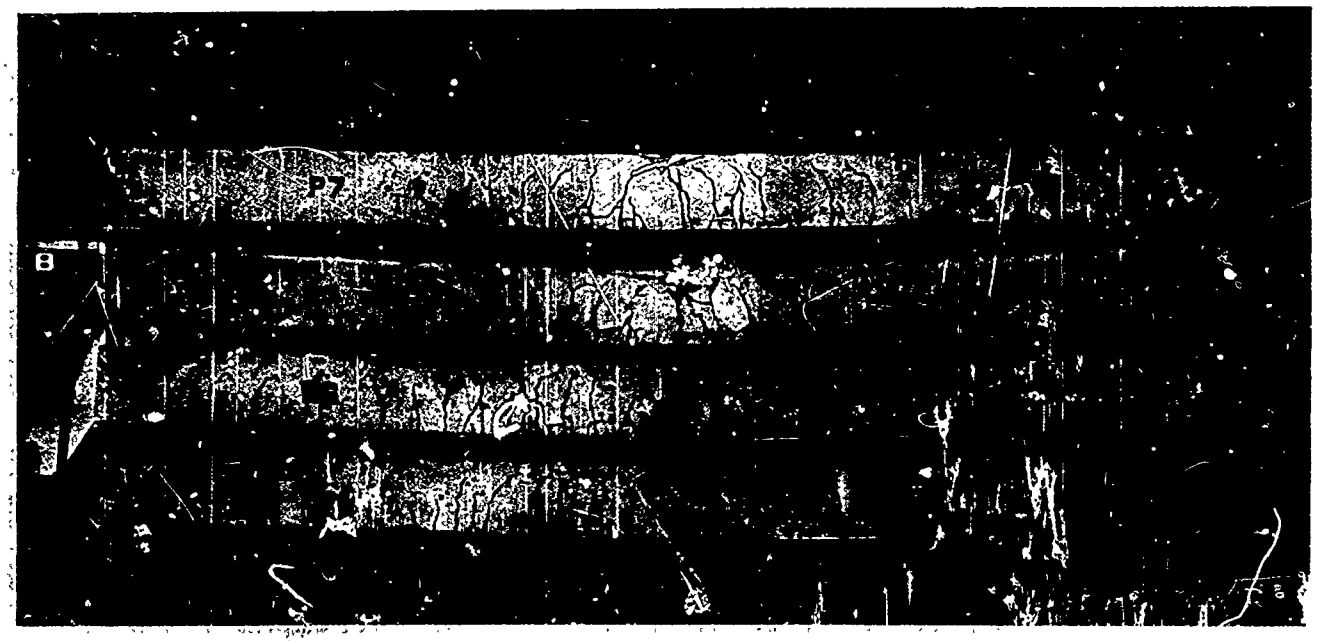

Figure C4. Post-shot view of crack patt ı for beams P6-2, R6-2, P7-4, and R7-4.

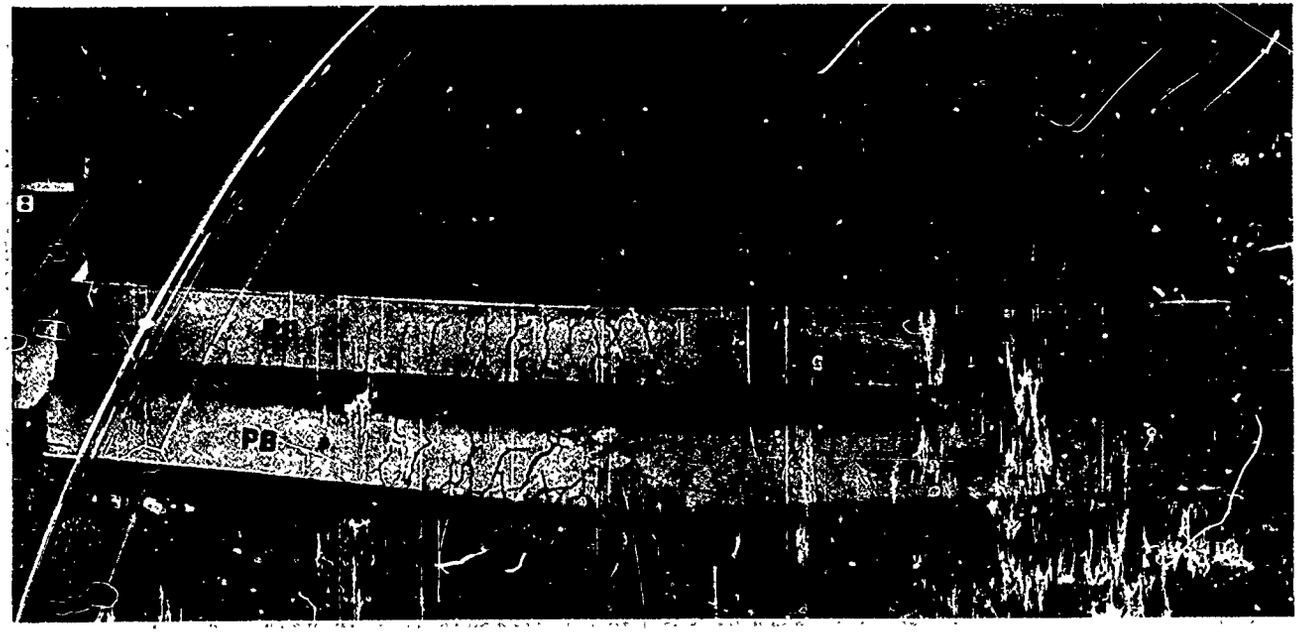

Figure C5. Post-shot view of crack pattern for beams P8 and R8-2.

Appendix D

TYPICAL OSCILLOGRAM TRACES FOR DYNAMIC TESTS
(Figures D1-D3)

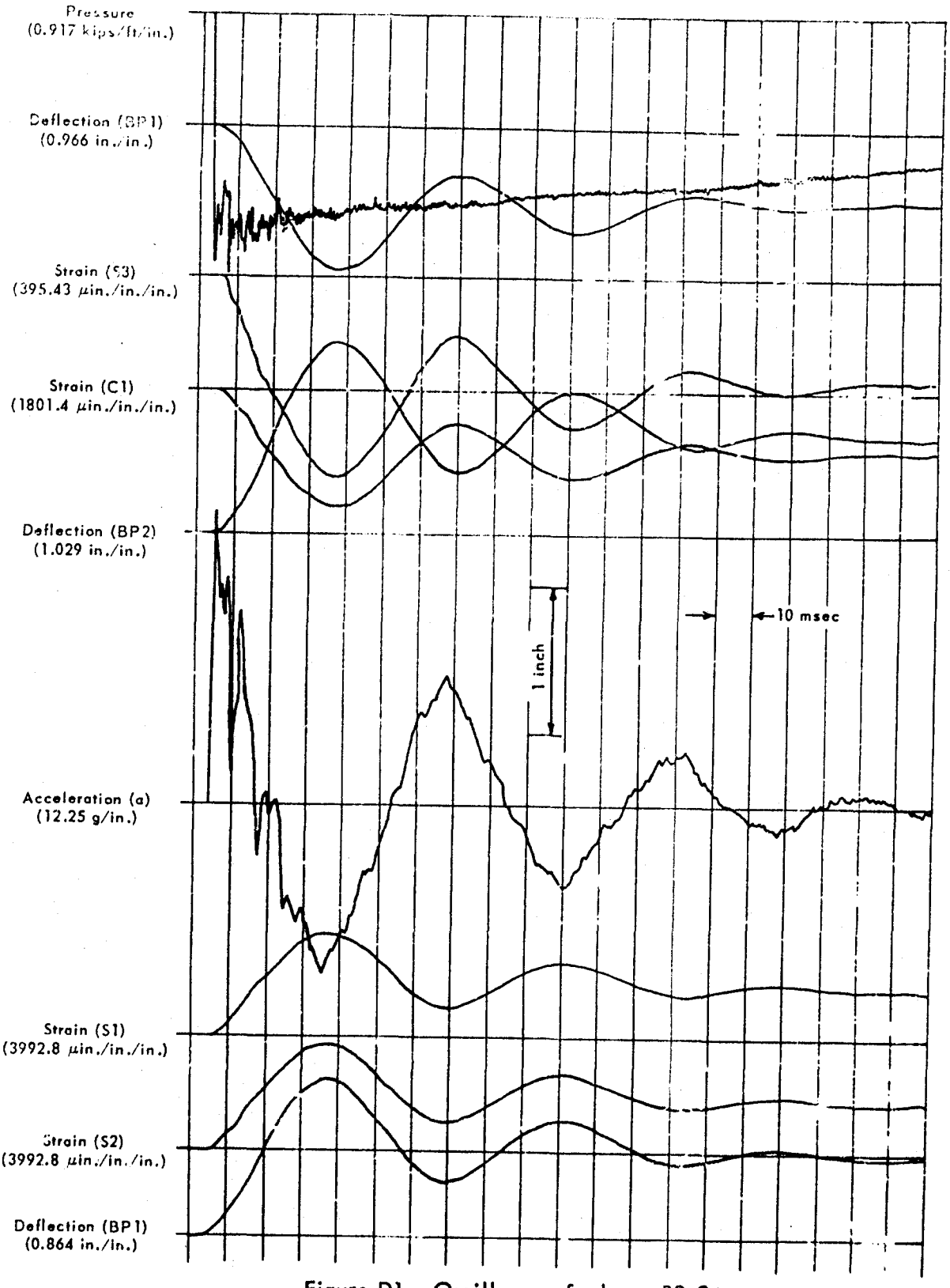

Figure D1. Oscillogram for beam R3-2.

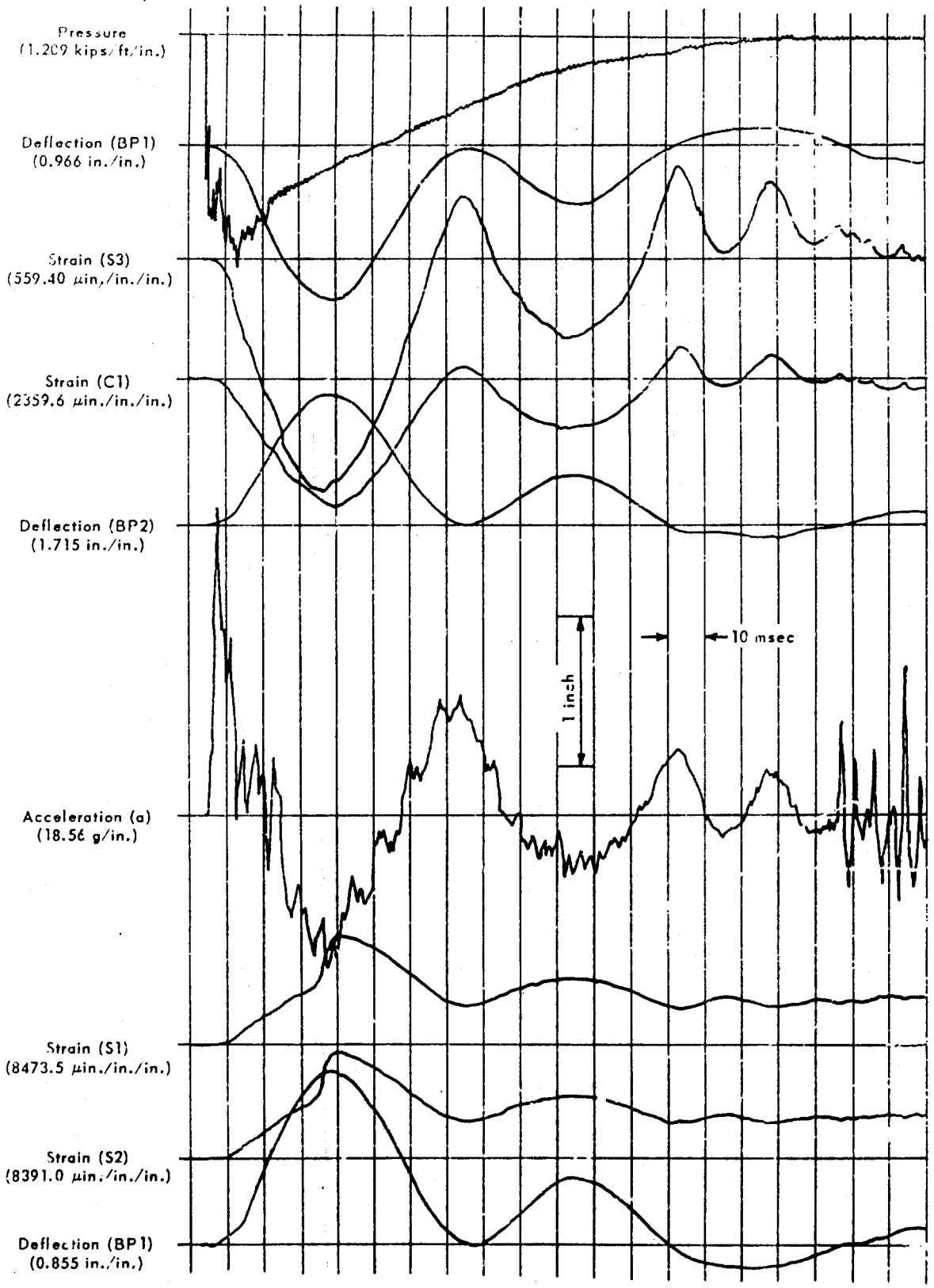

Figure D2. Oscillogram for beam R7-2.

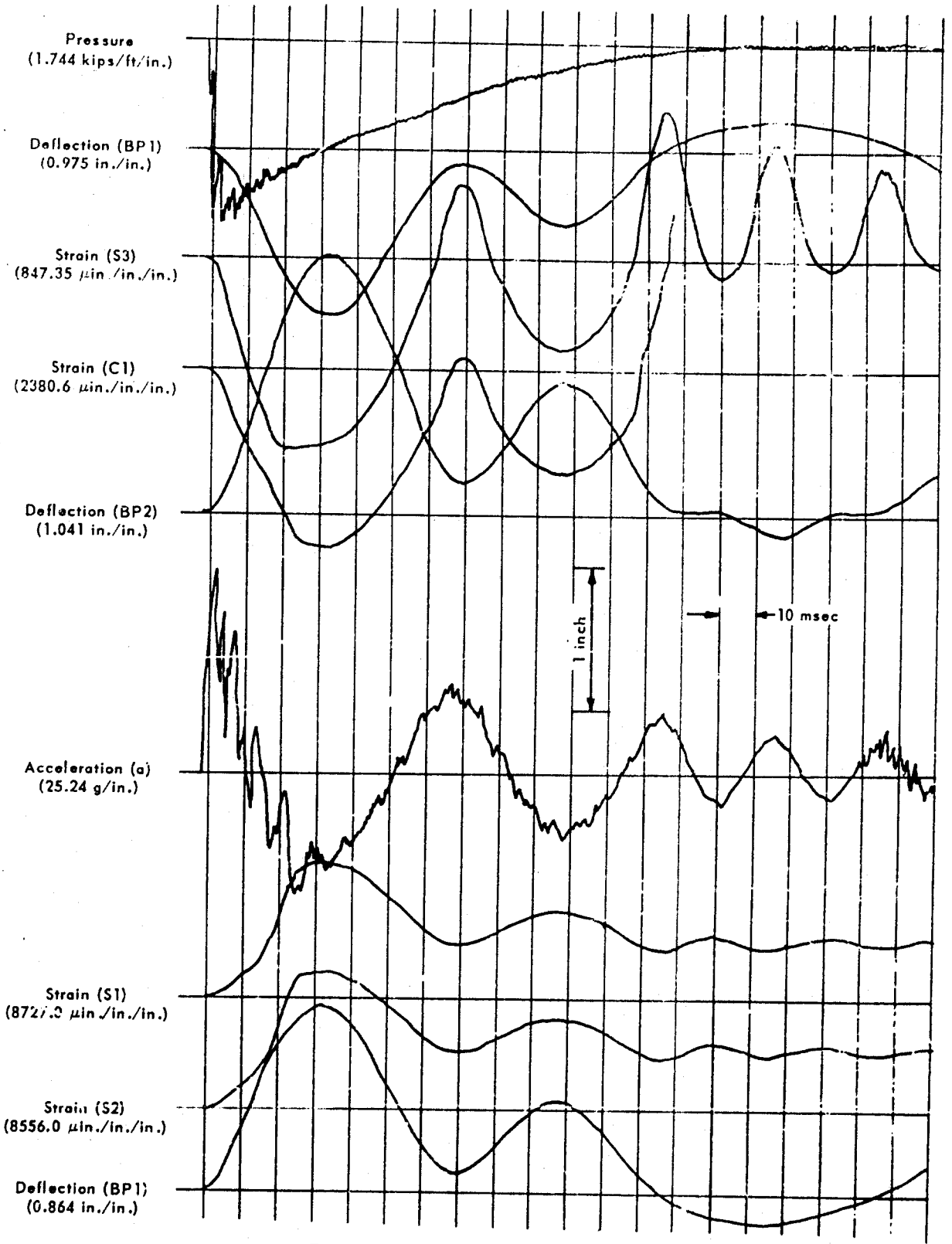

Figure D3. Oscillogram for beam P7-3.

DISTRIBUTION LIST

No. of copies	SNDL Code	
10		Chief, Bureau of Yards and Docks (Code 70)
1	23A	Naval Forces Commanders (Taiwan Only)
4	39B	Construction Battalions
10	39D	Mobile Construction Battalions
3	39E	Amphibious Construction Battalions
2	39F	Construction Battalion Base Units
1	A2A	Chief of Naval Research - Only
2	A3	Chief of Naval Operation (OP-07, OP-04)
5	A5	Bureaus
2	B3	Colleges
2	E4	Laboratory ONR (Washington, D. C. only)
1	E5	Research Office ONR (Pasadena only)
1	E16	Training Device Center
7	F9	Station - CNO (Boston; Key West; San Juan; Long Beach; San Diego; Treasure Island; and Rodman, C. Z. only)
6	F17	Communication Station (San Juan; San Francisco; Pearl Harbor; Adak, Alaska; and Guam only)
1	F41	Security Station
1	F42	Radio Station (Oso and Cheltanham only)
1	F48	Security Group Activities (Winter Harbor only)
8	H3	Hospital (Chelsea; St. Albans, Portsmouth, Va; Beaufort; Great Lakes; San Diego; Oakland; and Camp Pendleton only)
1	H6	Medical Center
2	J1	Administration Command and Unit - BuPers (Great Lakes and San Diego only)
1	J3	U. S. Fleet Anti-Air Warfare Training Center (Virginia Beach only)
2	J4	Amphibious Bases
1	J19	Receiving Station (Brooklyn only)
1	J34	Station - BuPers (Washington, D. C. only)
1	J37	Training Center (Bainbridge only)
1	J46	Personnel Center
1	J48	Construction Training Unit
1	J60	School Academy
1	J65	School CEC Officers
1	J84	School Postgraduate
1	J90	School Supply Corps

Distribution List (Cont'd)

No. of copies	SNDL Code	
1	J95	School War College
1	J99	Communication Training Center
11	L1	Shipyards
4	L7	Laboratory - BuShips (New London; Panama City; Carderock; and Annapolis only)
5	L26	Naval Facilities - BuShips (Antigua; Turks Island; Barbados; San Salvador; and Eleuthera only)
1	L30	Submarine Base (Groton, Conn. only)
2	L32	Naval Support Activities (London & Naples only)
2	L42	Fleet Activities - BuShips
4	M27	Supply Center
6	M28	Supply Depot (Except Guantanamo Bay; Subic Bay; and Yokosuka)
2	M61	Aviation Supply Office
18	N1	BuDocks Director, Overseas Division
25	N2	Public Works Offices
7	N5	Construction Battalion Center
5	N6	Construction Officer-in-Charge
1	N7	Construction Resident-Officer-in-Charge
12	N9	Public Works Center
1	N14	Housing Activity
2	R9	Recruit Depots
2	R10	Supply Installations (Albany and Barstow only)
1	R20	Marine Corps Schools, Quantico
3	R64	Marine Corps Base
1	R66	Marine Corps Camp Detachment (Tengan only)
6	W1A1	Air Station
35	W1A2	Air Station
8	W1B	Air Station Auxiliary
4	W1C	Air Facility (Phoenix; Monterey; Oppama; Naha; and Naples only)
6	W1E	Marine Corps Air Station (Except Quantico)
9	W1H	Station - BuWeps (Except Rota)
1		Deputy Chief of Staff, Research and Development, Headquarters, U. S. Marine Corps, Washington, D. C.
1		President, Marine Corps Equipment Board, Marine Corps School, Quantico, Va.
2		Library of Congress, Washington, D. C.
200		Director, Office of Technical Services, Department of Commerce, Washington, D. C.
1		Rivers and Harbor Library, Princeton University, Princeton, N. J.

Distribution List (Cont'd)

No. of copies	
1	Chief of Staff, U. S. Army, Chief of Research and Development, Department of the Army, Washington, D. C.
1	Office of the Chief of Engineers, Assistant Chief of Engineering for Civil Works, Department of the Army, Washington, D. C.
1	Chief of Engineers, Department of the Army, Washington, D. C., Attn: Engineering R & D Division
1	Chief of Engineers, Department of the Army, Washington, D. C., Attn: ENGCW-CE
1	Director, U. S. Army Engineer Research and Development Laboratories, Fort Belvoir, Va., Attn: Information Resources Branch
1	Headquarters, Wright Air Development Division, (WWAD-Library), Wright-Patterson Air Force Base, Ohio
3	Headquarters, U. S. Air Force, Directorate of Civil Engineering, Washington, D. C., Attn: AFOCE-ES
1	Commanding Officer, U. S. Naval Construction Battalion Center, Port Hueneme, Calif., Attn: Materiel Dept., Code 140
1	Deputy Chief of Staff, Development, Director of Research and Development, Department of the Air Force, Washington, D. C.
1	Director, National Bureau of Standards, Department of Commerce, Connecticut Ave., Washington, D. C.
2	Office of the Director, U. S. Coast and Geodetic Survey, Washington, D. C.
20	Armed Services Technical Information Agency, Arlington Hall Station, Arlington, Va.
2	Director of Defense Research and Engineering, Department of Defense, Washington, D. C.
2	Director, Division of Plans and Policies, Headquarters, U. S. Marine Corps, Washington, D. C.
2	Director, Bureau of Reclamation, Washington, D. C.
1	Commanding Officer, U. S. Navy Yards and Docks Supply Office, U. S. Naval Construction Battalion Center, Port Hueneme, Calif.
1	Facilities Officer (Code 108), Office of Naval Research, Washington, D. C.
1	Federal Aviation Agency, Office of Management Services, Administrative Services Division, Washington, D. C., Attn: Library Branch
1	Director, U. S. Naval Ordnance Laboratory, White Oak, Silver Springs, Md.
1	Office of Naval Research, Branch Office, Navy No. 100, Box 39, FPO, New York
1	U. S. Naval Radiological Defense Laboratory, San Francisco
1	Officer in Charge, CECOS, Port Hueneme, Calif., Attn: ADCE Course
1	U. S. Air Force, Asst. Chief of Staff, Intelligence, Bldg. B., AHS, Washington, D. C., Attn: Mr. Sargent White
1	Commander, Air Force Ballistic Missile Division, Air Research and Development Command, P.O. Box 262, Inglewood, Calif.
1	Directorate of Research, Air Force Special Weapons Center, Kirtland Air Force Base, N. Mex.
1	Director, U. S. Army Engineer Waterways Experiment Station, P.O. Box 631, Vicksburg, Miss., Attn: Mr. G. L. Arbuthnot, Jr.
1	U. S. Army Chemical Center, Nuclear Defense Laboratory, Edgewood, Md.
2	Chief, Defense Atomic Support Agency, Washington, D. C.

Distribution List (Cont'd)

No. of copies	
1	Director, Ballistic Research Laboratories, Aberdeen, Md.
1	U. S. Atomic Energy Commission, Technical Information Service, P.O. Box 62, Oak Ridge, Tenn
1	Director, Civil Effects Test Group, Atomic Energy Commission, Washington, D. C.
1	Headquarters, Field Command, Defense Atomic Support Agency, Sandia Base, Albuquerque, N. Mex.
1	Office of the Chief of Engineers, Department of the Army, T-7, Gravelly Point, Washington, D. C., Attn: ENGNB
1	Office of the Chief of Engineers, Department of the Army, T-7, Gravelly Point, Washington, D. C., Attn: ENG MC-EB
1	Commanding Officer, Engineer Research and Development Laboratories, Fort Belvoir, Va.
1	Sandia Corporation, Box 5800, Albuquerque, N. Mex.
1	Library, Engineering Department, University of California, 405 Hilgard Ave., Los Angeles
1	Director, Waterways Experiment Station, P. O. Box 631, Vicksburg, Miss.
1	Officer in Charge, U. S. Navy Unit, Rensselaer Polytechnic Institute, Troy, N. Y.
1	Commander, U. S. Naval Shipyard, Attn: Material Laboratory, Brooklyn
1	U. S. Army, Attn: Director of Research and Development Group, Washington, D. C.
1	Chief, Concrete Division, Waterways Experiment Station, P. O. Drawer 2131, Jackson, Miss.
1	Chief, Physical Research Branch, Research Division, U. S. Department of Commerce, Bureau of Public Roads, Washington, D. C.
1	Operation Civil, University of California, Richmond Field Station, Berkeley, Calif.
1	Director, Engineering Research Institute, University of Michigan, Ann Arbor, Mich.
1	Portland Cement Association, 5420 Old Orchard Road, Skokie, Ill., Attn: Research Librarian.
1	Formulation and Analysis Branch, Mathematics and Computation Laboratory, National Resource Evaluation Center, Office of Emergency Planning, Washington, D. C.
1	Mr. William J. Taylor, Terminal Ballistics Laboratory, Aberdeen Proving Ground, Aberdeen Proving Ground, Md.
1	CAPT W. M. McLellon, CEC, USN, Office of Civil Defense Support, Bldg. T-7, Washington, D. C.
1	LT Edward S. Perry, U. S. Naval Reserve Officers Training Corp Unit, University of Illinois, Urbana, Ill.
1	CAPT L. N. Saunders, CEC, USN, Code C10, U. S. Naval Construction Battalion Center, Port Hueneme, Calif.
1	CDR E. M. Saunders, CEC, USN, Bureau of Yards and Docks, Code 74, Washington, D. C.
1	CDR H. W. Stephens, CEC, USN, Bureau of Yards and Docks, Code E111, Washington, D. C.
1	LCDR Charles W. Gulick, Jr., CEC, USN, Navy No. 926, FPO, San Francisco
1	LCDR W. A. Walls, CEC, USN, Defense Atomic Support Agency, Washington, D. C.
1	LCDR C. R. Whipple, CEC, USN, U. S. Naval Ordnance Laboratory, White Oak, Md.
1	Major F. A. Verser, Jr., USA, Defense Atomic Support Agency, Washington, D. C.
1	Mr. L. Neal FitzSimons, Office of Civil Defense, Department of Defense, Washington, D. C.
1	Mr. Ben Taylor, Office of Civil Defense, Department of Defense, Washington, D. C.

Distribution List (Cont'd)

No. of copies	
1	Dr. T. H. Schiffman, Armour Research Foundation of Illinois Institute of Technology, Technology Center, Chicago, Ill.
1	Dr. Robert V. Whitman, Massachusetts Institute of Technology, Cambridge, Mass.
1	Mr. Werner Weber, Nuclear Engineering Consultant, N. Y. State Civil Defense Commission, P.O. Box 7007, State Office Bldg., Albany, N. Y.
1	LCDR J. D. Andrews, CEC, USN, SHAPE Headquarters, Paris, France, A.P.O. 55, New York
1	CDR W. J. Christensen, CEC, USN, U. S. Naval Civil Engineering Laboratory, Port Hueneme, Calif.
1	LCDR N. W. Clements, CEC, USN, Navy Nuclear Power Unit, Fort Belvoir, Va.
1	LTJG L. K. Donovan, CEC, USN, Navy Nuclear Power Unit, Fort Belvoir, Va.
1	LTJG Clinton W. Kelly, III, CEC, USN, Bureau of Yards and Docks, Program Officer, U. S. Naval Radiological Defense Laboratory, San Francisco
1	CDR W. J. Francy, CEC, USN, Bureau of Yards and Docks, Director, Southeast Division, U. S. Naval Base, Charleston, S. C.
1	CDR C. F. Krickenberger, CEC, USN, Bureau of Yards and Docks, Code 51, Washington, D. C.
1	Dr. Harold Brode, The Rand Corporation, 1700 Main St., Santa Monica, Calif.
1	Dr. William Kreger, Naval Radiological Defense Laboratory, San Francisco
1	Dr. Hans Tiller, Nuclear Defense Laboratory, Army Chemical Center, Md.
1	Mr. Irving Gaskill, National Resource Evaluation Center, Executive Office Bldg., Washington, D. C.
1	Major Robert S. Marcum, Defense Atomic Support Agency, Department of Defense, Washington, D. C.
1	Dr. Carl F. Miller, Office of Civil Defense, Department of Defense, Washington, D. C.
1	Mr. James C. Pettee, National Resource Evaluation Center, Executive Office Bldg., Washington, D. C.
1	Dr. A. B. Chilton, Civil Engineering Hall, University of Illinois, Urbana, Ill.
1	Mrs. Shea Valley, CRTZS, A. F. Cambridge Research Center, Bedford, Mass.
1	Dr. Ronald W. Shephard, University of California, Engineering Field Station, 1301 South 46th St., Richmond, Calif.
1	LTCOL Russell J. Hutchinson, 052921, Office of the Engineer, Camp Wolters, Mineral Wells, Tex.
1	LT R. B. Reeves, CEC, USN, Field Command, Defense Atomic Support Agency, Sandia Base, Albuquerque, N. Mex.
1	Professor J. T. Hanley, Department of Civil Engineering, University of Illinois, Urbana, Ill.
1	Asst. Professor J. Silverman, Department of Chemical Engineering, University of Maryland, College Park, Md.
1	Mr. R. D. Cavanaugh, Barry Controls, Inc., 700 Pleasant St., Watertown, Mass.
1	Mr. Kenneth Kaplan, Broadview Research Corporation, 1811 Trousdale Dr., Burlingame, Calif.
1	Mr. Thomas Morrison, American Machine and Foundry Co., 7501 North Natchez Ave., Niles, Ill.
1	Mr. W. R. Perret - 5112, Sandia Corporation, Sandia Base, Albuquerque, N. Mex.
1	Mr. Lyndon Welch, Eberle M. Smith Associates, Inc., 153 East Elizabeth St., Detroit, Mich.
1	Dr. Lauriston S. Taylor, Chief, Radiation Physics Division, National Bureau of Standards, Washington, D. C.
1	Professor Herbert M. Bosch, Public Health Engineering, School of Public Health, University of Minnesota, Minneapolis, Minn.

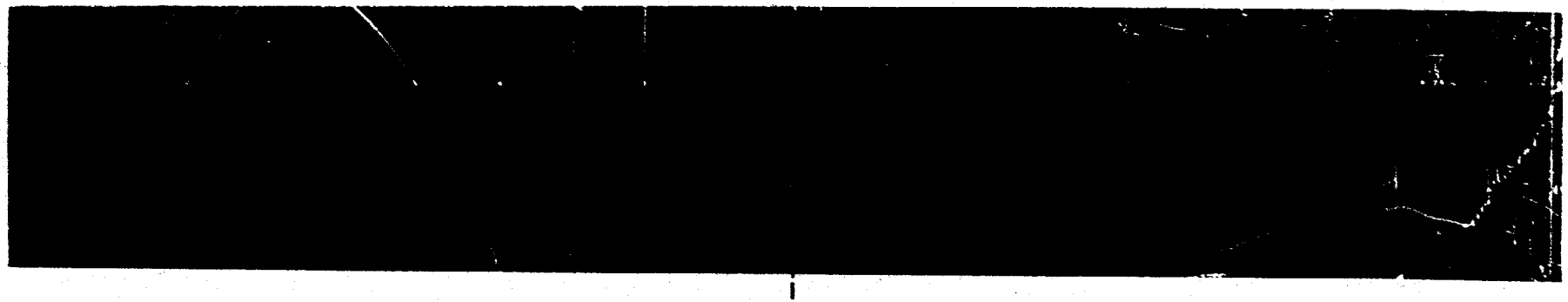

U. S. Naval Civil Engineering Laboratory
Technical Report R-226
BLAST LOADING OF CONCRETE BEAMS REINFORCED WITH HIGH-STRENGTH DEFORMED BARS, by William A. Keenan
99 p. illus. 22 Apr 63 UNCLASSIFIED

This report presents the theoretical study and subsequent test of concrete beams, reinforced with high-strength deformed bars, subjected to static and dynamic uniform loads of both long and short duration. Major considerations were adequate strength and ductility under dynamic loads and limited cracks and deflections under static service loads.

1. Reinforced Concrete Beams — High-Strength Reinforcement
I. Keenan, William A.
II. Y-F008-10-102A

U. S. Naval Civil Engineering Laboratory
Technical Report R-226
BLAST LOADING OF CONCRETE BEAMS REINFORCED WITH HIGH-STRENGTH DEFORMED BARS, by William A. Keenan
99 p. illus. 22 Apr 63 UNCLASSIFIED

This report presents the theoretical study and subsequent test of concrete beams, reinforced with high-strength deformed bars, subjected to static and dynamic uniform loads of both long and short duration. Major considerations were adequate strength and ductility under dynamic loads and limited cracks and deflections under static service loads.

1. Reinforced Concrete Beams — High-Strength Reinforcement
I. Keenan, William A.
II. Y-F008-10-102A

U. S. Naval Civil Engineering Laboratory
Technical Report R-226
BLAST LOADING OF CONCRETE BEAMS REINFORCED WITH HIGH-STRENGTH DEFORMED BARS, by William A. Keenan
99 p. illus. 22 Apr 63 UNCLASSIFIED

This report presents the theoretical study and subsequent test of concrete beams, reinforced with high-strength deformed bars, subjected to static and dynamic uniform loads of both long and short duration. Major considerations were adequate strength and ductility under dynamic loads and limited cracks and deflections under static service loads.

1. Reinforced Concrete Beams — High-Strength Reinforcement
I. Keenan, William A.
II. Y-F008-10-102A

U. S. Naval Civil Engineering Laboratory
Technical Report R-226
BLAST LOADING OF CONCRETE BEAMS REINFORCED WITH HIGH-STRENGTH DEFORMED BARS, by William A. Keenan
99 p. illus. 22 Apr 63 UNCLASSIFIED

This report presents the theoretical study and subsequent test of concrete beams, reinforced with high-strength deformed bars, subjected to static and dynamic uniform loads of both long and short duration. Major considerations were adequate strength and ductility under dynamic loads and limited cracks and deflections under static service loads.

1. Reinforced Concrete Beams — High-Strength Reinforcement
I. Keenan, William A.
II. Y-F008-10-102A

Distribution List (Cont'd)

No. of copies	
1	Dr. Merit P. White, Civil Engineering Department, School of Engineering, University of Massachusetts, Amherst, Mass.
1	Dr. Robert J. Hansen, Department of Civil and Sanitary Engineering, Massachusetts Institute of Technology, Cambridge, Mass.
1	Mr. Harold Horowitz, Building Research Institute, National Academy of Sciences, 2101 Constitution Ave., N.W., Washington, D. C.
1	Mr. Luke Vortman - 5112, Applied Experiments Division, Sandia Corporation, Albuquerque, N. Mex.
1	Mr. Richard Park, National Academy of Sciences, 2101 Constitution Ave., N.W., Washington, D. C.
1	Dr. Harold A. Knapp, Fallout Studies Branch, Division of Biology and Medicine, U. S. Atomic Energy Commission, Washington, D. C.
1	Dr. Karl Z. Morgan, Director, Health Physics Division, Oak Ridge National Laboratory, Oak Ridge, Tenn.
1	Mr. Frederick A. Pawley, AIA Research Secretary, American Institute of Architects, 1735 New York Ave., N.W., Washington, D. C.
1	Dr. David Kleinecke, Engineering Field Station, University of California, 1301 South 46th St., Richmond, Calif.
1	Dr. E. E. Massey, Defense Research Board, Department of National Defense, Ottawa, Canada
1	Dr. Joseph D. Coker, National Resource Evaluation Center, Executive Office Bldg. Washington, D. C.
1	Dr. Charles F. Ksanda, Military Evaluations Division, U. S. Naval Radiological Defense Laboratory, San Francisco
1	LT Parker Moreland, Department of Defense, Defense Atomic Support Agency, Washington, D. C.
1	Dr. George E. Pugh, Institute of Defense Analyses, Weapons Systems Evaluation Division, Washington, D. C.
1	Dr. Robert Rapp, The Rand Corporation, 1700 Main St., Santa Monica, Calif.
1	Dr. Stephen B. Withey, Program Director, Survey Research Center, University of Michigan, Ann Arbor, Mich.
1	Mr. John Auxier, Oak Ridge National Laboratory, Oak Ridge, Tenn.
1	Dr. Eric T. Clarke, Technical Operations, Inc., Burlington, Mass.
1	LT Walter J. Eager, Jr., CEC, USN, Naval Postgraduate School, Monterey, Calif.
1	LCDR C. Curione, CEC, USN, U. S. Naval Civil Engineering Laboratory, Port Hueneme, Calif.
1	LTCOL James R. Bohanan, USAF, Headquarters, U. S. Air Force, Directorate of Civil Engineering, Washington, D. C.
1	Mr. Walter Gunther, The Mitre Corporation, P.O. Box 208, Lexington, Mass.
1	LCDR R. C. Vance, Mobile Construction Battalion 11, FPO, San Francisco
1	LCDR J. C. LeDoux, Office of Civil Defense, Department of Defense, Washington, D. C.
1	LT I. D. Crowley, CEC, USN, U. S. Naval School, CEC Officers, Port Hueneme, Calif.
1	LT S. H. Mathes, CEC, USN, U. S. Naval Construction Battalion Center, Port Hueneme, Calif.
1	Dr. James O. Buchanan, Technical Operations, Inc., South Ave., Burlington, Mass.
1	Mr. Jack C. Greene, Office of Civil Defense, Department of Defense, Washington, D. C.
1	CAPT Robert Crawford, USAF, Air Force Special Weapons Center, Kirtland Air Force Base, Albuquerque, N. M.

Distribution List (Cont'd)

No. of copies	
1	Dr. C. P. Siess, Talbot Laboratory, University of Illinois, Urbana, Ill.
1	Dr. J. D. Haltiwanger, Department of Civil Engineering, University of Illinois, Urbana, Ill.
1	Dr. A. Feldman, Department of Civil Engineering, University of Colorado, Boulder, Colo.
1	Professor G. R. Swihart, Department of Civil Engineering, University of Nebraska, Lincoln, Neb.
1	Professor Phil M. Ferguson, Civil Engineering Department, University of Texas, Austin, Tex.
1	Dr. Ray E. Untrauer, Department of Civil Engineering, Iowa State University, Ames, Iowa
1	Dr. J. G. Hammer, The Rand Corporation, Santa Monica, Calif.
1	Dr. W. J. Austin, Department of Civil Engineering, Rice University, Houston, Tex.
1	Dr. George K. Wadlin, Civil Engineering Department, University of Maine, Orono, Me.
1	Dr. Ken Lenzen, Department of Engineering Mechanics, Kansas University, Lawrence, Kan.
1	Dr. Eivind Hognestad, Structural Development Section, PCA Research and Development Laboratories, Skokie, Ill.
1	Mr. David Watstein, National Bureau of Standards, Washington, D. C.
1	Dr. Joseph Penzien, Department of Civil Engineering, University of California, Berkeley, Calif.
1	Dr. F. T. Mavis, Dean, College of Engineering, University of Maryland, College Park, Md.
1	Dr. John Balloch, Director, Operations Analysis, 26th Air Division, (SAGE), Hancock Field, Syracuse, N. Y.
1	Mr. J. F. Tamanini, A & E Development Division, Office of Civil Defense, Department of Defense, Washington, D. C.
1	Mr. Charles M. Eisenhauer, Radiation Physics Laboratory, National Bureau of Standards, Washington, D. C.
1	Mr. O. H. Hill, Bldg. 12, Rm. 505, Radiation Physics Division, National Bureau of Standards, Washington, D. C.
1	Dr. Lewis V. Spencer, Ottawa University, Physics Department, Ottawa, Kan.
1	Mr. E. E. Shalowitz, Protective Construction, GSA Bldg. 19th and F St., N. W., Washington, D. C.
1	Mr. G. H. Albright, Pennsylvania State University, College of Engineering and Architecture, University Park, Pa.
1	Mr. A. F. Dill, Civil Engineering Hall, University of Illinois, Urbana, Ill.
1	Dr. N. M. Newmark, Civil Engineering Hall, University of Illinois, Urbana, Ill.
1	Professor J. Neils Thompson, Civil Engineering Department, University of Texas, Austin, Tex.
1	Mr. Fred Sauer, Physics Department, Stanford Research Institute, Menlo Park, Calif.
1	Mr. W. E. Fisher, Air Force Special Weapons Center, Kirtland Air Force Base, Albuquerque, N. M.
1	Dr. Boris Bresler, Department of Civil Engineering, University of California, Berkeley, Calif.
1	Dr. Arsham Amirikian, Bureau of Yards and Docks, Code E202C, Washington, D. C.